Препринти Інституту фізики конденсованих систем НАН України розповсюджуються серед наукових та інформаційних установ. Вони також доступні по електронній комп'ютерній мережі на WWW-сервері інституту за адресою http://www.icmp.lviv.ua/

The preprints of the Institute for Condensed Matter Physics of the National Academy of Sciences of Ukraine are distributed to scientific and informational institutions. They also are available by computer network from Institute's WWW server (http://www.icmp.lviv.ua/)

Роман Романович Левицький
Сергій Іванович Сороков
Ігор Романович Зачек
Андрій Степанович Вдович
Алла Пилипівна Моїна
Леонід Миколайович Коротков
Олексій Ігорович Бочаров

Роль п'єзоелектричного зв'язку в поведінці фізичних характеристик регулярних і невпорядкованих сегнетоактивних сполук сім'ї $KH_2PO_4$

Роботу отримано 19 грудня 2011 р.

Затверджено до друку Вченою радою ІФКС НАН України

Рекомендовано до друку семінаром відділу теорії модельних спінових систем

Виготовлено при ІФКС НАН України


**Національна академія наук України**

**ІНСТИТУТ ФІЗИКИ КОНДЕНСОВАНИХ СИСТЕМ**

ICMP–11–13E

R.R.Levitskii, S.I.Sorokov, I.R.Zachek[*], A.S.Vdovych, A.P.Moina, L.M.Korotkov[†], A.I.Bocharov[†]

# ROLE OF PIEZOELECTRIC COUPLING IN BEHAVIOR OF THE PHYSICAL CHARACTERISTICS OF REGULAR AND DISORDERED FERROELECTRIC COMPOUNDS OF THE $KH_2PO_4$ FAMILY

[*]Lviv National Polytechnic University, 79013 Lviv, 12 Bandera Street
[†]Voronezh State Technical University, Moskovsky Pr. 14, 394026 Voronezh, Russia

ЛЬВІВ

**УДК:** 537.226.83/.86, 538.91

**PACS:** 77.84.-s, 64.60.Cn, 77.22.-d, 77.80.-e, 77.80.Bh, 77.65.Bn

**Роль п'єзоелектричного зв'язку в поведінці фізичних характеристик регулярних і невпорядкованих сегнетоактивних сполук сім'ї $KH_2PO_4$**

Р.Р.Левицький, С.І.Сороков, І.Р.Зачек, А.С.Вдович, А.П.Моїна, Л.М.Коротков, О.І.Бочаров

**Анотація.** Представлено огляд результатів теоретичних та експериментальних робіт для матеріалів типу $Rb_{1-x}(NH_4)_xH_2PO_4$. Показано, що результати розрахунку фізичних характеристик цих матеріалів на основі запропонованої теорії задовільно узгоджуються з експериментальними даними, за винятком області фазового переходу. Представлено також результати розрахунку фізичних характеристик регулярних сполук сім'ї $KH_2PO_4$ з врахуванням п'єзоелектричного зв'язку. Вказано на необхідність врахування п'єзоелектричного зв'язку в змішаних матеріалах.

**Role of piezoelectric coupling in behavior of the physical characteristics of regular and disordered ferroelectric compounds of the $KH_2PO_4$ family**

R.R.Levitskii, S.I.Sorokov, I.R.Zachek, A.S.Vdovych, A.P.Moina, L.M.Korotkov, A.I.Bocharov

**Abstract.** The review of theoretical and experimental papers for $Rb_{1-x}(NH_4)_xH_2PO_4$ type materials are presented. It is shown, that results of calculation of physical characteristics of these materials within proposed theory satisfactorily agree with experimental data, with the exception of phase transition region. The results of calculation of physical characteristics of regular $KH_2PO_4$ family compounds with taking into account of piezoelectric coupling are also presented. We have pointed on necessity of taking into account of piezoelectric coupling in mixed crystals.

**Подається в** Condensed Matter Physics
**Submitted to** Condensed Matter Physics





## 1. Introduction

### 1.1. Experimental studies of the $Rb_{1-x}(NH_4)_xH_2PO_4$ type compounds

The hydrogen bonded compounds of the $Rb_{1-x}(NH_4)_xH_2PO_4$ type, which at certain compositions have a proton glass phase, have been intensively studied for more than 25 years. In order to describe possible proton configurations in the mixed $Rb_{1-x}(NH_4)_xH_2PO_4$ type compounds, let us consider first the structure of the pure RDP - $RbH_2PO_4$ and ADP - $NH_4H_2PO_4$ crystals. In figure 1 a unit cell of the KDP - $KH_2PO_4$ crystal, which is isomorphic to RDP, is shown. A primitive cell

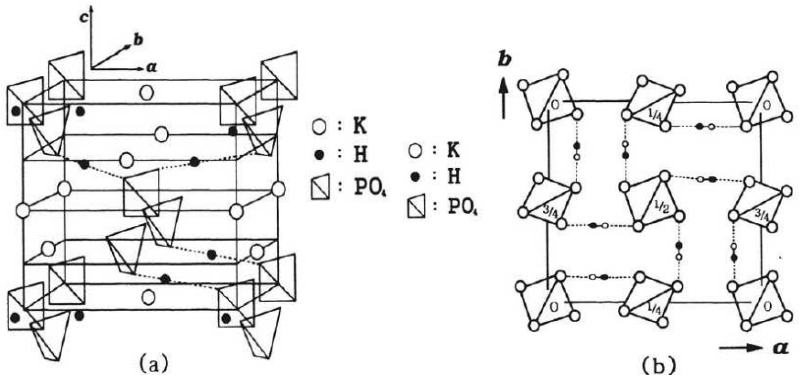


Figure 1. A unit cell (four formula units) of the KDP - $KH_2PO_4$ crystal.

of the $RbH_2PO_4$ type compounds contains one $PO_4$ tetrahedron of the "$A$" type and one $PO_4$ tetrahedron of the "$B$" type, two Rb atoms and four protons on four hydrogen bonds attached to the "$A$" type tetrahedron. In the ferroelectric phase the net dipole moment of the primitive cell, associated with displacements of heavy ions and deformations of the $PO_4$ groups, is directed along the $c$ axis. A triggering mechanism of the ionic displacements in these crystals is the proton ordering (their positions are described by pseudospin operators $S_f = \pm 1,\ f = 1, 2, 3, 4$) in double potential wells on the hydrogen bonds. The bond dipole moments lie almost in the $ab$ plane; the total dipole moment of protons in the cell of the RDP type crystals is zero. Thus,

$$\vec{\mu}_{1\alpha} = (\mu_\alpha^x, 0, 0),\ \vec{\mu}_{3\alpha} = (-\mu_\alpha^x, 0, 0),\ \vec{\mu}_{2\alpha} = (0, -\mu_\alpha^y, 0),\ \vec{\mu}_{4\alpha} = (0, \mu_\alpha^y, 0),$$

where $\vec{\mu}_{f\alpha}$ are the dipole moments of the $f$-th hydrogen bond; $\alpha = +$ for $x = 0$, and $\alpha = -$ for $x = 1$.

The composition range in these compounds can be divided into three regions of $x$, which we shall call the glass phase region, the ferroelectric phase region, and the antiferroelectric phase region. The glass phase region exists in the $Rb_{1-x}(NH_4)_xH_2PO_4$ system at $x \sim 0.22 - 0.75$, in the $Rb_{1-x}(ND_4)_xD_2PO_4$ at $x \sim 0.23 - 0.65$, in the $Rb_{1-x}(NH_4)_xH_2AsO_4$ at $x \sim 0.2 - 0.45$, and in the $K_{1-x}(NH_4)_xH_2PO_4$ system at $x \sim 0.23 - 0.67$. The ferroelectric phase region lies between $x = 0$ and the glass phase region; the antiferroelectric phase region lies between $x = 1$ and the glass phase region. An important characteristics of the $Rb_{1-x}(NH_4)_xH_2PO_4$ type compounds is the Edwards-Anderson parameter $q_{EA}$, which is the averaged over configurations square of the averaged over the Gibbs ensemble $S_f$-operator. It is different from zero at $0 < x < 1$ at all temperatures.

**Glass phase composition region.** In the proton glass phase the net spontaneous polarization is absent, but the unit cell polarization is different from zero. It means that the average over the sample square of the cell dipole moment (proportional to the Edwards-Anderson parameter) is different from zero.

Experimental measurements of the dielectric permittivity of $Rb_{1-x}(NH_4)_xH_2PO_4$ [1–8], $Rb_{1-x}(ND_4)_xD_2PO_4$ [7], [9–14], $Rb_{1-x}(NH_4)_xH_2AsO_4$ [15–18], and $K_{1-x}(NH_4)_xH_2PO_4$ [19–23] in the glass phase composition region have shown that the temperature curves of the longitudinal $\varepsilon_{33}(T,\nu)$ and transverse $\varepsilon_{11}(T,\nu)$ permittivities are qualitatively similar. At high temperatures the real parts of the permittivities are roughly described by the Curie-Weiss law. Below a certain temperature $T_f$, a deviation from the Curie-Weiss law is observed. Then $\varepsilon'_{33}(T,\nu)$ and $\varepsilon'_{11}(T,\nu)$ have maxima at temperature $T_m$ and slowly decrease after that. Below a certain temperature $T_g$ (the inflection points) $\varepsilon'_{33}(T,\nu)$ and $\varepsilon'_{11}(T,\nu)$ rapidly fall to their minimal values. The imaginary parts of the permittivities $\varepsilon''_{33}(T,\nu)$ and $\varepsilon''_{11}(T,\nu)$ have peaks at $T_g$ and fall nearly to zero at other temperatures. It should be noted that the temperatures $T_f$, $T_m$, and $T_g(\nu)$ determined from $\varepsilon'_{33}(T,\nu)$ are somewhat different from those determined from $\varepsilon'_{11}(T,\nu)$.

The temperature $T_g(\nu)$ decreases with decreasing frequency $\nu$, at which the permittivity is measured. The temperature of the transition to the glass phase is $T_0$, where $T_g(\nu) \to T_0$ at $\nu \to 0$. Character of the temperature curves of $\varepsilon''_{33}(T,\nu)$ and $\varepsilon''_{11}(T,\nu)$ indicates that this transition is strongly smeared out (it starts near $T_f$ and finishes at $T_0$).

The temperature $T_f$, in the vicinity of which the proton freezing



begins, is estimated by different methods. The EPR studies on paramagnetic $Tl^{2+}$ impurity ions [24–26], whose spectrum is sensitive to structural transformations, in the RADP crystals show that the energy levels of these ions are gradually split by local fields with lowering temperature. This confirms the existence of a significant static random field in $Rb_{1-x}(NH_4)_xH_2PO_4$.

The chaotic static electric fields governed by the piezoelectric interactions and static elastic strains are believed [27] to be formed by chaotic substitutional disorder of ions of different radii. It has been shown that these fields act, mainly, on the lattice polarization along the $c$-axis and on the configurations with two protons near the "upper" or "lower" (with respect to the $c$–axis) oxygen atoms. It is shown that in addition to these chaotic fields and pseudospin-pseudospin interactions with a random sign, a chaotic local anisotropy should be taken into account. The difference in the symmetry of "upper" or "lower" and lateral proton configurations and peculiarities of the proton-lattice interactions can lead to coexistence of the long-range order with the glass state or paraelectric state.

The temperature dependence of the spin-lattice relaxation time for protons of $NH_4$ ionic groups in $Rb_{0.65}(NH_4)_{0.35}H_2PO_4$ was studied by the NMR method in [28]. In these compounds such a dependence has a minimum at $\sim$ 180K, associated with the start of proton freezing and with formation of the hydrogen bonds between the $NH_4$ and $PO_4$ groups. In [29] the relaxation time of $^{31}P$ in $Rb_{1-x}(ND_4)_xD_2PO_4$ for different compositions was measured; a similar minimum in its temperature dependence was obtained near 170K.

The X-ray structural studies revealed [30] a deviation of the lattice constants in $Rb_{1-x}(NH_4)_xH_2PO_4$ from the Debye approximation below a certain temperature $T_f(x) \sim 90K$; these deviations increase with increasing ammonium concentration. Despite the changes in the lattice constants, these compounds remain tetragonal. Below $T_f(x)$ in the proton glass state a diffuse X-ray scattering increases [30–32]. It is particularly notable near the boundary between the ferroelectric and glass phases [32]. Possibly, it is related to formation of some heterogeneous structure, that is, to coexistence of two phases.

In the obtained in [33, 34] Raman spectra of $Rb_{1-x}(ND_4)_xD_2PO_4$ (x=0.5 and 0.25) some lines split below $T_f \sim 200K$, because of the nonequivalency of $PO_4$ groups (some of them are surrounded by $Rb^+$, while the others by $ND_4^+$). In the Raman spectra of $Rb_{0.3}(NH_4)_{0.7}H_2PO_4$ the orientational vibrations of $NH_4^+$ ions are revealed [35], indicating formation of the $PO_4$ – $NH_4^+$ bonds and of the proton glass. The tem-

perature dependence of the position of the peak, corresponding to the $\nu_2$ vibrations of the $PO_4$ tetrahedra, has a characteristic break near $T_f \sim 100K$. This break is related to the start of the proton freezing and their attaching to the $PO_4$ tetrahedra. A similar break was revealed in [36] for $K_{1-x}(NH_4)_xH_2PO_4$ ($x = 0.32, 0.53$) and in [37] for $Rb_{1-x}(NH_4)_xH_2AsO_4$ ($x = 0.35$).

The Edwards-Anderson parameter, which at moderately low temperatures is approximately proportional to the widths of various spectral lines, gradually increases with lowering temperature. This indicates that the transition to the proton glass state is smeared out. Thus, the NMR spectral line for $Rb_{1-x}(ND_4)_xD_2PO_4$ at different $x$ [38,39] and the NQR line for $_{0.5}(NH_4)_{0.5}H_2PO_4$ [41] widens at lowering temperature, and the intensity of elastic neutron scattering from $Rb_{0.38}(ND_4)_{0.62}D_2PO_4$ increases [42].

Below $T_0$ the system becomes non-ergodic. The temperature $T_0$ is estimated by approximation of the experimental data for the dielectric permittivities at low temperatures. In [11] using the results of dielectric measurements and the following phenomenological expression for the longitudinal dielectric susceptibility

$$\chi(T,\omega) = \chi_0(T) \cdot \int_0^\infty d\ln\tau \cdot \frac{g(\tau,T)}{1-i\omega\tau}$$

the distribution function of relaxation times $g(\tau,T)$ was analyzed. In the time range $\tau \approx [\tau_0, \tau_c]$ the function $g(\tau,T)$ was qualitatively approximated by a rectangular distribution with the critical relaxation time $\tau_c$. The best fit to the experimental data for x=0.35 was obtained using the Vogel-Fulcher law

$$\tau_c = \tau_0 \exp\left(\frac{E_c}{T-T_0}\right); \quad T_0 = 8.74K, \quad E_c = 268K,$$
$$\nu_0 = 1/2\pi\tau_0 = 3.49 \cdot 10^{12} Hz.$$

At $T = T_0$ the maximal relaxation time becomes infinite. In [10] using the measured dielectric permittivities of $Rb_{0.5}(ND_4)_{0.5}D_2PO_4$ the value of $T_0 \approx 32K$ was obtained.

In [43] it has been shown that for $Rb_{0.53}(ND_4)_{0.47}D_2PO_4$ the spectrum of the distribution function $g(\tau,T)$ consists of two wide lines; with decreasing temperature from 55K down to 35K a fast intensity redistribution from smaller times to larger ones takes place. These results are interpreted within a model of dynamically correlated domains [44, 45],



which form a system of classical dipoles. At the freezing temperature part of them form an infinite percolation cluster. In this model $T_0 = 0K$ (the Arrhenius law).

At low temperatures an essential role is, most likely, played by proton tunneling. This is indicated by the maximum on the temperature curve of the dielectric losses tangent in $Rb_{0.25}(NH_4)_{0.75}H_2PO_4$ [8] at $T \approx 0.2K$, as well as by splitting of NMR spectral lines of $Rb_{0.56}(ND_4)_{0.44}D_2PO_4$ [46]. This means that deuteron motion is not completely frozen out. Tunneling lowers down $T_0$.

Polarization relaxation and non-ergodic processes in proton glasses $M_{1-x}(NW_4)_xW_2AO_4$ (M=Rb, K; W=H, D; A=P, As) were explored by the Monte-Carlo method in [47]. The following interactions were taken into account: 1) between protons in the "upper" or "lower", lateral ($W_2AO_4$), and Takagi ($WAO_4$ and $W_3AO_4$) configurations; 2) between protons via $NH_4$ ions, which in pure ammonium compounds render the state with lateral configurations the ground state; 3) proton-lattice interactions, arising as a displacement field, if one of the nearest neighbors is the alkali ion, whereas the other is the ammonium ion; 4) interactions with an external electric field. At a given temperature the average value of polarization was calculated; the total number of proton jumps was up to $10^7$ for each temperature. The temperature variation of polarization at heating in zero external field ($P_{ZFH}$ with the initial value of $P_{ZFH}(T=0) = P_i$ ) and at heating in non-zero field ($P_{FH}$ with the initial $P_{FH}(T=0) = 0$) were approximated by the following dependences

$$P_{ZFH} = P_i \cdot \exp\left[-\left(T/T_e\right)^\gamma\right]; \quad P_{FH} = P_f \cdot \left(1 - \exp\left[-\left(T/T_e\right)^\gamma\right]\right).$$

At small fields $T_e \simeq T_{Slater} 0.53$, $\gamma = 6$, where the non-ergodicity temperature $T_e$ is introduced.

Little attention has been paid to investigation of the temperature dependence of specific heat of these systems in the glass phase region. We are aware of a single paper [48], where it has been shown that the molar specific heat C(T) of $Rb_{1-x}(NH_4)_xH_2PO_4$ at $x$=0.7 and $x$=0.74 increases monotonically with temperature. Near 60K the curve C(T) is somewhat convex upwards. This convexity is most likely related to the protonic contribution to the specific heat, which is difficult to separate from the lattice contribution.

**The ferroelectric phase composition region.** In this region at high temperatures the $q_{EA}$ parameter obtained from the NQR linewidths in $Rb_{1-x}(NH_4)_xH_2AsO_4$ with $x$=0.01, 0.02 [49] and NMR linewidths in $Rb_{1-x}(ND_4)_xD_2PO_4$ [39] with $x$=0.22 is different from zero. This indicates a partial proton freezing at high temperatures.

With lowering temperature, the transition to the ferroelectric phase takes place at $T_c(x)$; in this phase a spontaneous polarization $P_s$ exists. Unfortunately, the experimental data for $P_s$ and $q_{EA}$ are very limited, except for the case of $x = 0$. At $x = 0$ $P_s$ has a jump at $T_c(x)$. The temperature $T_c(x)$ is maximal at $x = 0$ and decreases with increasing $x$, whereas the jump in $P_s$ disappears (as observed in $Rb_{1-x}(NH_4)_xH_2AsO_4$ at $x = 0.08$ [18]), and the phase transition is smeared out. The temperature $T_c(x)$ can be also determined from the NMR data. Thus, in [50] by the NMR method it has been established that the temperature dependence of the spin-lattice relaxation time of $^{87}Rb$ ions in $Rb_{1-x}(ND_4)_xD_2PO_4$ has a minimum at $T_c(x)$.

The transverse dielectric permittivity $\varepsilon'_{11}(T,\nu)$ of the $Rb_{1-x}(NH_4)_xH_2PO_4$ type compounds in the ferroelectric phase composition region is somewhat smaller that in the glass phase region. It gradually increases at lowering temperature, then has a rounded maximum at $T_c(x)$, and rapidly decreases to a certain constant value below $T_c(x)$. At even lower temperature $T_g(x)$ (inflection point), the permittivity $\varepsilon'_{11}(T,\nu)$ decreases to a minimal value. At the same time $\varepsilon''_{11}(T,\nu)$ has two maxima at $T_c(x)$ and $T_g(x)$. The same behavior was experimentally detected also for $\varepsilon'_{11}(T,\nu)$ and $\varepsilon''_{11}(T,\nu)$ in $Rb_{1-x}(NH_4)_xH_2PO_4$ [51], $Rb_{1-x}(ND_4)_xD_2PO_4$ [12], $Rb_{1-x}(NH_4)_xH_2AsO_4$ [16, 18, 52, 53], and $K_{1-x}(NH_4)_xH_2PO_4$ [54].

The longitudinal permittivity $\varepsilon'_{33}(T,\nu)$ of the $Rb_{1-x}(NH_4)_xH_2PO_4$ type compounds in the ferroelectric phase composition region also has a rounded peak at $T_c(x)$, but its height is by two orders of magnitude larger than that of $\varepsilon'_{11}(T,\nu)$ and larger than in the glass phase composition region. It becomes larger and sharper with lowering $x$. Such a behavior of $\varepsilon'_{33}(T,\nu)$ was observed in $Rb_{1-x}(NH_4)_xH_2PO_4$ [3], $Rb_{1-x}(NH_4)_xH_2AsO_4$ [17], and $K_{1-x}(NH_4)_xH_2PO_4$ [22, 23, 55, 56].

Smearing of the transition to the ferroelectric phase is associated with fluctuations of ammonium concentration. In samples with smaller $x$ the transition to the ferroelectric phase takes place at higher temperatures than in samples with higher $x$. Such an explanation is confirmed by the data of [57], where in the neutron diffraction patterns of $Rb_{0.9}(ND_4)_{0.1}D_2AsO_4$ the intensity maxima characteristic for the paraelectric and for the ferroelectric phase were shown to coexist in a certain temperature range (7-10K). This fact indicates coexistence of the two phases.

Presence of the low-temperature peaks of $\varepsilon''_{11}(T,\nu)$ and $\varepsilon''_{33}(T,\nu)$ at $T_g(x)$ in the ferroelectric phase composition region is related to coexistence of the ferroelectric and glass phases. Such a coexistence was revealed by measurements of $\varepsilon''_{11}(T,\nu)$ in $Rb_{1-x}(NH_4)_xH_2PO_4$ at $x$=0.15 and 0.17 [51], $Rb_{1-x}(NH_4)_xH_2AsO_4$ [16, 18, 52, 58], $K_{1-x}(NH_4)_xH_2PO_4$ [54], $Rb_{0.96}(ND_4)_{0.04}D_2AsO_4$ [54, 59]. It is believed that in the ferroelectric phase composition region the samples have small inclusions, in which the concentration of $NH_4$ is characteristic for the glass phase composition region. These inclusions at the temperature $T_g(x)$ undergo a transition to the proton glass state. With lowering $x$ the temperature $T_g(x)$ decreases. This is associated with a decrease of the dimensions and correlation length of the clusters, where the transition to the glass state takes place; as a result, at low $x$ the system dynamics is faster than at $x$ close to the glass phase composition region.

In [58] the imaginary part of the permittivity $\varepsilon''_{11}(T,\nu)$ and the Cole-Cole curves were measured at different frequencies for low concentrations $x$=0; 0.01; 0.05; 0.1 in $Rb_{1-x}(NH_4)_xH_2AsO_4$ and $Rb_{1-x}(ND_4)_xD_2AsO_4$. At $x$=0.05; 0.1 a coexistence of the low-temperature proton glass phase and non-uniform ferroelectric phase has been detected below $T_g(\nu,x)$. From the Cole-Cole curves a presence of the relaxation time distribution below $T_g(\nu,x)$ is evident.

In [18] the temperature dependences of spontaneous polarization of $Rb_{1-x}(NH_4)_xH_2AsO_4$ and $Rb_{1-x}(ND_4)_xD_2AsO_4$ (at $x$=0.0; 0.08), as well as transverse permittivities $\varepsilon'_a(1kHz,T)$ (for $x$=0.0; 0.08; 0.4 in $Rb_{1-x}(NH_4)_xH_2AsO_4$ and $x$=0.0; 0.08; 0.28 in $Rb_{1-x}(ND_4)_xD_2AsO_4$) were measured. It has been shown that at $x$=0.08 in the temperature range between $T_g(x)$ and $T_c(x)$ the sample polarization is proportional to the contribution of the so-called lost dielectric response

$$P_{sd}(T)=P_{so}\frac{\Delta\varepsilon'_{a1}(T)}{\varepsilon'_a(T,x=0.4)};\ \Delta\varepsilon'_{a1}(T)=\varepsilon'_a(T,x=0.4)-\varepsilon'_a(T,x=0.08).$$

**Antiferroelectric phase composition region.** In this region the high-temperature proton glass phase exists at high temperatures, since the $q_{EA}$ parameter obtained from the NMR linewidths in the $Rb_{1-x}(ND_4)_xD_2PO_4$ system is different from zero and increases with decreasing temperature [39, 60].

At lowering temperature a phase transition to the antiferroelectric phase takes place at $T_N(x)$. The transition temperature $T_N(x)$ is maximal at $x$=1, decreases with lowering $x$, and vanishes at a certain critical value of $x$, where the glass phase composition region begins. The obtained in [35] temperature dependence of the Raman scattering line, corresponding to $\nu_2$ vibrations of $PO_4$ tetrahedra in $Rb_{1-x}(NH_4)_xH_2PO_4$ crystals at $x$=0.8, has two bends at 130K and 65K. The first bend corresponds to $T_f(x)$ and to the start of the proton freezing on the O-H...O

bonds, just like in the glass phase composition region. The second bend corresponds to the transition to the antiferroelectric phase at $T_N(x)$, because below $T_N(x)$ the frequency $\nu_2$ increases due to formation of the $NH_4$–$PO_4$ clusters. In [35] the two bends are observed also in the ferroelectric phase composition region at $x$=0.2: the first one at $T_f(x)$, the second one at $T_c(x)$.

Using the experimental data for the transverse dielectric permittivity of $Rb_{1-x}(NH_4)_xH_2PO_4$ [3, 4], $Rb_{1-x}(ND_4)_xD_2PO_4$ [12], $Rb_{1-x}(NH_4)_xH_2AsO_4$ [17], and $K_{1-x}(NH_4)_xH_2PO_4$ [19, 22, 61] it has been established that $\varepsilon'_{11}(T,\nu)$ in the antiferroelectric phase composition region at $T > T_N(x)$, just like in the glass and ferroelectric phase composition region, increases with lowering temperature, but the value of $\varepsilon'_{11}(T,\nu)$ here is somewhat larger. At $T < T_N(x)$ $\varepsilon'_{11}(T,\nu)$ is much smaller than at $T > T_N$ and slightly decreases with decreasing temperature. Near $T_N(x)$ a fast drop of $\varepsilon'_{11}(T,\nu)$ takes place, which at $x \to 1$ transforms into a break. At $x$ close to the glass phase composition region this decrease slows down, whereas the maximum of $\varepsilon'_{11}(T,\nu)$ at $T_N(x)$ becomes rounded, that is, the phase transition is smeared out. In [3] the observed $\varepsilon'_{11}(T,\nu)$ of $Rb_{1-x}(NH_4)_xH_2PO_4$ with $x$=0.75 has a rapid drop at a certain temperature $T_g(\nu)$.

As has been shown in [61], $\varepsilon_{33}(T,\nu)$ in $K_{1-x}(NH_4)_xH_2PO_4$ at $x$=0.8 and 0.9 is qualitatively similar to $\varepsilon_{11}(T,\nu)$, but twice smaller. This is the only experimental measurement of $\varepsilon_{33}(T,\nu)$ in the antiferroelectric phase composition region, except for the case $x$=1.

In the antiferroelectric part of the phase diagram, the coexistence of deuteron glass and antiferroelectric phases in $Rb_{1-x}(ND_4)_xD_2AsO_4$ at ($x$=0.39, 0.55, 0.69) was revealed [62] using the measured temperature and frequency dependences of $\varepsilon_{11}(T,\nu)$. This coexistence is indicated by a weak frequency dispersion of the temperature dependence of permittivity at $T \leq 100K$ (it is by two orders of magnitude smaller that in the region with the deuteron glass phase only at $x$=0.28).

In [63] by the example of the $Rb_{1-x}(NH_4)_xH_2AsO_4$ system a possibility of phase coexistence (of PE - dynamically disordered paraelectric phase, PG- structurally disordered proton glass state, FE - ferroelectric, and AFE - antiferroelectric phases) in this type of compounds is explored. Experimental evidence for this coexistence at different $x$ is presented.

The temperature dependence of specific heat in the antiferroelectric phase composition region, as shown in [48] for $Rb_{1-x}(NH_4)_xH_2PO_4$ at $x$=0.79 and 0.89, has two peaks: at $T_N$ and a much lower one at a few degrees below $T_N$. The second peak remains unexplained. Considering



the facts that i) the obtained results were not explained by their authors, and that ii) a too high peak of the specific heat for these values of $x$ was obtained, we can assume that these data are possibly unreliable.

Unfortunately, for all compositions and for both dielectric permittivities the experimental data obtained in different papers are in a poor agreement. Let us consider here examples of such discrepancies. It should be noted that $\varepsilon_{11}(T,\nu)$ and $\varepsilon_{33}(T,\nu)$ were measured at different frequencies. However, these frequencies are low enough, so the the dielectric permittivity hardly varies with frequency in this temperature range.

In $Rb_{1-x}(NH_4)_xH_2PO_4$ at $x = 0.25$ (ferroelectric phase), $T = 60K$ $\varepsilon'_{33}(T,\nu) \approx 340$ as measured in [2] at $\nu$=1 kHz and $\varepsilon'_{33}(T,\nu) \approx 250$ as measured in [3] at $\nu$=300 Hz. In [2] and [7] at $T = 60K$ and close compositions in the proton glass phase $x = 0.4$ and 0.4 and frequencies $\nu$=1 kHz and 12 kHz, respectively, it was obtained that $\varepsilon'_{33}(T,\nu) \approx 140$ and $\varepsilon'_{33}(T,\nu) \approx 65$, respectively, that is a nearly two-fold difference. The measured in [2](1 kHz) and [6](50 kHz) $\varepsilon'_{11}(T,\nu)$ for $x = 0.5$ is about 40% higher than measured in [3] (10 kHz); for $x = 0.7$ the measured in [2](1 kHz) $\varepsilon'_{11}(T,\nu)$ is about 30% larger than measured in [3] (10 kHz) and [4](70 kHz); whereas $\varepsilon'_{11}(T,\nu)$ at $x = 0.43$ [7](12 kHz) is about 80% smaller than found in [2](1 kHz) at a very close composition $x = 0.4$. In the system $Rb_{1-x}(ND_4)_xD_2PO_4$ with $x = 0.4$ (proton glass phase) $\varepsilon'_{11}(T,\nu)$ obtained in [7](12 kHz) is about twice smaller than in [14](116 Hz).

In $Rb_{1-x}(NH_4)_xH_2AsO_4$ $\varepsilon'_{11}(T,\nu)$ found in [18] (1 kHz) for $x = 0.4$ is about 20% smaller, whereas that found in [17](10 kHz) for $x = 0.44$ is about 10% smaller than measured in [15](30 kHz) for $x = 0.35$; in [17] $\varepsilon'_{11}(T,\nu)$ decreases with decreasing $x$. In $K_{1-x}(NH_4)_xH_2PO_4$ at $x = 0.39$ $\varepsilon'_{33}(T,\nu)$ measured in [21](20 Hz) is about twice larger than measured at $x = 0.32$ in [20] (0.1 Hz), even though $\varepsilon'_{33}(T,\nu)$ in [20] strongly increases with lowering $x$.

There are available lots of other experimental data, which disagree within 10%. Such discrepancies can be explained by errors in measurements of $\varepsilon_{11}(T,\nu)$ and $\varepsilon_{33}(T,\nu)$, as well as by an incorrect determination of $x$. For example, the concentration of ammonium $x$ in $K_{1-x}(NH_4)_xH_2PO_4$ depends non-linearly on its concentration in a solution during the sample growth [36].

The temperatures $T_g(x)$, corresponding to the maximum of $\varepsilon''_{11}(T,\nu)$ and to the rapid drop of $\varepsilon'_{11}(T,\nu)$, obtained in different experiments are also different. Thus, for $Rb_{0.5}(ND_4)_{0.5}D_2PO_4$ $T_g$=59K [12] at $\nu$=1 kHz and $T_g$=53K [9] at $\nu$=10kHz, and both in [12] and [9] $T_g(x)$ increases with frequency.

The data for the temperatures $T_c$ in the ferroelectric phase composition region are also contradictory. Thus, $T_c$ of $Rb_{1-x}(NH_4)_xH_2AsO_4$ determined from the maximum of $\varepsilon'_{33}(T,\nu)$ in [17] are about by 10 K larger than $T_c$ determined from the maximum of $\varepsilon'_{11}(T,\nu)$ in [16]. This means that the value of $x$ is either overestimated in [17] or underestimated in [16].

The experimental data for $\varepsilon'_{11}(T,\nu)$ in the antiferroelectric phase composition region are also in a poor agreement. The values of $\varepsilon'_{11}(T,\nu)$ for $Rb_{1-x}(NH_4)_xH_2PO_4$ at $x$=0.9 measured in [4] at cooling are by 20% larger than at heating and by about 10% larger than that obtained in [3]. The value of $\varepsilon'_{11}(T,\nu)$ measured in [61] for $K_{1-x}(NH_4)_xH_2PO_4$ at $x$=0.8 is almost three times smaller than that found in [19].

Unfortunately, the experimentalists who measured the components of the dielectric permittivity tensors did not comment on the discrepancies between their results and the previous measurements. We think that the major origin of these discrepancies is the difficulty of growing identical samples for a given $x$, because in these samples there are regions with different $x$. In spite of the quantitative differences, the qualitative behavior of the experimental curves of dielectric permittivities of the $Rb_{1-x}(NH_4)_xH_2PO_4$ type compounds is approximately the same. Therefore, very important are theoretical studies of these compounds.

### 1.2. Theoretical studies of the $Rb_{1-x}(NH_4)_xH_2PO_4$ compounds

From the point of view of a theoretical description, the $Rb_{1-x}(NH_4)_xH_2PO_4$ type compounds, which in a certain composition region can undergo a transition to the proton glass state, are quite similar to the magnetic compounds with a spin glass phase. Therefore, we can use the theoretical methods developed for the spin glass models. A detailed description of the proton glasses, however, is not possible within the spin glass models, since these models do not take into account the random electric fields and real crystal structure of proton glasses.

In [64,65] the Ising model in a transverse field with proton tunneling was explored. In [64] the interaction constants $J_{ij} = \pm J$ were taken to be different from zero only for the nearest neighbors. In [65], as in the Sherrington-Kirkpatrick model [66], $J_{ij}$ are long-range ones and fluctuate with the Gaussian distribution. Calculations performed therein in the mean field approximation have shown that in both cases tunneling lowers down the temperatures of the transitions between the paraelectric and glass phases $T_g$, as well as between the paraelectric and ferroelectric phase $T_c$ or antiferroelectric phase $T_N$.



In [46, 67, 68] the Ising model in a transverse field $\Omega_i$ also with a random internal longitudinal field $h_i$

$$H = -\frac{1}{2}\sum_{i,j} J_{ij} S_i^z S_j^z - \sum_i \Omega_i S_i^x - \sum_i (E + h_i)\, S_i^z, \qquad (1.1)$$

was explored, where $E$ is a uniform external field. Gaussian distributions are used for the random infinite range interactions with ($\left\langle J_{ij}^2 \right\rangle_c = x(1-x)\cdot const(i-j)$) and random deformational field $h_i$ ($\langle h_i \rangle = 0, \left\langle h_i^2 \right\rangle \sim x(1-x)$). In [67] within the replica symmetric approach a system of equations for unknown $p, q, r$

$$p = \langle S_\alpha^z \rangle_n ;\ q = \left\langle S_\alpha^z S_\beta^z \right\rangle_n ;\ r = \left\langle \left(S_\alpha^z\right)^2 \right\rangle_n \underset{\Omega\to 0}{\longrightarrow} 1;\ n \to 0,$$

(where $\alpha$, $\beta$ are the replica numbers), as well as as expressions for the free energy, susceptibility $\chi$, instability line of the replica symmetric solution (Almeida-Thouless line) are obtained and explored. It is shown that the temperature of the transition to the glass phase $T_g$ exists only at $\left\langle h_i^2 \right\rangle_c = 0$ and corresponds to the peak on the temperature curve of $\chi(T)$. The random internal field ($\left\langle h_i^2 \right\rangle_c \neq 0$) leads to existence of the proton glass state at any temperature above $T_g$ ($q_{EA} > 0$, $q_{EA} \underset{T\to\infty}{\longrightarrow} 0$) and smoothes the peak in the temperature curve of $\chi(T)$. The distribution function of the local fields $P(h) = \langle \delta(h - h_i - \sum_j J_{ij} S_j) \rangle$ was calculated at $\Omega_i = 0$. Its shape at high temperatures is close to the Gaussian one, whereas at lowering temperature or increasing $\left\langle h_i^2 \right\rangle_c$ it transforms into a two-peak curve with a minimum at $h = 0$. Such a shape of $P(h)$ qualitatively agrees with the experimentally observed shape of EPR [24] and NMR [69] spectral lines. The temperature dependence of $q_{EA}$ calculated within the model [67] well agrees with the second moment of the distribution function of the EPR [24] and NMR [39,69] spectral lines. In [25,70] for the model with Hamiltonian (1.1) at $\Omega_i = 0$, using the Glauber equation, a shape of the EPR line was calculated (a single-peak one at high temperatures and a two-peak one at low temperatures) that agrees well with the experiment in a wide temperature range ($T = [10K, 150K]$). For this model, as shown in [46], $q_{EA} \to 1$ at $\Omega_i = 0$, $T \to 0$. In presence of tunneling ($\Omega_i \neq 0$) $q_{EA} < 1$ at all temperatures, which means an incomplete freezing.

In [68] the order parameter $m$ and the parameter $q_{EA}$ for the model with Hamiltonian (1.1) are calculated by the replica method, and the phase diagrams at different values of the transverse field and of the random field dispersion are constructed. Since in presence of random

fields $q_{EA} > 0$ at all $T$, the temperature of the transition to the glass phase $T_g(x)$ here is introduced as a temperature below which the replica-symmetry solution is instable, that is, the replica symmetry is broken, and the system is in non-ergodic state. It is established that the random fields decrease the temperatures $T_g$, $T_c$, and $T_N$ and widen the glass phase region. It has been shown that between the glass and ferroelectric phases there exists a region where $m \neq 0$, and the replica symmetric solution is unstable; this region is called the region of coexistence of glass and ferroelectric phases.

If in (1.1) the distribution function of the fields $h_i$ consists of two Gaussians, then a critical point appears on the phase boundary between the ferroelectric and paraelectric phases, whereas the transition between the ferroelectric and paraelectric phases becomes the first order one [71].

In [72] a dynamic generalization of the static approach of [67] has been presented. The $Rb_{1-x}(ND_4)_xD_2PO_4$, $Rb_{1-x}(ND_4)_xD_2AsO_4$ compounds described by the Hamiltonian

$$H = -\frac{1}{2}\sum_{i,j} J_{ij} S_i^z S_j^z - \sum_i \left(E + h_i\right) S_i^z - g\sum_{i,k}\left(b_k + b_{-k}^{+}\right) S_i^x, \qquad (1.2)$$

$$\langle J_{ij}\rangle \Big/ \sqrt{N} = J_0 = (1-2x)J;\ \left\langle J_{ij}^2\right\rangle_c \Big/ N = \Delta = 4x\cdot(1-x)J^2;\ \left\langle h_i^2\right\rangle_c = \Delta_h.$$

are considered. Here an interaction of the pseudospins with the phonon thermostat is introduced into the Ising model Hamiltonian. This leads to the Debye-type relaxation [72]

$$\varepsilon(\omega) = 1 + \frac{\beta}{4\pi}\frac{1 - \left\langle th^2\left(\beta h(\xi)\right)\right\rangle_\xi}{1 + i\tau\omega};\ h(\xi) = \xi\Delta\Big/2J^2\sqrt{q + 4\Delta_h\Big/J^2} + J_0 p,$$

where polarization and the Edwards-Anderson parameter $p, q$ obey the following system of equations

$$p = \int_{-\infty}^{\infty}\frac{d\xi}{\sqrt{2\pi}}\exp\left(-\frac{\xi^2}{2}\right) th\left[\beta h(\xi)\right];\ q = \int_{-\infty}^{\infty}\frac{d\xi}{\sqrt{2\pi}}\exp\left(-\frac{\xi^2}{2}\right) th^2\left[\beta h(\xi)\right].$$

For the relaxation time a phenomenological Arrhenius-like expression is assumed

$$\tau^{-1} \approx \int_{-\infty}^{\infty} dt\left[\langle b(t)b(0)\rangle + \langle b(0)b(t)\rangle\right] \sim \tau_0^{-1}\cdot e^{-E/T};\ E \approx 100K.$$



A quantitative comparison of the obtained results with experiment was performed for the temperature behavior of the $\varepsilon''(\nu)$ peak only. It yielded

$$\varepsilon''_{teor}(\omega_p) = 0.027T - 0.10;$$

$$\varepsilon''_{\exp}(\omega_p) = 0.04T - 0.57\,(Rb_{0.7}(ND_4)_{0.3}D_2AsO);$$

$$\varepsilon''_{\exp}(\omega_p) = 0.11T - 3.411\,(Rb_{0.6}(ND_4)_{0.4}D_2PO_4).$$

It is claimed that the proposed simple approach can be useful for description of dielectric properties of deuteron glasses. However, the based on this model relaxation theory of deuterated mixtures [72] does not yield a correct frequency dependence of the dielectric permittivity.

The drawback of the described above calculations based on the Ising model with transverse field and random longitudinal field is that they do not take into account the real structure of the $Rb_{1-x}(NH_4)_xH_2PO_4$ type compounds. Also, the considered there interactions are long-range ones (of the Sherrington-Kirkpatrick type), whereas in the real systems the major role is played by the nearest neighbors interactions.

The first theory of the $Rb_{1-x}(NH_4)_xH_2PO_4$ mixtures that takes into account its real structure has been proposed in [73]. A pseudospin Hamiltonian was used to describe the energy levels of protons near the $PO_4$ groups; the critical lines $T_c(x), T_N(x)$ (an expansion over the order parameter $1/N\sum\limits_{i=1}^{N}\langle S_i\rangle$) and $T_g(x)$ (an expansion over $1/N\sum\limits_{i=1}^{N}\left(\langle S_i\rangle\right)^2$) were found in the cluster approach. A qualitative description of the experimentally observed phase diagram was obtained.

Later the cluster approach was used in [74, 75]. Thus, in [74] for description of the $Rb_{1-x}(NH_4)_xH_2PO_4$ a pseudospin model was proposed that takes into account the configurational energy of the cluster of hydrogen bonds near a $PO_4$ group and a long-range interaction $W$

$$H_{cl} = \frac{V}{4}\left(S_1S_2 + S_2S_3 + S_3S_4 + S_4S_1\right) + \frac{U}{4}\left(S_1S_3 + S_2S_4\right) - \\ - \sum_{i=1}^{4}\left(\varphi_{cl,i} + W\langle S_i\rangle\right) S_i.$$

Here $\varphi_{cl,i}$ are the cluster fields that take into account the interactions of $i$-th hydrogen bond with protons of the neighboring tetrahedra and are determined from the condition of the extremum of the free energy for the mixture of different phases. The Hamiltonian parameters $U$, $V$ are

related to the two lowest levels of the hydrogen cluster in $RDP(\varepsilon_0', \varepsilon_1')$ and $ADP$ $(\varepsilon_0, \varepsilon_1)$ as

$$U = \varepsilon_1'/2, V = \frac{1}{4}\left(\varepsilon_0' + 2\varepsilon_1'\right);\ U = \frac{1}{2}\left(\varepsilon_0 + \varepsilon_1\right)_1, V = \frac{1}{4}\left(\varepsilon_0 + 2\varepsilon_1\right).$$

The free energy is presented as a sum of the energies of three phases

$$F = p_+ F(\varepsilon_0 < 0, W = 0) + p_0 F(\varepsilon_0 = 0, W = 0) + p_- F(\varepsilon_0 > 0, W \neq 0)$$

with the probabilities $p_+$ for the ferroelectric phase, $p_-$ for the antiferroelectric phase, and $p_0$ for the neutral phase.

It is believed that the state of each tetrahedron is formed by the six ionic positions ($Rb$ or $NH_4$). Two of these six positions are the closest; therefore, the ferroelectric (antiferroelectric) state of the tetrahedron is formed if they are occupied with $Rb$ ($NH_4$). In other situations a neutral state is formed. From the analysis of the free energy expansion over the parameters $\langle S_1\rangle + \langle S_3\rangle$; $\langle S_1\rangle - \langle S_3\rangle$ the regions of ferroelectric ($0 < x < 0.2$ at $T = 0$) and antiferroelectric ($0.75 < x < 1$ at $T = 0$) phases on the phase diagram are found that are close to experimental.

This model was used to describe the diagram of the state in the proton glass region ($0.2 < x < 0.75$ at $T = 0$) in [75]. Here the replica symmetric approximation was used in averaging the system free energy with a parameter, being an analog of the Edwards-Anderson parameter $q = \langle S_{f\alpha} S_{f\beta}\rangle$ ($\alpha, \beta$ are the replica numbers). Analytical expressions for the partition function $L(n, q)$ and temperature of the glass transition $T_g(n)$ (when $q = 0$) are found for the number of replicas n=2, 3, 4. For $T_g(n)$ an expression is found for an arbitrary $n$. From here an expression $T_g$ was obtained

$$\left(\frac{kT_g}{\langle h^2\rangle}\right)^2 = \frac{1}{8}\frac{1 + 2\exp(-2\langle\varepsilon(x)\rangle/kT_g)}{\left(1 + 2\exp(-\langle\varepsilon(x)\rangle/kT_g)\right)^2};\ T_g = \lim_{n\to 0} T_g(n).$$

Hence, no consistent approach to description of all states of these compounds has been presented in [74, 75].

An original approach to description of thermodynamical properties of proton glasses has been proposed in [76–78]. The model Hamiltonian contains terms responsible for the ferroelectric ordering along the $Z$ axis ($S^z$-components of the classical spin) and for the antiferroelectric ordering ($S^x$-components). Restricting consideration by the quadratic in the Hamiltonian terms at averaging the system free energy over the concentrations by the replica method, in the replica symmetric approximation, a system of equations for the parameters of the ferroelectric $p$ and antiferroelectric $\xi$ ordering, as well as parameters of the short-range ordering $g_z$, $g_x$ (correlation between the nearest dipole moments)

$$p = \langle\langle S_{i1}^z\rangle\rangle_c = \langle\langle S_{i2}^z\rangle\rangle_c, \xi = \langle\langle S_{i1}^x\rangle\rangle_c = -\langle\langle S_{i2}^x\rangle\rangle_c;$$
$$g_z = \langle\langle S_{i1}^z S_{i2}^z\rangle\rangle_c, g_x = \langle\langle S_{i1}^x S_{i2}^x\rangle\rangle_c,$$

was obtained. Here 1, 2 are the sublattices of the site $i$; $\langle\ldots\rangle_c$ means configurational averaging.



The constructed phase diagram for $Rb_n(NH_4)_{1-n}H_2AsO_4$ qualitatively agrees with experiment. At high temperatures ($T \geq 210K$) $p = 0$, $\xi = 0$, whereas for $g_{z,1}$, $g_{x,1}$ there exist single solutions that correspond to the paraelectric region. The proton glass region is associated with appearance of additional solutions for $g_z$, $g_x$ at $p = 0$, $\xi = 0$ (at low temperatures the maximal number of solutions is equal to 5). Fluctuations of the dipole moments are described by the averages of the dipole moments of the nearest spins $g_z$, $g_x$. The self-correlations of the dipole moments of the $\langle\langle S_{i1}^z S_{i1}^z\rangle\rangle_c$ type, measured in EPR or NMR experiments as the Edwards-Anderson parameter, are not taken into account in this approach. We think that such correlations are more important than the correlations between the neighboring tetrahedra. Fluctuations of the deformational internal field, that can be estimated from the temperature dependence of the Edwards-Anderson parameter, are not taken into account in this approach either.

Hence, a theoretical description of thermodynamic and dielectric properties of hydrogen bonded compounds of the $Rb_{1-x}(NH_4)_xH_2PO_4$ type which can undergo a transition into the proton glass state, that would take into account the structural peculiarities and different types of interactions, is still a complicated and unsolved problem of the statistical physics. Particularly it concerns a microscopic description of the dynamical properties of these mixtures. The temperature curves of the real and imaginary parts of the longitudinal and transverse dielectric permittivities at different frequencies have to be described. Particularly interesting is to explore the low-temperature curves of the imaginary parts of the dielectric permittivity at low frequencies.

In [79–82] a theory of static characteristics of model proton glasses with an arbitrary range of competing interactions has been proposed. In [83–88] a cluster theory of the thermodynamick and dynamic characteristics of the $Rb_{1-x}(NH_4)_xH_2PO_4$ type system has been proposed. It has been shown that at the proper choice of the model parameters this theory yields a satisfactory quantitative description of experimental data for these systems. Inconsistency of different experimental data was also revealed.

In the paraelectric phase the ferroelectric compounds of the $MD_2XO_4$ type (M = K, Rb, $ND_4$; X = P, As) crystallize in the $\bar{4}\cdot m$ class of tetragonal syngony (the space group $I\bar{4}2d$ with non-centrosymmetric point group $D_{2d}$). These crystals are piezoelectric in both phases (paraelectric and ferroelectric or paraelectric and antiferroelectric), which essentially affects the behavior of their physical characteristics.

Description of the dielectric properties of the $MD_2XO_4$ type ferroelectrics within the framework of the conventional proton ordering model (see [89–95]) was restricted to the static limit and to the high-frequency relaxation. The Attempts to explore the piezoelectric resonance phenomenon within a model that does not take into account the piezoelectric coupling are pointless. The conventional proton ordering model does not distinguish free and clamped crystals and is not able to reproduce the effect of crystal clamping by high-frequency electric field. This leads to an incorrect description of the temperature behavior of the calculated polarization relaxation time and dynamic dielectric permittivitiy of the $MD_2XO_4$ type ferroelectrics in the phase transition region.

Application of electric fields and shear stresses of certain symmetries allows one to explore the role of the piezoelectric coupling in the phase transition, as well as their influence on the physical characteristics of these crystals.

Studies of the influence of the piezoelectric coupling on the physical characteristics of the $KH_2PO_4$ type ferrroelectric has been started in [96], where the Slater theory [97] has been modified by taking into account the splitting of the lowest ferroelectric level of the proton system caused by the strain $\varepsilon_6$. More extensive results for the deformed ferroelectrics of the $KH_2PO_4$ type were obtained in [98–107] . In [98, 99] a consistent microscopic formulation of the way with the strains of the different symmetries should be included into the proton ordering model has been made. In [98,99] the model of a deformed $KD_2PO_4$ type crystals was used for description of the effects of a symmetrized stress $\sigma_1 - \sigma_2$. That model took into account a splitting of the lateral configurations level. Later [100–103] all possible splittings of the proton configuration levels by the strains $\varepsilon_6$ were taken into account. In [100] the phase transition in a deformed $K(H_{0,12}D_{0,88})_2PO_4$ crystal has been explored for the first time. The thermodynamic, longitudinal dielectric, piezoelectric, and elastic characteristics of the crystal were calculated; their dependence on the stress $\sigma_6$ was studied. A thorough investigation of the thermodynamic and longitudinal dielectric, piezoelectric, and elastic characteristocs of the $K(H_{1-x}D_x)_2PO_4$ ferroelectrics was performed in [101]. The thermodynamic and longitudinal physical characteristcs of



$KH_2PO_4$ ferroelectrics with taking into account tunneling were studied in [102, 103]. A good quantitative description of the available experimental data for $KH_2PO_4$ type ferroelectrics and $NH_4H_2PO_4$ type antiferroelectrics in the paraelectric phase was obtained. In [105–107] the influence of the longitudinal electric field on the physical characteristics of $K(H_{0,12}D_{0,88})_2PO_4$ and $KH_2PO_4$ was studied; a satisfactory quantitative description of available experimental was obtained.

The mechanism of spontaneous strain $\varepsilon_6$ in the $KH_2PO_4$ type ferroelectrics and the influence of proton coupling with acoustic lattice vibrations on this strain were explored in [108].

In [104] a generalization of the proton ordering model for the $KH_2PO_4$ type ferroelectrics was proposed, in order to explore the piezoelectric, dielectric, and elastic characteristics associated with the strains $\varepsilon_4$ and $\varepsilon_5$. The expressions for the transverse physical characteristics of these crystals in the paraelectric phase have been obtained and explored within the four-particle cluster approximation. By the proper choice of the model parameters, a good agreement between the theory and experiment for $KH_2PO_4$ and $NH_4H_2PO_4$. A thorough investigation of transverse and longitudinal characteristics of the $NH_4H_2PO_4$ and $ND_4D_2PO_4$ antiferroelectric has been performed in [109].

In [100–104, 109] the dynamic properties of the $KH_2PO_4$ type ferroelectrics have not been explored. Such studie, however, are very important. Due to the established in [110–112] effect of tunneling suppression in the $KH_2PO_4$ type ferroelectics and principal difficulties, arising in calculations of the dynamic characteristics of these crystals when tunneling is taken into account, this problem should be solved with neglecting tunneling. The relaxation phenomena in the $KH_2PO_4$ type ferroelectrics and $NH_4H_2PO_4$ type antiferroelectrics were explored within the modified proton ordering model in [113,114] and $NH_4H_2PO_4$, respectively. The ultrasound velocity and attenuation were calculated. The experimentally observed phenomena of crystal clamping by the high-frequency electric field, piezoelectric resonance, and microwave dispersion were described explicitly.

In [21] a possibility of piezoelectric coupling in the $Rb_{1-x}(NH_4)_xH_2PO_4$ type systems was suggested. Unfortunately, this coupling was neglected in [83–88].

In the present paper we shall consider in detail the obtained in [83–88] results for the thermodynamic and dynamic characteristics of the $Rb_{1-x}(NH_4)_xH_2PO_4$ systems; we shall also discuss the discrepancies between the obtained therein theoretical results and the corresponding exprimental data. We shall also present a review of the results obtained

within the modified proton ordering model for the associated with the strains $\varepsilon_6$ and $\varepsilon_4$ longitudinal and transverse static dielectric, piezoelectric, elastic, and dynamic characeristics of the $M(H_{1-x}D_x)_2XO_4$ crystals in the paraelectric and ferroelectric phases.

Bearing in mind [21], we shall discuss in this paper a possible role of piezoelectric coupling in disordered compounds of the $Rb_{1-x}(NH_4)_xH_2PO_4$ type as well as ways of its experimental confirmation.

## 2. Thermodynamic properties of the $Rb_{1-x}$ $(NH_4)_x$ $H_2PO_4$ type compounds

It is well known, that for description of thermodynamic characteristics and dielectric properties (in a certain frequency range) of these crystals within the pseudospin-phonon model, the ionic variables can be excluded in the static approximation ( [95, 116]). The system description is then performed within the framework of a pseudospin model with renormalized moments of hydrogen bonds $\vec{d}_{f,\alpha}$ ($\alpha = +$ for $RDP$, $\alpha = -$ for $ADP$)

$$\vec{d}_{1\alpha}=(d^x_\alpha,0,d^z_\alpha),\ \vec{d}_{3\alpha}=(-d^x_\alpha,0,d^z_\alpha),\ \vec{d}_{2\alpha}=(0,-d^y_\alpha,d^z_\alpha),\ \vec{d}_{4\alpha}=(0,d^y_\alpha,d^z_\alpha);$$
$$\vec{P}^{A(B)}_\alpha=\sum_{f\in A(B)}\vec{d}_{f,\alpha}\eta^{A(B)}_{f,\alpha};\ \ \eta^{A(B)}_{f,\alpha}=\langle S_{f,\alpha}\rangle^{A(B)}. \tag{2.1}$$

Here we introduced an effective dipole moment of a tetrahedron $\vec{P}_\alpha$; $\langle....\rangle$ is the conventional Gibbs' thermodynamic average; summation $f = A(B)$ is carried out over the bonds, on which the protons order close to the given tetrahedron $A(B)$. For $RDP$ the tetrahedron polarization can have two opposite values along the $c$ axis, when two protons are ordered close to the upper edge of the tetrahedron ($\eta_f = \eta$) and close to the lower one ($\eta_f = -\eta$)

$$\eta_f=\eta\Rightarrow\vec{P}^{A(B)}_+=(0,0,2d^z_+\eta);\ \ \eta_f=-\eta\Rightarrow\vec{P}^{A(B)}_+=(0,0,-2d^z_+\eta). \tag{2.2}$$

For $ADP - NH_4H_2PO_4$ the primitive cell is twice as large as for $RDP$, and in addition to "$A$", "$B$" tetrahedra it contains "$A'$", "$B'$" tetrahedra. Since their polarizations are opposite to those of "$A$", "$B$", the total cell polarization is zero:

$$-\eta^A_{1,-}=-\eta^A_{2,-}=\eta^A_{3,-}=\eta^A_{4,-}=\eta;\ \ \vec{P}^A_-=-\vec{P}^{A'}_-=(-d^x_-\eta;+d^y_-\eta;0)$$
$$-\eta^B_{1,-}=\eta^B_{2,-}=\eta^B_{3,-}=-\eta^B_{4,-}=\eta;\ \ \vec{P}^B_-=-\vec{P}^{B'}_-=(-d^x_-\eta,-d^y_-\eta,0). \tag{2.3}$$



For an $ADP - NH_4H_2PO_4$ crystal the change of sign of $\eta^{A(B)}_{f,-}$ at transition to the "$A'$", "$B'$" tetrahedra can be taken into account as (here $\vec{n}$ the $RDP$ primitive cell vector; $\vec{k}^z_*$ is the vector at the Brillouin zone boundary directed along $Z$)

$$\eta^{A(B)}_{nf,-}=e^{i\vec{n}\vec{k}^z_*}\cdot\eta^{A(B)}_{f,-}. \tag{2.4}$$

Hence, in the cases of both $ADP$ and $RDP$ we use a primitive cell with "$A$" and "$B$" tetrahedra.

Hamiltonian of a mixed $Rb_{1-x}(NH_4)_xH_2PO_4$ system can be written as

$$H(\{h\})=-\sum_{n,f}\left(\langle\vec{d}_{nf}\rangle_c\cdot\left[\vec{E}+\vec{G}_n\right]\right)S_{nf}+\sum_n\left[H_A(n)+H_B(n)\right]-$$
$$-\frac{1}{2}\sum_{n,f}\sum_{n',f'}J_{nf,n'f'}S_{nf}S_{n'f'}; \tag{2.5}$$
$$H_A(n)=\frac{V_n}{4}\left(S_{n1}S_{n2}+S_{n2}S_{n3}+S_{n3}S_{n4}+S_{n4}S_{n1}\right)+$$
$$+\frac{U_n}{4}\left(S_{n1}S_{n3}+S_{n2}S_{n4}\right)+\frac{\Phi_n}{16}S_{n1}S_{n2}S_{n3}S_{n4}.$$

Here $S_{nf} = \pm1$ are spin operators describing position of a proton on the $f = 1, 2, 3, 4$ hydrogen bond in the $\vec{n}$ cell at the $R$ tetrahedron; $\vec{E}$ is an external uniform electric field; $\vec{G}_n$ is an internal random deformational field; $J_{nf,n'f'}$ is the long-range interaction between protons; $H_A(n), H_B(n)$ are the configurational energies of the "$A$", "$B$" tetrahedra. In this work we take into account two configurational states of a tetrahedron ($\alpha = +, -$):

$$V_\alpha=-\frac{1}{8}w_{1\alpha},\ U_\alpha=\frac{1}{8}\left(w_{1\alpha}-2\varepsilon_\alpha\right),\ \Phi_\alpha=\frac{1}{8}\left(w_{1\alpha}+2\varepsilon_\alpha-4w_\alpha\right),\ \alpha=+,-. \tag{2.6}$$

In the state $+$, the energy states of a tetrahedron are analogous to those in a pure $RDP$ crystal with the ground state level $\varepsilon_{s+}$

$$\varepsilon_+=\varepsilon_{a+}-\varepsilon_{s+},\ \ w_+=\varepsilon_{1+}-\varepsilon_{s+},\ \ w_{1+}=\varepsilon_{o+}-\varepsilon_{s+}. \tag{2.7}$$

In the state $-$ ($ADP$) we use the same relations for $V_\alpha$, $U_\alpha$, $\Phi_\alpha$ but with different values of $\varepsilon_\alpha$, $w_\alpha$, $w_{1\alpha}$.

In the case of a mixed $Rb_{1-x}(NH_4)_xH_2PO_4$ crystal, ionic positions are occupied by $Rb$ with the probability $c_+ = 1-x$ and by $NH_4$ with the probability $c_- = x$. Hence the distribution function of a strongly random

energy parameter $\varepsilon_\alpha$ (and similarly for $w_\alpha, w_{1\alpha}$) can be qualitatively written as

$$p(\sigma) = (1-x)\delta(\sigma-\varepsilon_+)+x\delta(\sigma-\varepsilon_-) = c_+\delta(\sigma-\varepsilon_+)+c_-\delta(\sigma-\varepsilon_-). \quad (2.8)$$

A state of the dipole moment on the bond $\vec{d}_{f,\alpha\alpha_f}$ is determined by the states $\alpha, \alpha_f$ of two tetrahedra connected by this bond. In the mean field approximation over the bonds, the averaged over configurations moment of a tetrahedron $\left\langle \vec{P}^B \right\rangle_c$ reads

$$\left\langle \vec{P} \right\rangle_c \approx \sum_{f=1}^{4} \left\langle \vec{d}_f \right\rangle_c \bar{\eta}_f, \ \left\langle \vec{d}_f \right\rangle_c = \sum_\alpha \sum_\beta c_\alpha c_\beta \vec{d}_{f,\alpha\beta}, \ \bar{\eta}_f = \langle\langle S_f \rangle\rangle_c . \quad (2.9)$$

In the present work we consider only two realizations of the sets of averaged over configurations values of $\bar{\eta}_f = \bar{\eta}$; $-\bar{\eta}^B_{1,-} = \bar{\eta}^B_{2,-} = \bar{\eta}^B_{3,-} = -\bar{\eta}^B_{4,-} = \bar{\eta}$, which correspond to ferroelectric and antiferroelectric ordering. This permits us to use the primitive cell of $RDP$ with 2 tetrahedra and 4 hydrogen bonds. The mean free energy per primitive cell $\langle \mathbf{F} \rangle$ can then be written as

$$-\beta \langle \mathbf{F} \rangle = -\sum_{f=1,\in A}^{4} \left\langle F_f^{(0)} \right\rangle_c + \left\langle F_A^{[0]} \right\rangle_c + \left\langle F_B^{[0]} \right\rangle_c - \quad (2.10)$$

$$-\beta \sum_{f=1,\in A}^{4} \bar{\varphi}_{L,f} \left\langle F_f^{(1)} \right\rangle_c + \frac{\beta}{2} \sum_{f,f'=1,\in A}^{4} \left\langle J_{f,f'}(\vec{k}_*) \right\rangle_c \left\langle F_f^{(1)} \right\rangle_c \left\langle F_{f'}^{(1)} \right\rangle_c ,$$

where $\vec{k}_* = \vec{0}_*$ for ferroelectric ordering $\left\langle F_f^{(1)} \right\rangle_c = \left\langle F^{(1)} \right\rangle_c$, $\vec{k}_* = \vec{k}^z_*$ for antiferroelectric ordering $-\left\langle F_1^{(1)} \right\rangle_c = \left\langle F_2^{(1)} \right\rangle_c = \left\langle F_3^{(1)} \right\rangle_c = -\left\langle F_4^{(1)} \right\rangle_c = \left\langle F^{(1)} \right\rangle_c$. We use the following notations for averages over different random fields of the single-particle $F_f^{(0)}$ and cluster $F_{1234}^{[0000]}$ generating functions

$$\left\langle F_f^{(0)} \right\rangle_c = \left\langle F^{(0)}(\zeta_f) \right\rangle_c = \left\langle F^{(0)} \left(\kappa_f + \sigma + g_x + g_y + g_z\right) \right\rangle_{\sigma,\vec{g}} =$$
$$= \int ... \int d\sigma R\left(\sigma, 2q\right) \rho_t(g_x)\rho_t(g_y)\rho_z(g_z) dg_x dg_y dg_z F^{(0)}(\kappa_f+\sigma+g_x+g_y+g_z), \quad (2.11)$$

$$\left\langle F_A^{[0]} \right\rangle_c = \left\langle F_{1234}^{[0000]} \right\rangle_c = \left\langle F^{[0000]}(\xi_1|\xi_2|\xi_3|\xi_4||R) \right\rangle_c =$$



$$= \int ... \int \prod_{f=1}^{4} d\sigma_f R\left(\sigma_f, q\right) \rho(g_x)\rho(g_y)\rho(g_z) dg_x dg_y dg_z \times$$
$$\times \left\langle F^{[0000]}\left(\kappa_{cl,1} + \sigma_1 + g_1 | ... | \kappa_{cl,4} + \sigma_4 + g_4 || R\right) \right\rangle_{\{\sigma\},\vec{g},R} . \quad (2.12)$$

Here we introduce notations for the average values of cluster $\bar{\varphi}_f$ and long-range $\bar{\varphi}_{L,f}$ fields, and

$$\kappa_f = h_f + \bar{\varphi}_{L,f} + 2\bar{\varphi}_f; \ \kappa_{cl,f} = h_f + \bar{\varphi}_{L,f} + \bar{\varphi}_f; \ h_f = \left( \left\langle \vec{d}_f \right\rangle_c \cdot \vec{E} \right),$$
$$g_1 = g_z - g_x, \ \ g_2 = g_z + g_y, \ \ g_3 = g_z + g_x, \ \ g_4 = g_z - g_y. \quad (2.13)$$

Averaging is performed over random cluster fields with dispersion $q$ and over random deformational fields with dispersion $\langle G^2 \rangle_c$ for tranverse and longitudinal field components

$$R\left(\sigma, q\right) = \frac{e^{-\frac{1}{2}\frac{\sigma^2}{q}}}{\sqrt{2\pi q}}, \ \ \rho\left(\sigma\right) = \frac{e^{-\frac{1}{2}\frac{\sigma^2}{\langle G^2 \rangle_c}}}{\sqrt{2\pi \langle G^2 \rangle_c}}, \ \ \langle G^2 \rangle_c = 4x(1-x)Q_G. \quad (2.14)$$

The expressions for the single-particle function $F_f^{(0)}$ and its derivatives $F_f^{(n)}$ are as follows

$$F_f^{(0)} = \ln\left[2\,\mathrm{ch}\left(\beta\zeta_f\right)\right], \ F_f^{(n)} = \partial^n / \partial(\beta\zeta_f)^n F_f^{(0)}, \ F_f^{(1)} = \mathrm{th}\left(\beta\zeta_f\right), \quad (2.15)$$
$$F_f^{(2)} = 1 - \left(F_f^{(1)}\right)^2, \ F_f^{(3)} = -2F_f^{(1)}F_f^{(2)}, \ F_f^{(4)} = -2F_f^{(2)}\left[1 - 3\left(F_f^{(1)}\right)^2\right].$$

The cluster function $F_{1234}^{[0000]}$ and its derivatives $F_{1234}^{[n_1n_2n_3n_4]}$ read

$$F^{[0000]}(\xi_1|\xi_2|\xi_3|\xi_4||R) = \ln\left[0.5 \cdot L(\xi_1,\xi_2,\xi_3,\xi_4||R_\alpha)\right];$$
$$F_{1234}^{[n_1n_2n_3n_4]} = \frac{\partial^{n_1}}{\partial(\beta\xi_1)^{n_1}} \cdots \frac{\partial^{n_4}}{\partial(\beta\xi_1)^{n_4}} F_{1234}^{[0000]}$$
$$F_{11}^{[1,1]} = F^{[2000]}(\xi_1|\xi_2|\xi_3|\xi_4||R) = 1 - M_1^{[1]}M_1^{[1]};$$
$$F_{12}^{[1,1]} = F^{[1100]}(\xi_1|\xi_2|\xi_3|\xi_4||R) = M_{12}^{[1,1]} - M_1^{[1]}M_2^{[1]};$$
$$F_{13}^{[1,1]} = F^{[1010]}(\xi_1|\xi_2|\xi_3|\xi_4||R) = M_{13}^{[1,1]} - M_1^{[1]}M_3^{[1]};$$
$$F_{14}^{[1,1]} = F^{[1001]}(\xi_1|\xi_2|\xi_3|\xi_4||R) = M_{14}^{[1,1]} - M_1^{[1]}M_4^{[1]};$$
$$F_{ff'}^{[21]} = -2F_f^{[1]}F_{ff'}^{[11]}; \ \ F_{ff'}^{[21]} = -2F_{ff'}^{[11]}F_{f'}^{[1]};$$

$$F^{[22]}_{ff'} = -2F^{[1,1]}_{ff'}\left[M^{[1,1]}_{ff'} - M^{[1]}_{f}M^{[1]}_{f'}\right];$$
$$M^{[1]}_{1} = L^{[1000]}_{1234}\Big/L^{[0000]}_{1234}, ...M^{[1]}_{4} = L^{[0001]}_{1234}\Big/L^{[0000]}_{1234};$$
$$M^{[1,1]}_{11} = L^{[2000]}_{1234}\Big/L^{[0000]}_{1234} \equiv 1,..., M^{[1,1]}_{14} = L^{[1001]}_{1234}\Big/L^{[0000]}_{1234}, \quad (2.16)$$

$$0.5L^{[0000]}_{1234} = 0.5L(\xi_1,\xi_2,\xi_3,\xi_4||R_\alpha) = 2a_\alpha ch(\beta\xi_1-\beta\xi_3)ch(\beta\xi_2-\beta\xi_4)+$$
$$+ch(\beta\xi_1+\beta\xi_2+\beta\xi_3+\beta\xi_4) + d_\alpha ch(\beta\xi_1-\beta\xi_2+\beta\xi_3-\beta\xi_4)+$$
$$+2b_\alpha\left[ch(\beta\xi_1+\beta\xi_3)ch(\beta\xi_2-\beta\xi_4)+ch(\beta\xi_1-\beta\xi_3)ch(\beta\xi_2+\beta\xi_4)\right], \quad (2.17)$$
$$a_\alpha = \exp(-\beta\varepsilon_\alpha), \quad b_\alpha = \exp(-\beta w_\alpha), \quad d_\alpha = \exp(-\beta w_{1\alpha}).$$

Here the partition function $0.5L\left(\{\xi\}\,||R_\alpha\right)$ is calculated with the cluster Hamiltonian

$$H_A(\{\xi\}\,;S_1,S_2,S_3,S_4||R) = H_A(\{0\}\,;S_1,S_2,S_3,S_4||R) - \sum_{f=1}^{4}\xi_f S_f$$
$$H_A(\{0\}\,;S_1,S_2,S_3,S_4||R) = \quad (2.18)$$
$$= \frac{V_\alpha}{4}\left(S_1S_2+S_2S_3+S_3S_4+S_4S_1\right)+\frac{U_\alpha}{4}\left(S_1S_3+S_2S_4\right)+\frac{\Phi_\alpha}{16}S_1S_2S_3S_4$$

We shall use the same model dependence of the average eigenvalues of the long-range interaction matrix as for the dipole moment of a hydrogen bond:

$$\left\langle \nu_\mu(\vec{k}_*)\right\rangle_c = \bar{\nu}_\mu(\vec{k}_*) = \sum_\alpha\sum_\beta c_\alpha c_\beta \nu_{\mu,\alpha\beta}(\vec{k}_*) \approx$$
$$\approx c_+^2\nu_{\mu,++}(\vec{k}_*) + c_-^2\nu_{\mu,--}(\vec{k}_*) + 2c_+c_-\nu_{\mu,00}(\vec{k}_*). \quad (2.19)$$

For these values of $\vec{k}_*$ the long-range interaction matrix $\bar{J}_{f,f'} = \left\langle J_{f,f'}\left(\vec{k}_*\right)\right\rangle_c$ and the unitary transformation matrix $\hat{U} = \{u_{\mu f}\}$ read

$$\hat{U} = \hat{U}^+ = \frac{1}{2}\begin{pmatrix} 1 & 1 & 1 & 1\\ 1 & 1 & -1 & -1\\ 1 & -1 & 1 & -1\\ 1 & -1 & -1 & 1\end{pmatrix}; \quad \langle J\rangle = \begin{pmatrix} \bar{J}_{11} & \bar{J}_{12} & \bar{J}_{13} & \bar{J}_{12}\\ \bar{J}_{12} & \bar{J}_{11} & \bar{J}_{12} & \bar{J}_{13}\\ \bar{J}_{13} & \bar{J}_{12} & \bar{J}_{11} & \bar{J}_{12}\\ \bar{J}_{12} & \bar{J}_{13} & \bar{J}_{12} & \bar{J}_{11}\end{pmatrix};$$
$$\hat{\bar{\nu}} = \hat{U}\hat{\bar{J}}\hat{U} = \begin{pmatrix} \bar{\nu}_1 & 0 & 0 & 0\\ 0 & \bar{\nu}_2 & 0 & 0\\ 0 & 0 & \bar{\nu}_3 & 0\\ 0 & 0 & 0 & \bar{\nu}_4\end{pmatrix}. \quad (2.20)$$



$$\bar{\nu}_1 = \bar{J}_{11}+2\bar{J}_{12}+\bar{J}_{13};\ \bar{\nu}_2 = \bar{\nu}_4 = \bar{J}_{11}-\bar{J}_{13};\ \bar{\nu}_3 = \bar{J}_{11}-2\bar{J}_{12}+\bar{J}_{13}. \quad (2.21)$$

From the condition of the free energy extremum we find and an expression for the average $\bar{\eta}_f = \langle\langle S_f\rangle\rangle_c$, reduced Edwards-Anderson parameter $Q_{EA,f}$, and an equation for unknown quantities $\bar{\varphi}_{L,f}, \bar{\varphi}_f, q_f$

$$\bar{\eta}_f = \left\langle F^{(1)}_f\right\rangle_c; \quad Q_{EA,f} = q_{EA,f} - \bar{\eta}_f^2; \quad q_{EA,f} = 1 - \left\langle F^{(2)}_f\right\rangle_c; \quad (2.22)$$
$$\left\langle F^{(1)}_f\right\rangle_c = \left\langle F^{[1000]}_f\right\rangle_c;\ \left\langle F^{(2)}_f\right\rangle_c = \left\langle F^{[2000]}_f\right\rangle_c;\ \bar{\varphi}_{L,f} = \sum_{f_1}^{4}\bar{J}_{ff_1}(\vec{k}_*)\bar{\eta}_{f_1}.$$

In absence of external field and for the ferroelectric ordering we obtain the following expressions for the free energy, for the average $\bar{\eta} = \bar{\eta}_f$, reduced Edwards-Anderson parameter $Q_{EA} = Q_{EA,f}$ and for equations for $\bar{\varphi}_L, \bar{\varphi}, q$

$$\bar{\eta} = \bar{\eta}_f; \quad \bar{\varphi} = \bar{\varphi}_f; \quad \bar{\varphi}_L = \bar{\varphi}_{L,f}; \quad q = q_f;$$
$$-\beta\left\langle \mathbf{F}_F\right\rangle_c = -4\left\langle F^{(0)}\right\rangle_c + 2\left\langle F_A\right\rangle_c - 4\beta\bar{\varphi}_L\left\langle F^{(1)}\right\rangle_c + 2\beta\bar{\nu}_1(\vec{0}_*)\left\langle F^{(1)}\right\rangle_c^2;$$
$$\bar{\eta} = \left\langle F^{(1)}\right\rangle_c; \quad Q_{EA} = q_{EA} - \bar{\eta}^2; \quad q_{EA,f} = 1 - \left\langle F^{(2)}\right\rangle_c;$$
$$\left\langle F^{(1)}\right\rangle_c = \left\langle F^{[1000]}\right\rangle_c; \quad \left\langle F^{(2)}\right\rangle_c = \left\langle F^{[2000]}\right\rangle_c; \quad \bar{\varphi}_L = \bar{\nu}_1(\vec{0}_*)\bar{\eta}. \quad (2.23)$$

In the case of an antiferroelectric ordering in absence of external field, the free energy, for the average $\bar{\eta} = -\bar{\eta}_1 = \bar{\eta}_2$, reduced Edwards-Anderson parameter $Q_{EA} = Q_{EA,f}$ and equations for $\bar{\varphi}_L, \bar{\varphi}, q$ read

$$\bar{\eta} = -\bar{\eta}_{1(4)} = \eta_{2(3)};\ \bar{\varphi} = -\bar{\varphi}_{1(4)} = \bar{\varphi}_{2(3)};\ \bar{\varphi}_L = -\bar{\varphi}_{L,1(4)} = \bar{\varphi}_{L,2(3)};\ q = q_f;$$
$$-\beta\left\langle \mathbf{F}_{AF}\right\rangle_c = -4\left\langle F^{(0)}\right\rangle_c + 2\left\langle F_A\right\rangle_c - 4\beta\bar{\varphi}_L\left\langle F^{(1)}\right\rangle_c + 2\beta\nu_2(\vec{k}^z_*)\left\langle F^{(1)}\right\rangle_c^2;$$
$$\bar{\eta} = \left\langle F^{(1)}\right\rangle_c = -\left\langle F^{(1)}_1\right\rangle_c; \quad Q_{EA} = q_{EA} - \bar{\eta}^2; \quad q_{EA,f} = 1 - \left\langle F^{(2)}\right\rangle_c;$$
$$\left\langle F^{(1)}\right\rangle_c = \left\langle F^{[0100]}\right\rangle_c; \quad \left\langle F^{(2)}\right\rangle_c = \left\langle F^{[0200]}\right\rangle_c; \quad \bar{\varphi}_L = \bar{\nu}_2(\vec{k}^z_*)\bar{\eta}. \quad (2.24)$$

As numerical calculations for the free energy show, the antiferroelectric state is realized in the region close to the $x = 1 - c \to 1$ limit; the ferroelectric state is realized in the region $1 - x = c \to 1$, and a proton glass state ($\bar{\varphi} = \bar{\varphi}_L = 0, q > 0$) takes place at intermediate compositions.

The static susceptibility of the system reads ($v_e$ is the cell volume)

$$\chi_{ab} = -\frac{1}{Tv_e}\sum_{f,f'}\langle d^a_f\rangle_c\langle d^b_{f'}\rangle_c\cdot\bar{\eta}'_{ff'} = -\frac{1}{Tv_e}\sum_\mu \tilde{d}^a_\mu\tilde{d}^b_\mu\cdot\tilde{\eta}'_\mu;$$

$$\bar{\eta}'_{ff'} = \frac{\partial \bar{\eta}_f}{\partial(\beta h_{f'})}; \quad \tilde{d}^a_\mu = \sum_f u_{\mu f} \langle d^a_f \rangle_c; \quad \tilde{\eta}'_\mu = \sum_{f,f'} u_{\mu f} u_{\mu f'} \bar{\eta}'_{ff'} \quad (2.25)$$

Here we used the fact that after the unitary transformation with $\hat{U}$, the matrix of $\tilde{\eta}'_{\mu\mu'} = \delta_{\mu\mu'}\tilde{\eta}'_\mu$ correlators is diagonal for ferroelectric and antiferroelectric orderings, and

$$\begin{aligned} &\tilde{\eta}'_1 = \bar{\eta}'_{11} + \bar{\eta}'_{12} + \bar{\eta}'_{13} + \bar{\eta}'_{14}; \quad \tilde{\eta}'_2 = \bar{\eta}'_{11} + \bar{\eta}'_{12} - \bar{\eta}'_{13} - \bar{\eta}'_{14}; \\ &\tilde{\eta}'_3 = \bar{\eta}'_{11} - \bar{\eta}'_{12} + \bar{\eta}'_{13} - \bar{\eta}'_{14}; \quad \tilde{\eta}'_4 = \bar{\eta}'_{11} - \bar{\eta}'_{12} - \bar{\eta}'_{13} + \bar{\eta}'_{14}. \end{aligned} \quad (2.26)$$

In this work we shall explore temperature and composition dependences of the longitudinal $\varepsilon_{33}(T)$ and transverse $\varepsilon_{11}(T)$ permittivity of the system

$$\begin{aligned} &\varepsilon_{aa}(T) = \varepsilon^0_{aa} + 4\pi\chi_{aa}(T), \quad \varepsilon^0_{aa} = 1 + 4\pi\chi^0_{aa}, \quad (a = 1,2,3); \\ &\chi_{33}(T) = -4\frac{1}{Tv_e}\left(\langle d^z \rangle_c\right)^2 \tilde{\eta}'_1(T); \\ &\chi_{aa}(T) = -\frac{1}{Tv_e}\left(\langle d^a \rangle_c\right)^2 \left(\tilde{\eta}'_2(T) + \tilde{\eta}'_4(T)\right), a = 1,2. \end{aligned} \quad (2.27)$$

In order to find the quantities $\tilde{\eta}'_\mu$ occurring in the expression for the susceptibility, we differentiate $\bar{\eta}_f$ and eq. (2.22) for $\bar{\varphi}_{L,f}, \bar{\varphi}_f, q_f$ with respect to the fields $\beta h_{f'}$ and obtain equations for $\bar{\eta}'_{ff'}$, $\bar{\varphi}'_{ff'}$, and $q'_{ff'}$

$$\begin{aligned} &\left[1 - \left\langle \hat{F}^{(2)} \right\rangle_c \beta\hat{\tilde{J}}(\vec{0})\right]\hat{\tilde{\eta}}' = \left\langle \hat{F}^{(2)} \right\rangle_c \left[1 + 2\beta\hat{\bar{\varphi}}'\right] + \frac{1}{2}\left\langle \hat{F}^{(2)} \right\rangle_c \beta^2 2\hat{q}', \\ &\left[2\left\langle \hat{F}^{(2)} \right\rangle_c - \left\langle \hat{F}^{[11]} \right\rangle_c\right]\beta\hat{\bar{\varphi}}' + \frac{1}{2}\left[2\left\langle \hat{F}^{(3)} \right\rangle_c - \left\langle \hat{F}^{[12]} \right\rangle_c\right]\beta^2\hat{q}' = \\ &= \left[-\left\langle \hat{F}^{(2)} \right\rangle_c + \left\langle \hat{F}^{[11]} \right\rangle_c\right]\left[1 + \beta\hat{\tilde{J}}(\vec{0})\hat{\tilde{\eta}}'\right], \\ &\left[2\left\langle \hat{F}^{(3)} \right\rangle_c - \left\langle \hat{F}^{[21]} \right\rangle_c\right]\beta\hat{\bar{\varphi}}' + \frac{1}{2}\left[2\left\langle \hat{F}^{(4)} \right\rangle_c - \left\langle \hat{F}^{[22]} \right\rangle_c\right]\beta^2\hat{q}' = \\ &= \left[-\left\langle \hat{F}^{(2)} \right\rangle_c + \left\langle \hat{F}^{[21]} \right\rangle_c\right]\left[1 + \beta\hat{\tilde{J}}(\vec{0})\hat{\tilde{\eta}}'\right]. \end{aligned} \quad (2.28)$$

We multiply these equations by the unitary matrix $\hat{U}$ (2.20) from the left, rendering all the matrices in eqs. (2.28) diagonal or antidiagonal.

Let us explore the symmetry of the matrices in these equations in the case of the antiferroelectric ordering (in the case of ferroelectric ordering all minus signs are changed to plus signs), as well as the form of the matrices after the unitary transformation

$$\langle \hat{F}^{(2n)} \rangle_c = \langle F^{(2n)} \rangle_c \cdot \hat{I}; \ \hat{\tilde{F}}^{(2n)} = \hat{U}^+ \cdot \langle F^{(2n)} \rangle_c \cdot \hat{U} \equiv \langle \hat{F}^{(2n)} \rangle_c; \quad (2.29)$$



$$\langle \hat{F}^{(2n+1)} \rangle_c = \langle F^{(2n+1)} \rangle_c \begin{pmatrix} 1 & 0 & 0 & 0 \\ 0 & -1 & 0 & 0 \\ 0 & 0 & -1 & 0 \\ 0 & 0 & 0 & 1 \end{pmatrix};$$

$$\hat{\tilde{F}}^{(2n+1)} = \langle F^{(2n+1)} \rangle_c \begin{pmatrix} 0 & 0 & 0 & 1 \\ 0 & 0 & 1 & 0 \\ 0 & 1 & 0 & 0 \\ 1 & 0 & 0 & 0 \end{pmatrix};$$

$$\hat{\bar{\varphi}}' = \begin{pmatrix} \bar{\varphi}'_{11} & \bar{\varphi}'_{12} & \bar{\varphi}'_{13} & \bar{\varphi}'_{14} \\ \bar{\varphi}'_{12} & \bar{\varphi}'_{11} & \bar{\varphi}'_{14} & \bar{\varphi}'_{13} \\ \bar{\varphi}'_{13} & \bar{\varphi}'_{14} & \bar{\varphi}'_{11} & \bar{\varphi}'_{12} \\ \bar{\varphi}'_{14} & \bar{\varphi}'_{13} & \bar{\varphi}'_{12} & \bar{\varphi}'_{11} \end{pmatrix}; \ \hat{\tilde{\varphi}}' = \hat{U}\hat{\bar{\varphi}}'\hat{U} = \begin{pmatrix} \tilde{\varphi}'_1 & 0 & 0 & 0 \\ 0 & \tilde{\varphi}'_2 & 0 & 0 \\ 0 & 0 & \tilde{\varphi}'_3 & 0 \\ 0 & 0 & 0 & \tilde{\varphi}'_4 \end{pmatrix};$$
$$\begin{aligned} &\tilde{\varphi}'_1 = \bar{\varphi}'_{11} + \bar{\varphi}'_{12} + \bar{\varphi}'_{13} + \bar{\varphi}'_{14}; \ \tilde{\varphi}'_2 = \bar{\varphi}'_{11} + \bar{\varphi}'_{12} - \bar{\varphi}'_{13} - \bar{\varphi}'_{14}; \\ &\tilde{\varphi}'_3 = \bar{\varphi}'_{11} - \bar{\varphi}'_{12} + \bar{\varphi}'_{13} - \bar{\varphi}'_{14}; \ \tilde{\varphi}'_4 = \bar{\varphi}'_{11} - \bar{\varphi}'_{12} - \bar{\varphi}'_{13} + \bar{\varphi}'_{14}; \end{aligned} \quad (2.30)$$

$$\hat{q}' = \begin{pmatrix} q'_{11} & -q'_{12} & -q'_{13} & q'_{14} \\ q'_{12} & -q'_{11} & -q'_{14} & q'_{13} \\ q'_{13} & -q'_{14} & -q'_{11} & q'_{12} \\ q'_{14} & -q'_{13} & -q'_{12} & q'_{11} \end{pmatrix}; \ \hat{\tilde{q}}' = \begin{pmatrix} 0 & 0 & 0 & \tilde{q}'_4 \\ 0 & 0 & \tilde{q}'_3 & 0 \\ 0 & \tilde{q}'_2 & 0 & 0 \\ \tilde{q}'_1 & 0 & 0 & 0 \end{pmatrix}$$
$$\begin{aligned} &\tilde{q}'_1 = q'_{11} - q'_{12} - q'_{13} + q'_{14}, \ \tilde{q}'_2 = q'_{11} - q'_{12} + q'_{13} - q'_{14}, \\ &\tilde{q}'_3 = q'_{11} + q'_{12} - q'_{13} - q'_{14}, \ \tilde{q}'_4 = q'_{11} + q'_{12} + q'_{13} + q'_{14}. \end{aligned} \quad (2.31)$$

The averaged matrices of the second derivatives $\langle \hat{F}^{[11]} \rangle_c; \langle \hat{F}^{[22]} \rangle_c$ for the antiferroelectric phase are of the same symmetry as the matrix $\hat{\tilde{\varphi}}'$, and the eigenvalues of these matrices $\tilde{F}^{[11]}_\mu; \tilde{F}^{[22]}_\mu$ are written as linear combinations similar to $\tilde{\varphi}'_\mu$. Symmetry of the matrix $\langle \hat{F}^{[21]} \rangle_c$ is the same as of $\hat{q}'$; after the unitary transformation it becomes analogous to the antidiagonal matrix $\hat{\tilde{q}}'$ with the corresponding elements $\tilde{F}^{[21]}_\mu$. The matrix $\langle \hat{F}^{[12]} \rangle_c$ is transposed to $\langle \hat{F}^{[21]} \rangle_c$. After the unitary transformation and exclusion of the parameters $\tilde{\varphi}'_\mu, \tilde{q}'_\mu$ we obtain expressions for the correlators $\tilde{\eta}'_\mu$, entering the expression for the system susceptibility.

$$\begin{aligned} \tilde{\eta}'_\mu = &-\left[D_\mu/B_\mu - \beta\bar{\nu}_\mu(\vec{0})\right]^{-1} \underset{ProtonGlassState}{\longrightarrow} \\ &-\left[2/\tilde{F}^{[11]}_\mu - \left(1 - \langle F^{(1)} \rangle_c\right)^{-1} - \beta\bar{\nu}_\mu(\vec{0})\right]^{-1}, \end{aligned} \quad (2.32)$$

$$D_\mu = \left[2\langle F^{(2)}\rangle_c - \tilde{F}_\mu^{[11]}\right]\left[2\langle F^{(4)}\rangle_c - \tilde{F}_\mu^{[22]}\right] -$$
$$- \left[2\langle F^{(3)}\rangle_c - \tilde{F}_\mu^{[12]}\right]\left[2\langle F^{(3)}\rangle_c - \tilde{F}_\mu^{[21]}\right],$$
$$B_\mu = \bar{F}^{(2)} \cdot \tilde{F}_\mu^{[11]}\left[2\langle F^{(4)}\rangle_c - \tilde{F}_\mu^{[22]}\right] +$$
$$+\langle F^{(2)}\rangle_c \tilde{F}_\mu^{[12]}\tilde{F}_\mu^{[21]} - 2\left[\langle F^{(3)}\rangle_c\right]^2 \tilde{F}_\mu^{[11]}.$$

In the case of the ferroelectric ordering the matrices $\hat{\tilde{\eta}}', \hat{\tilde{\varphi}}', \hat{q}', \left\langle \hat{F}^{[nn']} \right\rangle_c$ have the same symmetry. As a result, we obtain the same expression for $\tilde{\eta}'_\mu$, except that for the eigenvalues $\tilde{F}_\mu^{[12]}$ we have to use the linear combination like for $\tilde{\varphi'}_\mu$.

Let us note that dynamic susceptibility $\chi_{aa}(\nu, T)$ of the system is expressed via the dynamic eigenvalues $\tilde{\eta}'_\mu(\nu)$ as in the static case (2.27) after the replacement $\tilde{\eta}'_\mu \to \tilde{\eta}'_\mu(\nu)$. The expressions for $\tilde{\eta}'_\mu(\nu)$ are derived in [83].

## 3. Relaxational dynamics of the $Rb_{1-x}(NH_4)_x\ H_2PO_4$ type mixtures

Dynamics of the mixed system $Rb_{1-x}(NH_4)_xH_2PO_4$ will be described on the basis of Glauber equations for the n-th order correlation functions:

$$\left(\sum_{j=1}^{n}\nu_j + \partial/\partial t\right)\eta_{12\ldots n}(t) =$$
$$\sum_j^n \nu_j \left\langle S_1 \ldots S_n F^{(1)}(h_j(t) + \bar{\varphi}_{L,j}(t) + \hat{\varphi}_j^- + \hat{\varphi}_j^+)\right\rangle_{\rho(t)};$$
$$\eta_{12\ldots n}(t) = \langle S_1 \ldots S_n\rangle_{\rho(t)}; \quad \nu_j = 1/\tau_{0,j}; \quad \bar{\varphi}_{L,j}(t) = \sum_j \bar{J}_{jj'}(\vec{k}_*)\bar{\eta}'_j(t). \tag{3.1}$$

Here we introduce operator fields $\varphi_j^+, \varphi_j^-$ exerted on the bond $j$ by the two tetrahedral connected by this bond

$$\begin{aligned}\hat{\varphi}_j^+ &= -\,V_j\,/\,4\,(S_{j_2} + S_{j_4}) - \,U_j\,/\,4\,S_{j_3} - \,\Phi_j\,/\,16\,S_{j_2}S_{j_3}S_{j_4};\\ \hat{\varphi}_j^- &= -\,V_j\,/\,4\,(S_{j'_2} + S_{j'_4}) - \,U_j\,/\,4\,S_{j'_3} - \,\Phi_j\,/\,16\,S_{j'_2}S_{j'_3}S_{j'_4}.\end{aligned} \tag{3.2}$$

The seed relaxation time $\tau_{0,j}$ can be expressed via correlation functions of an ionic subsystem. Within the given below cluster approximation, the bonds $i, j$ belong to the same tetrahedron (as an example we use



the "$B$" tetrahedron with indices $f, f' = 1 \div 4$). Averaging over configurations will also be performed for each tetrahedron with its hydrogen bonds independently. Therefore in our equations the primitive cell index is absent.

We shall explain the approximation by the example of an equation for a single-particle correlator. In the mean field approximation we make a replacement $\hat{\varphi}_j^\pm \to \varphi_j(t)$ and obtain an equation

$$[\nu_1 + \partial/\partial t]\cdot\eta_1(t) = \nu_1 \cdot F^{(1)}(\kappa_1(t)); \quad \kappa_1(t) = h_1(t) + 2\varphi_1(t) + \bar{\varphi}_{L,1}(t). \tag{3.3}$$

Within the cluster approximation such a replacement is performed for a field $\hat{\varphi}_f^- \to \varphi_f$ only

$$\begin{aligned}&[\nu_1 + \partial/\partial t]\cdot\eta_1(t) = \nu_1 \cdot F^{(1)}\left(\kappa_{cl,1}(t) + \varphi_1^+\right);\\ &\kappa_{cl,1}(t) = h_1(t) + \varphi_1(t) + \bar{\varphi}_{L,1}(t);\\ &\nu_1 \cdot F^{(1)}\left(\kappa_{cl,1}(t) + \varphi_1^+\right) = L_1 + P_1\cdot\eta_3(t) + Q_1\left(\eta_2(t) + \eta_4(t)\right) +\\ &+N_1\eta_{24}(t) + M_1\left(\eta_{23}(t) + \eta_{34}(t)\right) + R_1\eta_{234}(t).\end{aligned} \tag{3.4}$$

The expansion coefficients are found from the relations

$$\begin{aligned}&L_1(t) = \frac{\nu_1}{8}\sum_{2,3,4} F_1^{(1)}; \quad P_1(t) = \frac{\nu_1}{8}\sum_{2,3,4} S_3F_1^{(1)};\\ &Q_1(t) = \frac{\nu_1}{8}\sum_{2,3,4} S_2F_1^{(1)} \equiv \frac{\nu_1}{8}\sum_{2,3,4} S_2F_1^{(1)};\ N_1(t) = \frac{\nu_1}{8}\sum_{2,3,4} S_2S_4F_1^{(1)};\\ &M_1(t) = \frac{\nu_1}{8}\sum_{2,3,4} S_2S_3F_1^{(1)} = \frac{\nu_1}{8}\sum_{2,3,4} S_4S_3F_1^{(1)};\\ &R_1(t) = \frac{\nu_1}{8}\sum_{2,3,4} S_2S_3S_4F_1^{(1)}.\end{aligned} \tag{3.5}$$

In equations (3.3), (3.4) the $t$-dependent distribution functions $\eta_f(t)$, $\eta_{fg}(t)$, $\eta_{fgk}(t)$ and random dynamic cluster field $\varphi_f(t)$ are unknown. In the cluster approximation we need to write down a system of 14 closed equations for 14 unknown correlation functions. In the matrix form

$$\begin{aligned}\hat{A}\left(\{\nu_f\}; \{L_f, P_f, Q_f, N_f, M_f, R_f\}; \partial/\partial t\right)\cdot\vec{\eta}(t) =\\ = \vec{C}\left(\{L_f, P_f, Q_f, N_f, M_f, R_f\}\right).\end{aligned} \tag{3.6}$$

Here we introduce notations for the column vectors

$$\vec{\eta}(t) = (\eta_1; \eta_2; \eta_3; \eta_4|\eta_{23}; \eta_{34}; \eta_{41}; \eta_{12}; \eta_{24}; \eta_{13}|\eta_{234}; \eta_{341}; \eta_{412}; \eta_{123});$$

$$-\vec{C}\left(\{L_f,P_f,Q_f,N_f,M_f,R_f\}\right)=(L_1;L_2;L_3;L_4|Q_2+Q_3;Q_3+Q_4;$$
$$Q_1+Q_4;Q_1+Q_2;P_2+P_4;P_1+P_3|M_2+M_4+N_3;$$
$$M_1+M_3+N_4;M_2+M_4+N_1;M_1+M_3+N_2). \quad (3.7)$$

The matrix contains the $\partial/\partial t$ operators only in its diagonal elements. It is too cumbersome to be presented here.

In the present work we are interested in the linear response of the system to a frequency-dependent field

$$h_f(t)=h_f+\delta h_f(t);\quad \kappa_f(t)=\kappa_f+\delta\kappa_f(t);\quad \kappa_{cl,f}(t)=\kappa_{cl,f}+\delta\kappa_{cl,f}(t);$$
$$\eta'_{ff'}(t)=\frac{\delta\eta_f(t)}{\delta h_{f'}(t)};\quad \kappa'_{ff'}(t)=\frac{\delta\kappa_f(t)}{\delta h_{f'}(t)};\quad \varphi'_{ff'}(t)=\frac{\delta\varphi_f(t)}{\delta h_{f'}(t)}. \quad (3.8)$$

Expanding (3.3) in powers of $\delta\kappa_f(t)$ and differentiating the dynamic part with respect to $\delta h_{f'}(t)$, we obtain expressions for the static $\eta_f$ and dynamic $\eta'_{ff'}(\omega)$ (after the Fourier transformation $t\to\omega$) parts

$$\eta_f=F_f^{(1)}(\kappa_f);\quad \kappa_f=h_f+2\varphi_f+\sum_{f_1}\bar{J}_{ff_1}(\vec{k}_*)\bar{\eta}_{f_1};$$
$$\eta'_{ff'}(\omega)=F_f^{(2)}(\omega)\cdot\kappa'_{ff'}(\omega);\qquad F_f^{(2)}(\omega)=\nu_f F_f^{(2)}(\kappa_f)/(\nu_f+i\omega);$$
$$\bar{\kappa}'_{ff'}(\omega)=\delta_{ff'}+2\varphi'_{ff'}(\omega)+\sum_{f_1=1}^{4}\bar{J}_{ff_1}(\vec{0})\cdot\bar{\eta}'_{f_1f'}(\omega). \quad (3.9)$$

Static solutions of the cluster equation (3.6), apparently, have the form

$$\vec{\eta}_0=\left(\hat{A}_0\left(\{\nu_f\};\{\};0\right)\right)^{-1}\cdot\vec{C}_0\left(\{\}\right);$$
$$\hat{A}_0\left(\{\nu_f\};\{\};0\right)=\hat{A}\left(\{\nu_f\};\{L_f,P_f,Q_f,N_f,M_f,R_f\}_{h_f(t)=h_f};0\right);$$
$$\vec{C}_0\left(\{\}\right)=\vec{C}\left(\{L_f,P_f,Q_f,N_f,M_f,R_f\}_{h_f(t)=h_f}\right). \quad (3.10)$$

Linear dynamic response can be expressed via the static solutions $\vec{\eta}_0$ as

$$\delta\vec{\eta}(\omega)=\left(\hat{A}_0\left(\{\nu_f\};\{\};i\omega\right)\right)^{-1}\left[\delta\vec{C}\left(\{\}\right)-\delta\hat{A}\left(\{\nu_f\};\{\};i\omega\right)\cdot\vec{\eta}_0\right]. \quad (3.11)$$

Expanding the linear responses $\delta\vec{C}\left(\{\}\right),\delta\hat{A}\left(\{\nu_f\};\{\};i\omega\right)$ in powers of $\delta\kappa_{cl,f}(i\omega)$ and differentiating with respect to $\delta h'_f(\omega)$, we obtain an expression for $\eta'_{ff'}(\omega)$



$$\eta'_{ff'}(\omega)=\sum_{f_1=1}^{4}\Omega_{ff_1}(\omega)\kappa'_{cl,f_1f'}(\omega); \quad (3.12)$$

$$\kappa'_{cl,ff'}(\omega)=\delta_{ff'}+\varphi'_{ff'}(\omega)+\sum_{f_1=1}^{4}\bar{J}_{ff_1}(\vec{0})\cdot\bar{\eta}'_{f_1f'}(\omega);$$

$$\Omega_{ff'}(\omega)=\sum_{i=1}^{14}\left(A_0^{-1}\right)_{f,i}\cdot\frac{\partial\left(C_0\right)_i}{\partial\kappa_{cl,f'}}-\sum_{i,j=1}^{14}\left(A_0^{-1}\right)_{f,i}\cdot\frac{\partial\left(A_0\right)_{i,j}}{\partial\kappa_{cl,f'}}\cdot\eta_{0,j}.$$

After averaging over configurations with taking into account the Gaussian fluctuations, we obtain from (3.9) and (3.12)

$$\bar{\eta}'_{ff'}(\omega)=\left\langle\eta'_{ff'}(\omega)\right\rangle_c=\left\langle F_f^{(3)}(\omega)\right\rangle_c q'_{ff'}(\omega)+$$
$$+\left\langle F_f^{(2)}(\omega)\right\rangle_c\left[\delta_{ff'}+2\bar{\varphi}'_{ff'}(\omega)+\sum_{f_1=1}^{4}\bar{J}_{ff_1}(\vec{0})\cdot\bar{\eta}'_{f_1f'}(\omega)\right],$$
$$\bar{\eta}'_{ff'}(\omega)=\sum_{f_1=1}^{4}\left\langle\Omega_{ff_1}(\omega)\right\rangle_c\left[\delta_{f_1f'}+\bar{\varphi}'_{f_1f'}(\omega)+\sum_{f_2=1}^{4}\bar{J}_{f_1f_2}(\vec{0})\cdot\bar{\eta}'_{f_2f'}(\omega)\right]+$$
$$+\sum_{f_1=1}^{4}\left\langle\Omega'_{ff_1}(\omega)\right\rangle_c\frac{1}{2}q'_{f_1f'}(\omega), \quad (3.13)$$

Here we introduce the notations

$$\left\langle\varphi_{f_1}\cdot\varphi'_{f_1f'}(\omega)\right\rangle_c^{cum}=q'_{f_1f'}(\omega)/2;\quad \left\langle\Omega'_{ff'}(\omega)\right\rangle_c=\left\langle\frac{\partial\Omega_{ff'}(\omega)}{\partial\kappa_{cl,f'}}\right\rangle_c. \quad (3.14)$$

Equating the mean values of correlators $\bar{\eta}'_{ff'}(\omega)$ calculated within the single-particle and cluster approximations, we obtain the first matrix equation for unknown matrices $\hat{\varphi}'(\omega)$, $\hat{q}'(\omega)$

$$\left[2\left\langle\hat{F}^{(2)}(\omega)\right\rangle_c-\left\langle\hat{\Omega}(\omega)\right\rangle_c\right]\hat{\bar{\varphi}}'(\omega)+\frac{1}{2}\left[2\left\langle\hat{F}^{(3)}(\omega)\right\rangle_c-\left\langle\hat{\Omega}'(\omega)\right\rangle_c\right]\hat{q}'(\omega)=$$
$$=\left[-\left\langle\hat{F}^{(2)}(\omega)\right\rangle_c+\left\langle\hat{\Omega}(\omega)\right\rangle_c\right]\cdot\left[1+\hat{\bar{J}}\left(\vec{0}\right)\hat{\bar{\eta}}'(\omega)\right]. \quad (3.15)$$

Equating the mean values of correlators $\left\langle Q'_{ff'}(\omega)\right\rangle_c=-2\left\langle\eta_{0,f}\cdot\eta'_{ff'}(\omega)\right\rangle_c$ calculated within the single-particle and cluster approximations, we obtain the second matrix equation for unknown

matrices $\hat{\varphi}'(\omega)$, $\hat{q}'(\omega)$

$$\left[2\left\langle \hat{F}^{(3)}(\omega)\right\rangle_c - \left\langle \hat{\Omega}_Q(\omega)\right\rangle_c\right]\hat{\bar{\varphi}}'(\omega) + \frac{1}{2}\left[2\left\langle \hat{F}^{(4)}(\omega)\right\rangle_c - \left\langle \hat{\Omega}'_Q(\omega)\right\rangle_c\right]\hat{q}'(\omega) =$$
$$= \left[-\left\langle \hat{F}^{(3)}(\omega)\right\rangle_c + \left\langle \hat{\Omega}_Q(\omega)\right\rangle_c\right]\left[1 + \hat{\tilde{J}}\left(\vec{0}\right)\hat{\bar{\eta}}'(\omega)\right]. \quad (3.16)$$

Here we introduce matrix notations

$$\langle \Omega_{Q,ff'}(\omega)\rangle_c = \langle -2\eta_{0,f}\cdot\Omega_{ff'}(\omega)\rangle_c; \quad \left\langle \Omega'_{Q,ff'}(\omega)\right\rangle_c = \left\langle \frac{\partial\Omega_{Q,ff'}(\omega)}{\partial\kappa_{cl,f'}}\right\rangle_c. \quad (3.17)$$

From equations (3.15), (3.16) we derive expressions for $\hat{\varphi}'(\omega)$, $\hat{q}'(\omega)$ used to find $\bar{\eta}'_{ff'}(\omega)$ (3.13). For the sake of simplicity, in what follows we shall use an effective relaxation time $\bar{\tau}_0$

$$\frac{1}{\bar{\tau}_0} = \langle \nu_f\rangle_c \approx c_+^2\frac{1}{\tau_{0,+}} + c_-^2\frac{1}{\tau_{0,-}} + 2c_+c_-\frac{1}{\tau_{0,0}}. \quad (3.18)$$

Let us consider the symmetry of matrices, entering these equations in the case of antiferroelectric ordering (in the case of ferroelectric ordering all minus signs should be replaced by plus signs), as well as the form of the matrices after a unitary transformation (for the sake of simplicity we omit the argument of $\omega$ in the matrix elements)

$$\left\langle \hat{F}^{(2n)}(\omega)\right\rangle_c = \left\langle F^{(2n)}(\omega)\right\rangle_c \hat{I};$$
$$\widetilde{\left\langle \hat{F}^{(2n)}(\omega)\right\rangle_c} = U^+\left\langle \hat{F}^{(2n)}(\omega)\right\rangle_c U \equiv \left\langle \hat{F}^{(2n)}(\omega)\right\rangle_c; \quad (3.19)$$

$$\left\langle \hat{F}^{(2n+1)}(\omega)\right\rangle_c = \left\langle F^{(2n+1)}(\omega)\right\rangle_c \begin{pmatrix} 1 & 0 & 0 & 0\\ 0 & -1 & 0 & 0\\ 0 & 0 & -1 & 0\\ 0 & 0 & 0 & 1\end{pmatrix};$$
$$\widetilde{\left\langle \hat{F}^{(2n+1)}(\omega)\right\rangle_c} = \left\langle F^{(2n+1)}(\omega)\right\rangle_c \begin{pmatrix} 0 & 0 & 0 & 1\\ 0 & 0 & 1 & 0\\ 0 & 1 & 0 & 0\\ 1 & 0 & 0 & 0\end{pmatrix}; \quad (3.20)$$

$$\hat{\bar{\varphi}}'(\omega) = \begin{pmatrix} \bar{\varphi}'_{11} & \bar{\varphi}'_{12} & \bar{\varphi}'_{13} & \bar{\varphi}'_{14}\\ \varphi'_{12} & \varphi'_{11} & \varphi'_{14} & \varphi'_{13}\\ \varphi'_{13} & \varphi'_{14} & \varphi'_{11} & \varphi'_{12}\\ \varphi'_{14} & \varphi'_{13} & \varphi'_{12} & \varphi'_{11}\end{pmatrix};$$



$$\widetilde{\hat{\bar{\varphi}}'(\omega)} = \hat{U}\hat{\bar{\varphi}}'(\omega)\hat{U} = \begin{pmatrix} \tilde{\bar{\varphi}}'_1 & 0 & 0 & 0\\ 0 & \tilde{\bar{\varphi}}'_2 & 0 & 0\\ 0 & 0 & \tilde{\bar{\varphi}}'_3 & 0\\ 0 & 0 & 0 & \tilde{\bar{\varphi}}'_4\end{pmatrix}; \quad (3.21)$$
$$\tilde{\bar{\varphi}}'_1(\omega) = \bar{\varphi}'_{11} + \bar{\varphi}'_{12} + \bar{\varphi}'_{13} + \bar{\varphi}'_{14}; \quad \tilde{\bar{\varphi}}'_2(\omega) = \bar{\varphi}'_{11} + \bar{\varphi}'_{12} - \bar{\varphi}'_{13} - \bar{\varphi}'_{14};$$
$$\tilde{\bar{\varphi}}'_3(\omega) = \bar{\varphi}'_{11} - \bar{\varphi}'_{12} + \bar{\varphi}'_{13} - \bar{\varphi}'_{14}; \quad \tilde{\bar{\varphi}}'_4(\omega) = \bar{\varphi}'_{11} - \bar{\varphi}'_{12} - \bar{\varphi}'_{13} + \bar{\varphi}'_{14};$$

$$\hat{q}'(\omega) = \begin{pmatrix} q'_{11} & -q'_{12} & -q'_{13} & q'_{14}\\ q'_{12} & -q'_{11} & -q'_{14} & q'_{13}\\ q'_{13} & -q'_{14} & -q'_{11} & q'_{12}\\ q'_{14} & -q'_{13} & -q'_{12} & q'_{11}\end{pmatrix};$$
$$\widetilde{\hat{q}'(\omega)} = \hat{U}\hat{q}'(\omega)\hat{U} = \begin{pmatrix} 0 & 0 & 0 & \tilde{q}'_4\\ 0 & 0 & \tilde{q}'_3 & 0\\ 0 & \tilde{q}'_2 & 0 & 0\\ \tilde{q}'_1 & 0 & 0 & 0\end{pmatrix}; \quad (3.22)$$
$$\tilde{q}'_1(\omega) = q'_{11} - q'_{12} - q'_{13} + q'_{14}, \quad \tilde{q}'_2(\omega) = q'_{11} - q'_{12} + q'_{13} - q'_{14},$$
$$\tilde{q}'_3(\omega) = q'_{11} + q'_{12} - q'_{13} - q'_{14}, \quad \tilde{q}'_4(\omega) = q'_{11} + q'_{12} + q'_{13} + q'_{14}.$$

The symmetry of $\left\langle \hat{\Omega}(\omega)\right\rangle_c$, $\left\langle \hat{\Omega}'_Q(\omega)\right\rangle_c$ matrices in the antiferroelectric phase is the same as of $\hat{\bar{\varphi}}'(\omega)$, and their eigenvalues $\tilde{\Omega}_\mu(\omega)$, $\tilde{\Omega}'_{Q,\mu}(\omega)$ can be written as linear combinations similar to $\tilde{\bar{\varphi}}'_\mu(\omega)$. Symmetry of the $\left\langle \hat{\Omega}'(\omega)\right\rangle_c$, $\left\langle \hat{\Omega}_Q(\omega)\right\rangle_c$ matrices coincides with the symmetry of a matrix transposed to $\hat{q}'(\omega)$; after the unitary transformation its form is analogous to the transposed $\widetilde{\hat{q}'(\omega)}$ matrix with the corresponding $\tilde{\Omega}'_\mu(\omega)$, $\tilde{\Omega}_{Q,\mu}(\omega)$ elements. After the unitary transformation, the matrix equation (3.15) becomes diagonal, and equation (3.16) becomes antidiagonal. In order to have in transformed equation (3.16) products with the same indices $\mu$, that is, $\tilde{\Omega}_{Q,\mu}(\omega)\cdot\tilde{\bar{\varphi}}'_\mu(\omega)$, $\tilde{\Omega}'_{Q,\mu}(\omega)\cdot\tilde{q}'_1(\omega)$ (instead of $\tilde{\Omega}_{Q,4}(\omega)\cdot\tilde{\bar{\varphi}}'_1(\omega)$, $\tilde{\Omega}'_{Q,4}(\omega)\cdot\tilde{q}'_1(\omega)$), one should change numbering of the $\tilde{\Omega}_{Q,\mu}(\omega)$, $\tilde{\Omega}'_{Q,\mu}(\omega)$ matrices eigenvalues to the opposite one $((1,2,3,4)\to(4,3,2,1))$. Then, when the parameters $\tilde{\bar{\varphi}}'_\mu(\omega), \tilde{q}'_\mu(\omega)$ are found and substituted to the expression for $\tilde{\bar{\eta}}'_\mu(\omega)$ (diagonalized first equation of (3.13)), we obtain

$$-\tilde{\bar{\eta}}'_\mu(\omega) = \left[D_\mu(\omega)/B_\mu(\omega) - \beta\nu_\mu(\vec{0})\right]^{-1}, \quad (3.23)$$

$$D_\mu(\omega) = \left[2\left\langle F^{(2)}(\omega)\right\rangle_c - \tilde{\Omega}_\mu(\omega)\right]\left[2\left\langle F^{(4)}(\omega)\right\rangle_c - \tilde{\Omega}'_{Q,\mu}(\omega)\right] -$$
$$- \left[2\left\langle F^{(3)}(\omega)\right\rangle_c - \tilde{\Omega}'_\mu(\omega)\right]\left[2\left\langle F^{(3)}(\omega)\right\rangle_c - \tilde{\Omega}_{Q,\mu}(\omega)\right]$$
$$B_\mu(\omega) = \left\langle F^{(2)}(\omega)\right\rangle_c \cdot \tilde{\Omega}_\mu(\omega)\left[2\left\langle F^{(4)}(\omega)\right\rangle_c - \tilde{\Omega}'_{Q,\mu}(\omega)\right] +$$
$$+ \left\langle F^{(2)}(\omega)\right\rangle_c \cdot \tilde{\Omega}_{Q,\mu}(\omega) \cdot \tilde{\Omega}'_\mu(\omega) - 2\left[\left\langle F^{(3)}(\omega)\right\rangle_c\right]^2 \tilde{\Omega}_\mu(\omega). \quad (3.24)$$

In the case of ferroelectric ordering in (3.23), (3.24) the eigenvalues of $\tilde{\Omega}_\mu(\omega)$, $\tilde{\Omega}_{Q,\mu}(\omega)$, $\tilde{\Omega}'_\mu(\omega)$, $\tilde{\Omega}'_{Q,\mu}(\omega)$ matrices are constructed on the matrix elements $\langle\Omega_{ff'}(\omega)\rangle_c$, $\langle\Omega_{Q,ff'}(\omega)\rangle_c$, $\left\langle\Omega'_{ff'}(\omega)\right\rangle_c$ $\left\langle\Omega'_{Q,ff'}(\omega)\right\rangle_c$, similarly as the matrix $\hat{\tilde{\varphi}}'(\omega)$ (3.21). In the case of antiferroelectric ordering, in these expressions the eigenvalues of $\tilde{\Omega}_\mu(\omega)$, $\tilde{\Omega}_{Q,\mu}(\omega)$ matrices are constructed on the matrix elements $\langle\Omega_{ff'}(\omega)\rangle_c$; $\langle\Omega_{Q,ff'}(\omega)\rangle_c$, similarly to the matrix $\hat{\tilde{\varphi}}'(\omega)$ (3.21), and of the $\tilde{\Omega}'_\mu(\omega)$, $\tilde{\Omega}'_{Q,\mu}(\omega)$ matrices are constructed on the matrix elements $\left\langle\Omega'_{ff'}(\omega)\right\rangle_c$; $\left\langle\Omega'_{Q,ff'}(\omega)\right\rangle_c$ similarly to the matrix $\hat{q}'(\omega)$ (3.22). Let us note that in the case of a pure system the expression for $\tilde{\eta}'_\mu(\omega)$ is analogous to (3.23) in the proton glass region, except that it does not contain the configurational averaging, and coincides with the expression given in [117].

In this work we shall explore temperature and composition dependences of the complex permittivity of the system

$$\varepsilon_{aa}(\omega,T) = \varepsilon^0_{aa} + 4\pi\chi_{aa}(\omega,T), \quad \varepsilon^0_{aa} = 1 + 4\pi\chi^0_{aa}, \quad (a=1,2,3). \quad (3.25)$$

Dynamic susceptibility $\chi_{aa}(\omega,T)$of the system is expressed via dynamic eigenvalues $\tilde{\tilde{\eta}}'_\mu(\omega)$ (3.23) as in the static case (2.27) after the replacement $\tilde{\tilde{\eta}}'_\mu \to \tilde{\tilde{\eta}}'_\mu(\omega)$.

## 4. Discussion

### 4.1. Optimal sets of model parameters

Using the obtained in previous Sections expressions, let us evaluate the dielectric and thermal characteristics of the $Rb_{1-x}(NH_4)_xH_2PO_4$ type compounds and compare them with the corresponding experimental data. Values of the theory parameters should provide the best possible fit to the experiment.

The found sets of the model parameters for the $Rb_{1-x}(NH_4)_xH_2PO_4$ mixtures ($T_c(x=0)=147.6$K, $T_N(x=1)=148$K), $Rb_{1-x}(ND_4)_xD_2PO_4$ ($T_c(x=0)=235$K, $T_N(x=1)=242$K), $Rb_{1-x}(NH_4)_xH_2AsO_4$ ($T_c(x=0)=110$K, $T_N(x=1)=216$K),



Table 1. Parameters for $Rb_{1-x}(NH_4)_xH_2PO_4$

| tetrahedron state | $\varepsilon_\alpha$ K | $w_\alpha$ K | $\nu_{1,\alpha\alpha}(0)$ K | $\nu_{2,\alpha\alpha}(k^z)$ K | $\nu_{2,\alpha\alpha}(0)$ K |
|---|---|---|---|---|---|
| +(Ferro) | 80 | 600 | 14.33 | -50 | -40 |
| 0(Glass) | — | — | -34 | -2 | -65 |
| -(Antiferro) | -60 | 500 | 10 | 46.8 | -35 |

| tetrahedron state | $d^z_\alpha(G), 10^{-18}$ esu·cm | $d^z_\alpha(F), 10^{-18}$ esu·cm | $d^x_\alpha(G), 10^{-18}$ esu·cm | $d^x_\alpha(F), 10^{-18}$ esu·cm |
|---|---|---|---|---|
| +(Ferro) | 0.93 | 0.73 | 2.7 | 2.7 |
| 0(Glass) | 1.05 | 0.7 | 3.25 | 0.8 |
| -(Antiferro) | 1.18 | 1.18 | 2.9 | 0.85 |

| tetrahedron state | $\chi^0_{33}$ | $\chi^0_{11}$ | $v_e$ $10^{-21}$cm | $\sqrt{\langle g^2\rangle}$, K | $\tau^z_{0,\alpha}$, s $10^{-16}$ | $\tau^x_{0,\alpha}$, s $10^{-16}$ |
|---|---|---|---|---|---|---|
| +(Ferro) | 0.55 | 1.25 | 0.209 | — | 100 | — |
| 0(Glass) | 2.9 | 2.3 | — | 14.1 | 0.05 | — |
| -(Antiferro) | 0.23 | 0.7 | 0.211 | — | 40 | — |

Table 2. Parameters for $Rb_{1-x}(ND_4)_xD_2PO_4$

| tetrahedron state | $\varepsilon_\alpha$ K | $w_\alpha$ K | $\nu_{1,\alpha\alpha}(0)$ K | $\nu_{2,\alpha\alpha}(k^z)$ K | $\nu_{2,\alpha\alpha}(0)$ K |
|---|---|---|---|---|---|
| +(Ferro) | 160 | 1100 | 22.76 | 25 | 20 |
| 0(Glass) | — | — | -44 | 40 | -60 |
| -(Antiferro) | -140 | 750 | -40 | 67.44 | -20 |

| tetrahedron state | $d^z_\alpha(G), 10^{-18}$ esu·cm | $d^z_\alpha(F), 10^{-18}$ esu·cm | $d^x_\alpha(G), 10^{-18}$ esu·cm | $d^x_\alpha(F), 10^{-18}$ esu·cm |
|---|---|---|---|---|
| +(Ferro) | 0.95 | 0.95 | 3.25 | 3.25 |
| 0(Glass) | 1.7 | 0.9 | 3.55 | 1.0 |
| -(Antiferro) | 1.65 | 1.65 | 3.15 | 1.0 |

| tetrahedron state | $\chi^0_{33}$ | $\chi^0_{11}$ | $v_e$ $10^{-21}$cm | $\sqrt{\langle g^2\rangle}$, K | $\tau^z_{0,\alpha}$, s $10^{-14}$ | $\tau^x_{0,\alpha}$, s $10^{-14}$ |
|---|---|---|---|---|---|---|
| +(Ferro) | 0.8 | 0.8 | 0.209 | — | 2.0 | 3 |
| 0(Glass) | 0.6 | 0.7 | — | 24.5 | 0.55 | 6 |
| -(Antiferro) | 0.34 | 0.58 | 0.211 | — | 6.0 | 3 |

$K_{1-x}(NH_4)_xH_2PO_4$ ($T_c(x=0)=122$K, $T_N(x=1)=148$K) are presented in Tables 1-4, respectively. The dashes in the tables means that the given tetrahedron is averaged over two states only (without the neutral state 0 (Glass)).

Table 3. Parameters for $Rb_{1-x}(NH_4)_xH_2AsO_4$

| tetrahedron state | $\varepsilon_\alpha$ K | $w_\alpha$ K | $\nu_{1,\alpha\alpha}(0)$ K | $\nu_{2,\alpha\alpha}(k^z)$ K | $\nu_{2,\alpha\alpha}(0)$ K |
|---|---|---|---|---|---|
| +(Ferro) | 60 | 500 | 9.83 | 5 | 5 |
| 0(Glass) | — | — | -15 | 22 | -25 |
| -(Antiferro) | -100 | 470 | -80 | 75.19 | 5 |

| tetrahedron state | $d^z_\alpha(G), 10^{-18}$ esu·cm | $d^z_\alpha(F), 10^{-18}$ esu·cm | $d^x_\alpha(G), 10^{-18}$ esu·cm | $d^x_\alpha(F), 10^{-18}$ esu·cm |
|---|---|---|---|---|
| +(Ferro) | 0.88 | 0.59 | 2.55 | 2.55 |
| 0(Glass) | 1.2 | 0.59 | 3.2 | 3.2 |
| -(Antiferro) | 1.35 | 1.35 | 3.15 | 1.0 |

| tetrahedron state | $\chi^0_{33}$ | $\chi^0_{11}$ | $v_e$ $10^{-21}$cm | $\sqrt{\langle g^2\rangle}$, K | $\tau^z_{0,\alpha}$, s $10^{-14}$ | $\tau^x_{0,\alpha}$, s $10^{-14}$ |
|---|---|---|---|---|---|---|
| +(Ferro) | 0.5 | 0.7 | 0.2236 | — | 60 | 7 |
| 0(Glass) | 0.45 | 1.1 | — | 10 | 60 | 7 |
| -(Antiferro) | 0.3 | 0.7 | 0.2275 | — | 60 | 7 |

Table 4. Parameters for $K_{1-x}(NH_4)_xH_2PO_4$

| tetrahedron state | $\varepsilon_\alpha$ K | $w_\alpha$ K | $\nu_{1,\alpha\alpha}(0)$ K | $\nu_{2,\alpha\alpha}(k^z)$ K | $\nu_{2,\alpha\alpha}(0)$ K |
|---|---|---|---|---|---|
| +(Ferro) | 65 | 450 | 13.54 | -70 | -60 |
| 0(Glass) | — | — | -28 | 5 | -50 |
| -(Antiferro) | -60 | 500 | 10 | 46.8 | -35 |

| tetrahedron state | $d^z_\alpha(G), 10^{-18}$ esu·cm | $d^z_\alpha(F), 10^{-18}$ esu·cm | $d^x_\alpha(G), 10^{-18}$ esu·cm | $d^x_\alpha(F), 10^{-18}$ esu·cm |
|---|---|---|---|---|
| +(Ferro) | 0.84 | 0.73 | 2.75 | 2.75 |
| 0(Glass) | 0.85 | 0.73 | 2.95 | 1.75 |
| -(Antiferro) | 1.18 | 1.18 | 2.9 | 0.85 |

| tetrahedron state | $\chi^0_{33}$ | $\chi^0_{11}$ | $v_e$ $10^{-21}$cm | $\sqrt{\langle g^2\rangle}$, K | $\tau^z_{0,\alpha}$, s $10^{-14}$ | $\tau^x_{0,\alpha}$, s $10^{-14}$ |
|---|---|---|---|---|---|---|
| +(Ferro) | 0.85 | 0.8 | 0.1946 | — | — | — |
| 0(Glass) | 0.55 | 0.75 | — | 10 | — | — |
| -(Antiferro) | 0.23 | 0.7 | 0.2110 | — | — | — |

### 4.2. Spontaneous polarization

The calculated temperature curves of spontaneous polarization for $Rb_{1-x}(NH_4)_xH_2PO_4$, $Rb_{1-x}(ND_4)_xD_2PO_4$, $Rb_{1-x}(NH_4)_xH_2AsO_4$, $K_{1-x}(NH_4)_xH_2PO_4$ compounds along with the available experimental



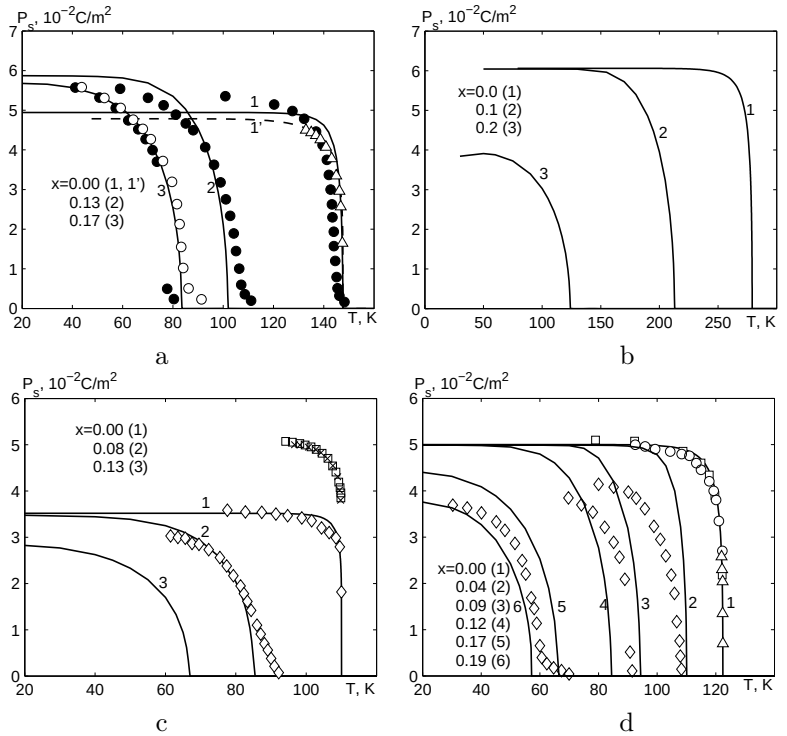


Figure 2. Temperature behavior of spontaneous polarization of a tetrahedron $P^z_s = P^z/v_e$ in the ferroelectric region of the phase diagram for $Rb_{1-x}(NH_4)_xH_2PO_4$ (a) at $x$: 0.0 – 1, 1' [95], Δ [118]; 0.1 – 2; 0.15 – 3; for $Rb_{1-x}(ND_4)_xD_2PO_4$ (b) at $x$: 0.0 – 1; 0.1 – 2; 0.2 – 3; for $Rb_{1-x}(NH_4)_xH_2AsO_4$ (c) at $x$: 0.0 – 1, ◇ [18], ▫ [119], × [120]; 0.08 – 2; 0.13 – 3; for $K_{1-x}(NH_4)_xH_2PO_4$ (d) at $x$: 0.0 – 1, ○ - [121], ▫ [122], △ [123]; 0.12 – 2; 0.17 – 3.

data are shown in fig. 2.

The calculated dependences $P_s(T)$ well describe the experimental data at $x$=0. With increasing $x$ the theory predicts a decrease of spontaneous polarization, until it completely vanishes at the concentration corresponding to the transition into the glass phase composition region. The temperatures, at which the spontaneous polarization arises in the ferroelectric phase, or the spontaneous sublattice polarization arises in the antiferroelectric phase, at different $x$ yield the $T_c(x)$ or $T_N(x)$

dependences, respectively.

Let us note that at small $x$ the saturation polarization is almost independent of $x$ (curves 1 and 2 for all compounds), even though the order parameter $\bar{\eta}(x,T)$ at small $T$ decreases with $x$. As seen from Eq. (2.9) the polarization is determined by the product $\langle d^z \rangle_c \bar{\eta}$. For all explored compounds the following relation is obeyed $d^z_-(F) > d^z_+(F)$, and the average $\langle d^z \rangle$ increases with $x$, whereas the low-temperature polarization of a tetrahedron is almost independent of $x$. With increasing $x$ the parameter $\bar{\eta}$ rapidly decreases at low $T$, which leads to a rapid decrease of saturation polarization. The calculated curves for $Rb_{1-x}(NH_4)_xH_2PO_4$ in the composition range indicate a certain increase of the saturation polarization with increasing x. In the discussed model the spontaneous polarization is given by the product . The parameter weakly decreases with increasing at small ammonium concentrations. However, rapidly tends to zero, when , which leads to disappearance of polarization. Besides, the component of the dipole moment increases monotonically with increasing , which follows from (2) and from the analysis of experimental data: esu cm, esu cm, esu cm.

The calculated temperature curves of spontaneous polarization for the $K_{1-x}(NH_4)_xH_2PO_4$ compounds well describe the experimental data at 0.0 and 0.19. However, the calculated saturation polarizations at 0.0; 0.04; 0.09 are close each to other but at 0.04; 0.09 is by 20higher than the experimental data. In our opinion, the spontaneous polarization for experimental samples with 0.4; 0.9 did not reached its saturation value, because samples could contain domains with opposite polarizations.

### 4.3. Molar specific heat

The experimental points for the proton contribution $\Delta C_p$ to the specific heat of the considered systems should be determined by subtracting the lattice contribution from the measured specific heat; the lattice contribution in the phase transition region is approximated by a linear dependence. The proposed theory, as seen in figs. 3-6, properly describes the temperature dependence of proton contribution to the molar specific heat of the $Rb_{1-x}(NH_4)_xH_2PO_4$, $Rb_{1-x}(ND_4)_xD_2PO_4$, $Rb_{1-x}(NH_4)_xH_2AsO_4$, $K_{1-x}(NH_4)_xH_2PO_4$ compounds at $x$=0 and $x$=1. At compositions other than $x$=0 or $x$=1 the theory predicts a decrease of the jump of specific heat at $T_c$ and $T_N$ and its vanishing at $x$ in the proton glass composition region. To answer the question about the validity of the proposed theory for the $Rb_{1-x}(NH_4)_xH_2PO_4$ type systems, further experimental investigation of the temperature dependences of specific heat of these crystals in a wide composition range are required.



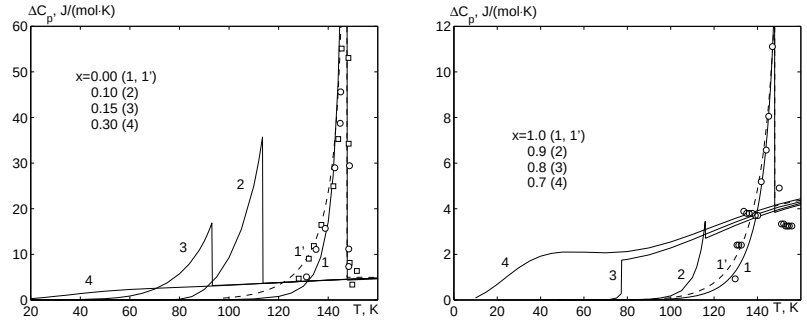


Figure 3. Temperature behavior of the proton contribution $\Delta C_p$ into the specific heat of $Rb_{1-x}(NH_4)_xH_2PO_4$ in the ferroelectric (a) region of the phase diagram at $x$: 0.0 – 1, 1' [95], ▫ [124], ○ [125]; 0.1 – 2; 0.15 – 3; 0.3 – 4 and in the antiferroelectric region at $x$: 1.0 – 1, 1' [95], ○ [126]; 0.9 – 2; 0.8 – 3; 0.7 – 4; 0.74 – ◇ [48].

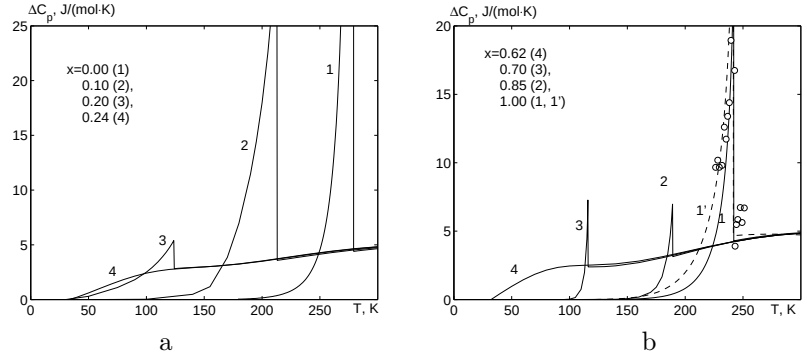


Figure 4. Temperature behavior of the proton contribution $\Delta C_p$ into the specific heat of $Rb_{1-x}(ND_4)_xD_2PO_4$ in the ferroelectric (a) region of the phase diagram at $x$: 0.0 – 1; 0.1 – 2; 0.2 – 3; 0.24 – 4 and in the antiferroelectric region at $x$: 1.0 – 1, ○ [126], 1' [95]; 0.85 – 2; 0.7 – 3; 0.62 – 4.

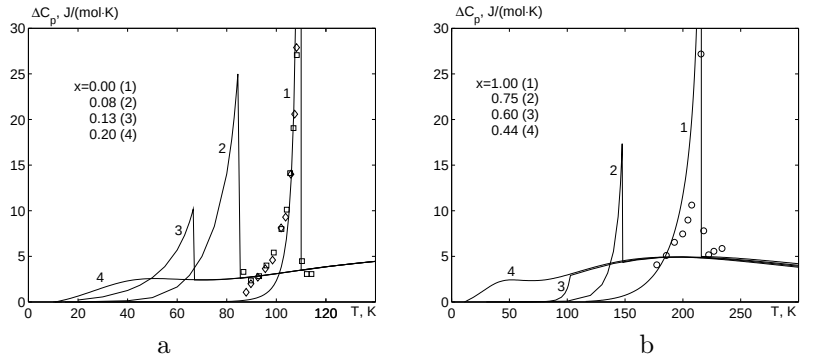


Figure 5. Temperature behavior of the proton contribution $\Delta C_p$ into the specific heat of $Rb_{1-x}(NH_4)_xH_2AsO_4$ in the ferroelectric (a) region of the phase diagram at $x$: 0.0 – 1, ▫ [119], ◇ [120]; 0.08 – 2; 0.13 – 3; 0.2 – 4 and in the antiferroelectric region at $x$: 1.0 – 1, ○ [127]; 0.75 – 2; 0.6 – 3; 0.45 – 4.

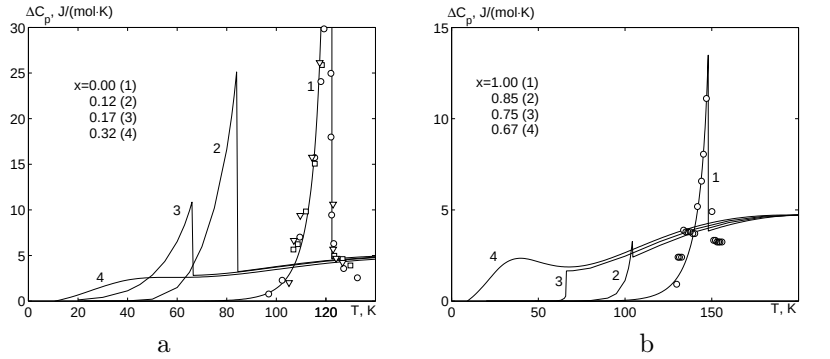


Figure 6. Temperature behavior of the proton contribution $\Delta C_p$ into the specific heat of $K_{1-x}(NH_4)_xH_2PO_4$ in the ferroelectric (a) region of the phase diagram at $x$: 0.0 – 1, ○ [128], ▽ [129], ▫ [130]; 0.12 – 2; 0.17 – 3; 0.32 – 4 and in the antiferroelectric region at $x$: 1.0 – 1, ○ [126]; 0.85 – 2; 0.75 – 3; 0.67 – 4.

### 4.4. The Edwards-Anderson parameter

The cumulant Edwards-Anderson parameter $Q_{EA}(T)$ of the $Rb_{1-x}(NH_4)_xH_2PO_4$ type compounds is different from zero at all



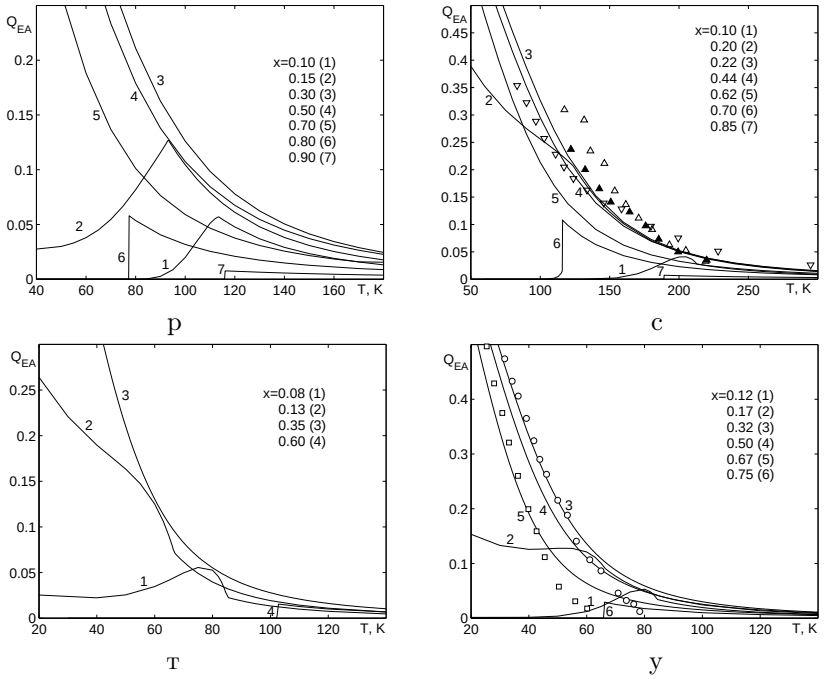


Figure 7. The temperature dependence of the Edwards-Anderson parameter $Q_{EA}$ for $Rb_{1-x}(NH_4)_xH_2PO_4$ (a) at $x$: 0.1 – 1; 0.15 – 2; 0.3 – 3; 0.5 – 4; 0.7 – 5; 0.8 – 6; 0.9 – 7; for $Rb_{1-x}(ND_4)_xD_2PO_4$ at different $x$: 0.1 – 1; 0.2 – 2; 0.22 – 3, ▲ [39]; 0.44 – 4, △ [39], ▽ [69]; 0.62 – 5; 0.7 – 6; 0.85 – 7; for $Rb_{1-x}(NH_4)_xH_2AsO_4$ at different $x$: 0.08 – 1; 0.13 – 2; 0.35 – 3; 0.6 – 4; for $K_{1-x}(NH_4)_xH_2PO_4$ at different $x$: 0.12 – 1; 0.17 – 2; 0.32 – 3; 0.5 – 4; 0.67 – 5; 0.75 – 6.

temperatures and concentrations $x$, except for $x = 0$ and $x = 1$ (fig. 7). This is attributed to the internal random deformational fields, which arise due to different properties of NH4+ and K+, Rb+ ions. Let us note that the temperature and composition dependences of $Q_{EA}(T)$ are similar for all compounds. The parameter $Q_{EA}(T)$ has a rounded peak at the transition from the high-temperature paraelectric phase to the ferroelectric phase. This indicates a large local fluctuation of proton ordering parameter ( is the unit cell vector) at $T < T_c(x)$ , especially at compositions close to the boundary of the ferroelectric phase. It can be explained by existence of microdomains with different

polarization (up and down proton configuration) and microregions with antiferroelectric ordering of proton on bonds (lateral proton configuration). The parameter $Q_{EA}(T)$ rapidly falls to zero at the transition to the antiferroelectric phase. This indicates, mainly, the lateral proton configuration ordering at or $T < T_N(x)$ . The parameter $Q_{EA}(T)$ is the largest in the proton glass composition region and increases with decreasing temperature. The parameter $Q_{EA}(T)$ (curves 3, 4, 5 for $Rb_{1-x}(NH_4)_xH_2PO_4$, $Rb_{1-x}(ND_4)_xD_2PO_4$, $K_{1-x}(NH_4)_xH_2PO_4$, 3 for $Rb_{1-x}(NH_4)_xH_2AsO_4$,) increases quickly from about 0.05-0.1 , which corresponds approximately to the upper inflection points of the $\varepsilon'_{33}(T,0)$ and $\varepsilon'_{11}(T,0)$ dependences at the transition from the high-temperature to the low-temperature region of the paraelectric phase (here $Q_{EA}(T)$ = 0.3-0.4), lying below the temperature maximum of $\varepsilon'_{33}(T,0)$ and $\varepsilon'_{11}(T,0)$ dependences. For $Rb_{1-x}(ND_4)_xD_2PO_4$ at $x = 0.22$ the theoretical curve 3 (fig. 7 (b)) satisfactorily describes the experimental data of [39]. At the same time, at $x = 0.44$ our calculations agree with the data of [69] but the obtained values are lower than those of [39], both for $x = 0.44$ and $x = 0.22$. We think that this can be explained by an incorrectly determined composition $x$ of the samples in [39].

For $K_{1-x}(NH_4)_xH_2PO_4$ for the temperatures above the inflection points the experimental data for $Q_{EA}(T)$ calculated from the dielectric data [40], lie below the theoretical curves. However, for the deuterated system $Rb_{1-x}(ND_4)_xD_2PO_4$ the data of our calculations [83] and NMR measurements [39, 69] coincide. So one can assume that the different temperature behavior of $Q_{EA}(T)$ for $K_{1-x}(NH_4)_xH_2PO_4$ and $Rb_{1-x}(ND_4)_xD_2PO_4$ may be caused either by tunneling not taken into account in our calculations or by different methods of determination of $Q_{EA}(T)$ dependences from different experimental data.

Unfortunately, no experimental data for $Q_{EA}(T)$ in other compounds of this type were available.

### 4.5. Longitudinal dielectric permittivity

In fig. 8–11 we show the temperature cures of the longitudinal static permittivity of $\varepsilon'_{33}(T,0)$ ($\varepsilon'_{33}(T,0) = \varepsilon_{33}(T)$) of the $Rb_{1-x}(NH_4)_xH_2PO_4$ type compounds at different $x$ along with the experimental data for $\varepsilon'_{33}(T,\omega)$ at low frequencies.

An essential difference between these quantities arises only in the proton glass composition region and at temperatures below the maximum of $\varepsilon'_{33}(T,\nu)$. Here $\varepsilon'_{33}(T,\nu)$ even at small $\nu$ always tends to $\varepsilon^0_{33}$, whereas the theoretical static permittivity $\varepsilon'_{33}(T,0)$ at $T \to 0$ tends to a certain finite value, larger than $\varepsilon^0_{33}$. At high temperatures the static and



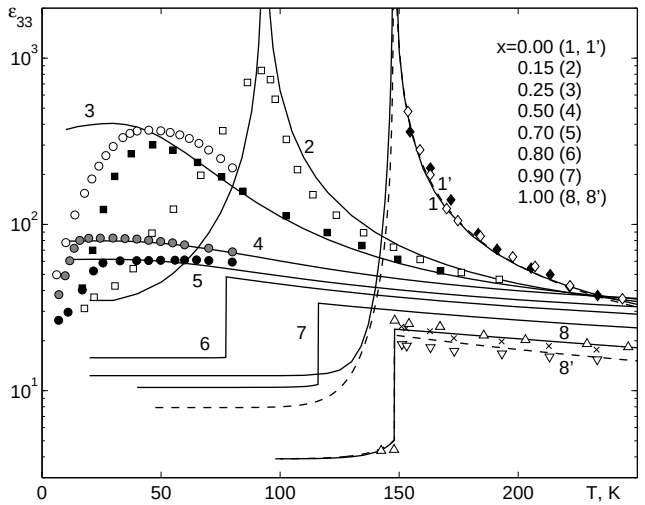


Figure 8. The temperature dependence of the longitudinal permittivity $\varepsilon'_{33}(T,0)$ of $Rb_{1-x}(NH_4)_xH_2PO_4$ at different $x$: 0.0 – 1, 1' [95], ◇ [131], ◆ [132]; 0.15 – 2, ▫ [3]; 0.25 – 3, ○ [2], ■ [3]; 0.5 – 4, ● [2] (1 kHz); 0.7 – 5, ● [2]; 0.8 – 6; 0.9 – 7; 1.0 – 8, 8' [95], △ [133], × [134], ▽ [133].

dynamic permittivities practically coincide; this permits us to talk about qualitative agreement or disagreement between the theoretical curves for $\varepsilon'_{33}(T,0)$ and experimental points for $\varepsilon'_{33}(T,\nu \neq 0)$.

In figure 8 we plot the temperature dependences of the longitudinal permittivity $\varepsilon'_{33}(T,0)$ for $Rb_{1-x}(NH_4)_xH_2PO_4$ at different $x$. The compositions with $x$=0.0 (curves 1, 1' and the experimental points), 0.15 (2) correspond to the transition to the ferroelectric phase, $x$=0.25 (3), 0.5 (4), 0.7 (5) correspond to the transition to the proton glass phase, whereas $x$=0.8 (6), 0.9 (7), 1.0 (8, 8') correspond to the transition to the antiferroelectric phase (experimental data are available for $x$=1.0 only). In the regions with the transition to the ferroelectric phase the calculated curves of $\varepsilon'_{33}(T,0)$ qualitatively correctly describe the temperature behavior of experimental data, but their values in the vicinity of the peak are much larger than experimental. This peak can be smeared out and lowered down, if we take into account macroscopic fluctuations of concentration $x$ as well as the piezoelectric effect. In the regions where the transition to the low-temperature proton glass takes place, the theory and experiment coincide quantitatively at temperatures above the

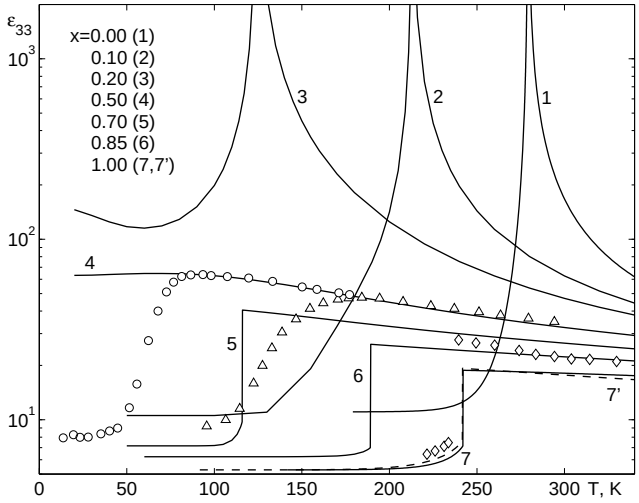


Figure 9. The temperature dependence of the longitudinal permittivity $\varepsilon'_{33}(T,\nu)$ of $Rb_{1-x}(ND_4)_xD_2PO_4$ at different $x$: 0.0 – 1; 0.1 – 2; 0.2 – 3; 0.5 – 4, ○ [9] (10 kHz), △ [10] (10 GHz); 0.7 – 5; 0.85 – 6; 1.0 – 7, 7' [95], ◇ [135].

peak of $\varepsilon'_{33}(T,\omega)$. At $x$=0.0, 1.0, considering the dispersion of experiment points, we can talk about a quantitative agreement of theoretical results with experimental points. For these compositions we also present the theoretical results [95] (dashed lines 1', 8', respectively), obtained with somewhat different values of the model parameters. Note that the changes in these values, as compared to those of [95], did not perceptibly change $\varepsilon'_{33}(T,0)$.

In figure 9 we show the temperature dependence of the longitudinal permittivity $\varepsilon'_{33}(T,\nu)$ of $Rb_{1-x}(ND_4)_xD_2PO_4$ at different $x$. At $x$=0.0 (1), 0.1 (2), 0.2 (3) (ferroelectric composition region) no experimental data were available. The experimental points for $x$=0.5 [9] (10 kHz), Δ [10] (10 GHz) correspond to the glass phase composition region (static curve 4). At $x$=0.7 (5), $x$=0.85 (6), $x$=1.0 (7) we have the antiferroelectric ordering region. Let us note that for $x$=1.0 the agreement with experiment for $\varepsilon_{33}(T)$ (curve 7') would be slightly better if a different set of the model parameter values was used [95].

In figure 10 the calculated longitudinal static permittivity $\varepsilon_{33}(T)$ for $Rb_{1-x}(NH_4)_xH_2AsO_4$ is compared with the experimental data for



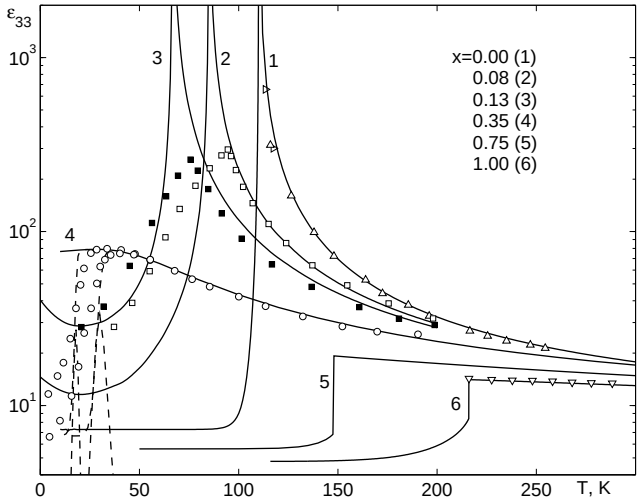


Figure 10. The temperature dependence of the longitudinal permittivity $\varepsilon'_{33}(T,\nu)$ of $Rb_{1-x}(NH_4)_xH_2AsO_4$ at different $x$: 0.0 – 1, △ [131], ▷ [136]; 0.08 – 2, ▫ [17] (1 MHz); 0.13 – 3, ▪ [17] (1 MHz); 0.35 – 4, ○ [15] (1 Hz, 30 KHz); 0.75 – 5; 1.0 – 6, ▽ [137]. The dashed lines correspond to the theoretical curves for $x$=0.35, $\nu$=1 Hz, 30 kHz.

$\varepsilon'_{33}(T,\nu\neq 0)$ for different compositions $x$ at low frequencies $\nu$. In the ferroelectric phase composition region ($x$=0; 0.08; 0.13) the static theory correctly describes parts of the curves above $T_c(x)$ as well as the position of the maximum of $\varepsilon'_{33}(T,\nu\to 0)$, but their values in the vicinity of the peak are much larger than experimental. This peak can be smeared out and lowered down, if we take into account macroscopic fluctuations of concentration $x$ as well as the piezoelectric effect. In the proton glass composition region the theory and experiment coincide quantitatively at temperatures above the peak of $\varepsilon'_{33}(T,\nu)$. At $x$=0.0, 1.0, considering the dispersion of experiment points, we can talk about a quantitative agreement of theoretical results with experimental points.

In figure 11 we plot the temperature curve of the longitudinal permittivity $\varepsilon'_{33}(T,\omega)$ for $K_{1-x}(NH_4)_xH_2PO_4$ at different $x$. Like for other systems, in the ferroelectric region the calculated values of $\varepsilon_{33}(T)$ in the vicinity of the peak are too high. The best agreement with experiment is obtained in regions of the so-called "pure" phases, that is, $x\to 0$, $x\to 1$, and $x$ in the middle of the glass phase composition range.

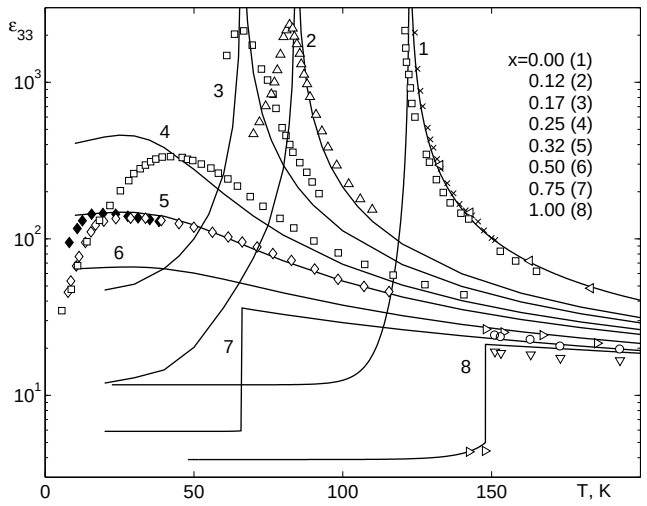


Figure 11. The temperature dependence of the longitudinal permittivity $\varepsilon'_{33}(T,0)$ of $K_{1-x}(NH_4)_xH_2PO_4$ in the ferroelectric region of the phase diagram at different $x$: 0.0 – 1, ▫ [22] (100 kHz), × [138], ◁ [121]; 0.12 – 2, △ [55] (175 Hz); 0.17 – 3, ▫ [22] (100 kHz); 0.25 – 4, ▫ [22] (100 kHz); 0.32 – 5, ◇ [19] (1к+ц), ◆ [20] (0.1 Hz); 0.5 – 6; 0.75 – 7; 1.0 – 8, ▷ [133], ○ - [134], ▽ - [139].

At low temperatures the experimental $\varepsilon'_{33}(T,\nu)$ rapidly decreases, because it is measured at non-zero frequencies. This decrease is qualitatively correctly described by the calculated real part of the dynamic permittivity $\varepsilon'_{33}(T,\nu)$ in the glass phase composition region, as shown in fig. 12 for $Rb_{1-x}(ND_4)_xD_2PO_4$ at $x$=0.5 and in fig. 10 (dashed lines) for $Rb_{1-x}(NH_4)_xH_2AsO_4$ $x$=0.35 (at $\nu$=1 Hz, 30 kHz).

In the glass phase composition region the maximum of $\varepsilon''_{33}(T,\nu)$ (approximately coincides with the low-temperature inflection point of $\varepsilon'_{33}(T,\nu)$) corresponds to the temperature, at which the relaxation time is close to the field period. For $Rb_{1-x}(ND_4)_xD_2PO_4$ at $x$=0.5 the calculated real and imaginary parts of $\varepsilon_{33}(T,\nu)$ at different frequencies satisfactorily describe the experimental data. The theory yields a faster decrease than the experiment for $\varepsilon'_{33}(T,\nu)$ and a more narrow and high peak for $\varepsilon''_{33}(T,\nu)$. We attribute this drawback to the imperfect procedure of configurational averaging of the susceptibility. In the case of $Rb_{1-x}(NH_4)_xH_2AsO_4$ the calculated imaginary part of $\varepsilon_{33}(T,\nu)$ has a



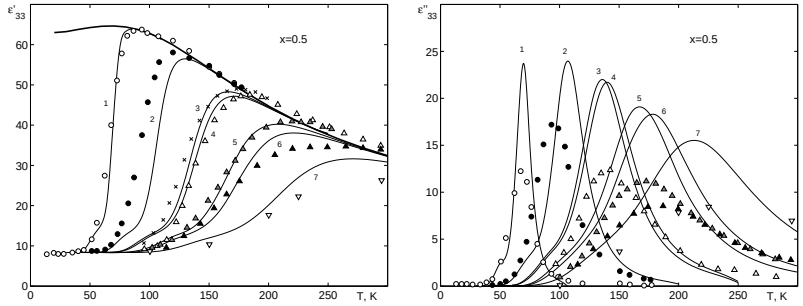


Figure 12. The temperature dependences of real $\varepsilon'_{33}(T,\nu)$ (a) and imaginary $\varepsilon''_{33}(T,\nu)$ (b) parts of longitudinal permittivity for $Rb_{1-x}(ND_4)_xD_2PO_4$ at $x$=0.5 and at different frequencies: 6 MHz – 1, 1' ○ [9]; 1 GHz – 2, 2', ● [9]; 8 GHz – 3, 3', × [10]; 10 GHz – 4, 4', △ [10]; 36 GHz – 5, 5', ▲ [10]; 52 GHz – 6, 6', ▲ [10]; 150 GHz – 7, 7', ▽ [10];

very narrow and high peak. This discrepancy can be possibly caused by the tunneling effects, essential in undeuterated compounds, which are not taken into account in our calculations performed within the Glauber dynamics approach.

At high temperatures the frequency dependence of the complex permittivity $\varepsilon(T,\nu)$ is close to the Debye type (fig. 13). At low temperatures the Debye-type behavior disappears. In the imaginary part of the permittivity a clear two-peak structure of the dielectric spectrum is observed. In the antiferroelectric phase the low-frequency peak is less pronounced.

We also calculated $\varepsilon'_{aa}(T,\nu)$, $\varepsilon''_{aa}(T,\nu)$ $(a=1,3)$ in the regions of ferroelectric and antiferroelectric ordering. At low frequencies and at temperatures near and above $T_c(x)$ $\varepsilon'_{aa}(T,\nu)$ practically coincides with the static permittivity $\varepsilon_{aa}(T)$. At low temperatures $\varepsilon''_{33}(T,\nu)$ has a peak (correspondingly, $\varepsilon'_{33}(T,\nu)$ has a bend ) (see fig. 14 for $x=0.2$).

With lowering $x$ the temperature position of this peak in $\varepsilon''_{aa}(T,\nu)$ practically does not change, but its height rapidly decreases. We failed to find this peak numerically at $x<0.15$. A similar peak is detected in the antiferroelectric phase region at $0.65<x<0.70$. Let us note that for the same frequency $\varepsilon''_{11}(T,\nu)<\varepsilon''_{33}(T,\nu)$ for all concentrations $x$, what agrees with the experimental data.

This sharp peak can be smeared out if we put $\omega\neq 0$ and perform

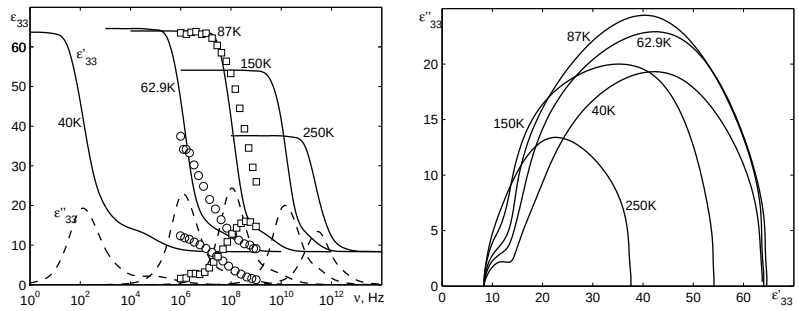


Figure 13. The frequency dependence of real $\varepsilon'_{33}(T,\nu)$ and imagine $\varepsilon''_{33}(T,\nu)$ parts of longitudinal permittivity (a) for $Rb_{1-x}(ND_4)_xD_2PO_4$ at $x$=0.5 at different temperatures: 40K, 62.9K $\circ$ [9], 87K $\square$ [9], 150K, 250K, and also the Cole-Cole curves (b) for these temperatures.

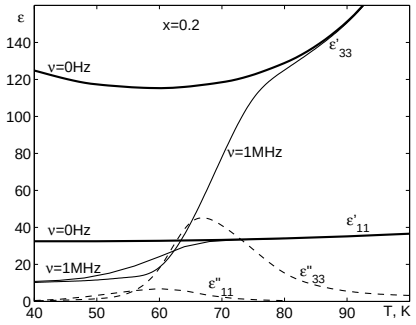


Figure 14. The temperature dependence of longitudinal $\varepsilon'_{11}(T,\nu)$ and transverse permittivities $\varepsilon'_{33}(T,\nu)$ for $Rb_{1-x}(ND_4)_xD_2PO_4$ compound for $x$=0.2 at 1 MHz.

an additional averaging over macroscopic fluctuations of concentration. For $x = 0.35$ the theory yields a faster decrease than experiment for $\varepsilon'_{33}(T,\omega)$, as well as a very narrow and sharp peak of $\varepsilon''_{33}(T,\omega)$.

In the case of undeuterated compounds of the $Rb_{1-x}(NH_4)_xH_2PO_4$ type a certain role in the low-temperature dynamics can be played by tunneling of protons on hydrogen bonds. To describe it we need to go beyond the scope of the method of Glauber kinetic equations. At the same time, the proposed here approach can be used for a qualitative evaluation of the behavior of the dynamic characteristics in this type of compounds.



It should be noted that both for the transverse and longitudinal permittivities the best description of experimental data is obtained in the regions of the so-called "pure" phases, that is $x \to 0$, $x \to 1$, and the glass phase region at $x \sim 0.5$ for $Rb_{1-x}(NH_4)_xH_2PO_4$, $Rb_{1-x}(ND_4)_xD_2PO_4$, $K_{1-x}(NH_4)_xH_2PO_4$ and $x \sim 0.35$ for $Rb_{1-x}(NH_4)_xH_2AsO_4$.

The proposed here approach can be used to describe of the dynamic characteristics of $Rb_{1-x}(ND_4)_xD_2PO_4$ compounds and to evaluate the qualitative behavior of the permittivities of $Rb_{1-x}(NH_4)_xH_2PO_4$, $Rb_{1-x}(NH_4)_xH_2AsO_4$, $K_{1-x}(NH_4)_xH_2PO_4$.

### 4.6. Transverse dielectric permittivity

In figures 15-18 we present the calculated temperature dependences of static transverse permittivity $\varepsilon'_{11}(T,0)$ ($\varepsilon'_{11}(T,0) = \varepsilon_{11}(T)$) of the $Rb_{1-x}(NH_4)_xH_2PO_4$ type compounds as well as experimental data for $\varepsilon'_{11}(T,\omega)$ at low frequencies. The transverse permittivity, in contrast to the longitudinal one, is finite at all compositions. At temperatures above $T_c(x)$ and $T_N(x)$ $\varepsilon_{11}(T)$ monotonically increases with increasing $x$, whereas $\varepsilon_{33}(T)$ monotonically decreases. Just like for $\varepsilon'_{33}(T,0)$, an essential difference between $\varepsilon'_{11}(T,0)$ and $\varepsilon'_{11}(T,\omega \neq 0)$ exists only in the composition range of the glass phase and at temperatures below the maximum of $\varepsilon'_{11}(T,\omega)$. Here $\varepsilon'_{11}(T,\omega)$ always tends to $\varepsilon^0_{11}$, whereas the theoretical static permittivity $\varepsilon'_{11}(T,0)$ at $T \to 0$ tends to a certain finite value larger than $\varepsilon^0_{11}(x)$. However, at high temperatures, like the longitudinal permittivity, the dynamic and static curves of the transverse permittivity practically coincide. This fact enables us to talk about qualitative agreement or disagreement between the theoretical curves for $\varepsilon'_{11}(T,0)$ and the experimental points for $\varepsilon'_{11}(T,\omega \neq 0)$.

In figure 15 we show the temperature behavior of the transverse permittivity $\varepsilon'_{11}(T,0)$ of $Rb_{1-x}(NH_4)_xH_2PO_4$ at different $x$. In the ferroelectric (curves 1, 1', 2) and antiferroelectric (curves 6, 7, 7') phase composition ranges the temperature curves of $\varepsilon'_{11}(T,0)$ have jumps at $T_c(x)$ and $T_N(x)$, respectively. The curves 3, 4, 5 correspond to the glass phase composition range. A similar temperature dependence of $\varepsilon'_{11}(T,0)$ is observed also for the other compounds of the $Rb_{1-x}(NH_4)_xH_2PO_4$ type. Overall the theoretical results satisfactorily agree with the experimental data. However, at $x$=0.8 (the antiferroelectric phase composition range) the theory yields a lower peak and a faster decrease of permittivity at the Neel temperature, than it is experimentally observed. In the ferro-

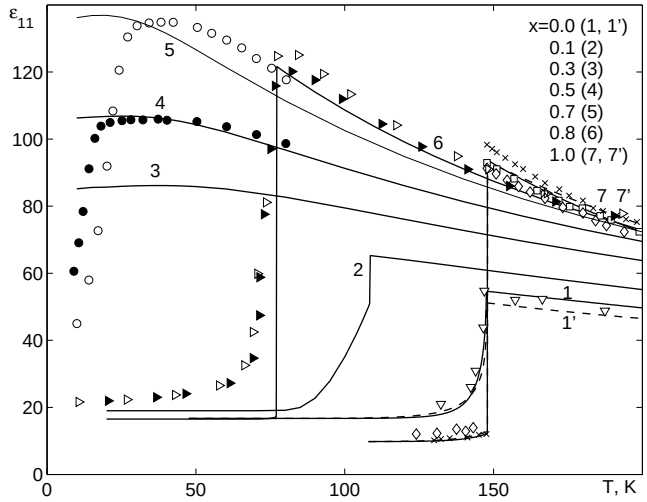


Figure 15. The temperature dependences of transverse permittivity $\varepsilon'_{11}(T,0)$ of $Rb_{1-x}(NH_4)_xH_2PO_4$ at different $x$: 0.0 – 1, 1' [95], ▽ [140]; 0.1 – 2; 0.3 – 3; 0.5 – 4, ● [2]; 0.7 – 5, ○ [2]; 0.8 – 6, ▷ (cool) [4], ▶ (heat) [4]; 1.0 – 7, 7' [95], × [141], ▫ [142], ◇ [22].



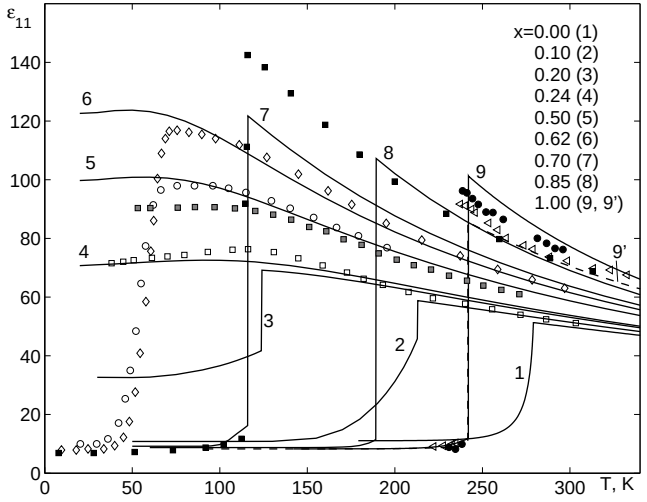


Figure 16. The temperature dependences of transverse permittivity $\varepsilon'_{11}(T,0)$ of $Rb_{1-x}(ND_4)_xD_2PO_4$ at different $x$: 0.0 – 1; 0.1 – 2; 0.2 – 3; 0.24 – 4, ▫ [12] (stat); 0.5 – 5, ▪ [12] (stat), ○ [9] (10 kHz); 0.62 – 6, ◇ [11] (300 Hz); 0.7 – 7, ▪ [12] (1к+ц); 0.85 – 8; 1.0 – 9, 9' [95], ● [141], ◁ [135].

electric phase the experimental data are available only for $x$=0.0. The curves 1' for $x$=0 and 7' for $x$=1 in fig. 15 are the theoretical calculations of [95], where a certain relation was used, being a partial case of (2.27) at $x$=0; 1. However, in that paper a somewhat different values of the model parameters is used. The found here sets of the model parameters permit us to describe the thermodynamic and dielectric characteristics at all compositions $x = [0, 1]$.

In figure 16 the theoretical static transverse permittivity $\varepsilon'_{11}(T,0)$ of $Rb_{1-x}(ND_4)_xD_2PO_4$ is compared with experimental data, including the data for the real part of the transverse permittivity $\varepsilon'_{11}(T,\omega \neq 0)$ at low frequencies $\omega$ [9, 11, 12, 135, 141]. For $x$=0.0 (curve 1), $x$=0.1 (2), $x$=0.2 (3) only the theoretical results are shown. As one can see, for $x$=0.24 (4), 0.50 (5), 0.62 (6) the theoretical calculations well agree with experimental data. At $x$=0.50 the presented experimental values for $\varepsilon'_{11}(T, \nu = 10kHz)$ of [9] are larger than the values of $\varepsilon'_{11}(T,0)$ obtained in [12] even at high temperatures. This can indicate an unreliable estimation of concentration $x$=0.50 in either of these papers or an uncertainty of the experimental data for $\varepsilon'_{11}(T,0)$. At $x$=0.7 (7) the calculated curve of $\varepsilon'_{11}(T,0)$ lies below the experimental points of [12] for 1 kHz. The most essential deviation from the experimental data is obtained at compositions close to $x \sim$0.2 and $x \sim$0.65, which are the transition regions between the ferroelectric and glass phases and between the antiferroelectric and glass phases. In these composition ranges we need to taken into account a possible coexistence of different phases. This will be a subject of a separate study.

In figure 17 the theoretical transverse permittivity $\varepsilon'_{11}(T,\omega)$ of $Rb_{1-x}(NH_4)_xH_2AsO_4$ is compared with available experimental data at low frequencies. The phase diagram is strongly asymmetric, and the proton glass state exists in the region $x = [0.2; 0.45]$. As seen, a good agreement with experiment takes place in the regions far from the phase boundaries (curves 1,2 for the ferroelectric state and 5, 6 for the antiferroelectric state). The value of $x$=0.15 corresponds to the intermediate region between the ferroelectric and proton glass phases. The rounded maximum in the experimental curve, most likely, is related to coexistence of ferroelectric and glass phases. Below the permittivity maximum

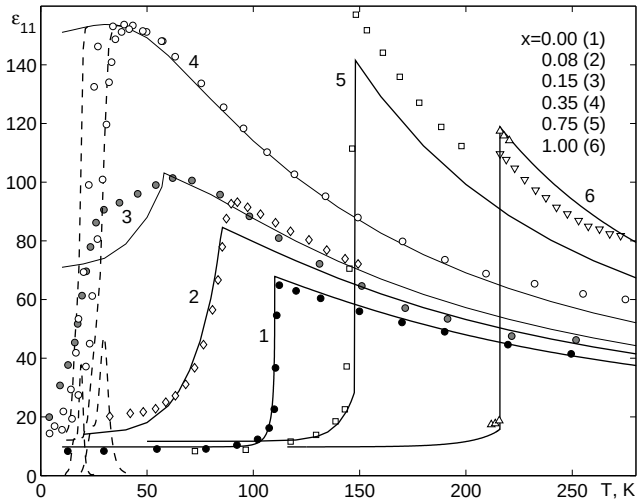


Figure 17. The temperature dependences of transverse permittivity $\varepsilon'_{11}(T,\omega)$ of $Rb_{1-x}(NH_4)_xH_2AsO_4$ at different $x$: 0.0 – 1, ● [16]; 0.08 – 2, ◇ [18] (1 kHz); 0.15 – 3, ◍ [16] (1+ц, 30 kHz); 0.35 – 4, ○ [15] (1 Hz, 30 kHz); 0.75 – 5, ▫ [17] (1 MHz); 1.0 – 6, ▽ [137], △ [143].

a similar to the described above for the glass phase deviation of the static theoretical curve from the experimental points at $\omega \neq 0$ takes place.

There is a lot of experimental data for the transverse permittivity of the $K_{1-x}(NH_4)_xH_2PO_4$ mixture (see fig. 18) for the compositions from the ferroelectric ($x$=0.0; 0.047; 0.166) and antiferroelectric ($x$=0.75; 0.85; 0.85; 1.0) regions. Just like in the above discussed compounds, the most prominent discrepancy between the theory and experiment is observed for the compositions of the transition regions (curves 3 and 7). Unfortunately, the experimental data for $K_{1-x}(NH_4)_xH_2PO_4$ at $x \sim 0.5$ are very limited. Most likely, this is caused by difficulties in growing these crystals at $x \sim 0.5$, since $x$ in the obtained samples depends on $x$ in the solution in a non-linear manner [36].

Let us consider now the dynamic permittivity $\varepsilon_{11}(T,\omega)$ in the proton glass phase ($x$=0.5) for $Rb_{1-x}(ND_4)_xD_2PO_4$. In figure 19 along with the available experimental data we plot the calculated temperature dependences of the real $\varepsilon'_{11}(T,\omega)$ and imaginary $\varepsilon''_{11}(T,\omega)$ parts of the permittivity at different frequencies. The maximum of $\varepsilon''_{11}(T,\omega)$ corresponds to the inflection point of the $\varepsilon'_{11}(T,\omega)$ curve. A large dispersion of the



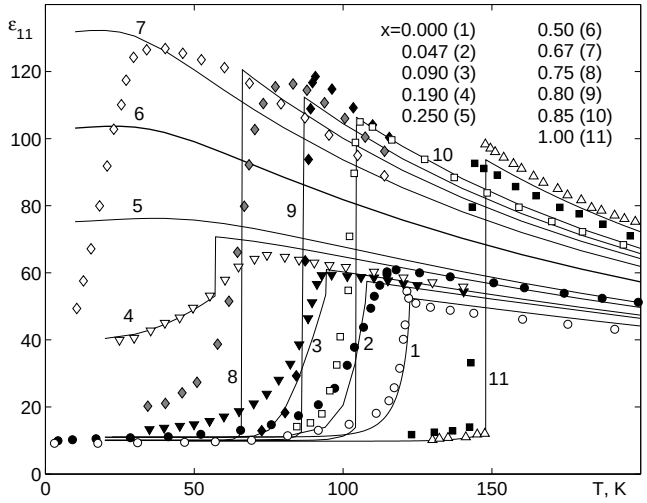


Figure 18. The temperature dependences of transverse permittivity $\varepsilon'_{11}(T,0)$ of $K_{1-x}(NH_4)_xH_2PO_4$ at different $x$: 0.0 – 1, ○ [54] (10 kHz), ◁ [139], ▷ [144]; 0.047 – 2, ● [54] (10 kHz); 0.166 – 3, ◍ [54] (10 kHz); 0.25 – 4; 0.5 – 5; 0.67 – 6, ◇ [19] (1 kHz); 0.75 - 7, ◇ [19] (1 kHz); 0.8 - 8, ◆ [19] (1 kHz); 0.85 - 9, ▫ [22] (100 kHz); 1.0 - 10, △ [141], × [142], ■ [22] (100 kHz).

experimental data takes place. For $\varepsilon'_{11}(T,\omega)$ the data of [9] (in the region of the low-temperature decrease) approximately correspond to the data of [12] for essentially lower frequencies. The points for $\nu$=10 kHz [12] ] in the decrease region are shifted to higher temperatures as compared to the points of [9] for $\nu$=10 kHz. The latters are very close to the data for $\nu$=1 Hz [12]. Then the points of [9] for $\varepsilon'_{33}(T,\omega)$ at $\nu$=10 MHz are shifted to lower temperatures as compared to the points of [12] at $\nu$=1 MHz. Our theoretical curves for $\nu$=10 kHz (curve 2), 10 MHz(3), 1 GHz (4) qualitatively well describe the experimental temperature behavior of $\varepsilon'_{11}(T,\omega)$ and $\varepsilon''_{11}(T,\omega)$ obtained in [9]. However, the theory yields a larger shift of the curves at changing frequency and a sharper shape and larger values of the imaginary part of the permittivity.

For $Rb_{1-x}(NH_4)_xH_2AsO_4$ (see fig. 17) at $x = 0.35$ (approximately the center of the glass phase) we also compared the theoretical results with the experimental data of [16] at frequencies $\nu$=1 Hz, 30 kHz. The theory also yields a faster, as compared to experimental, decrease of

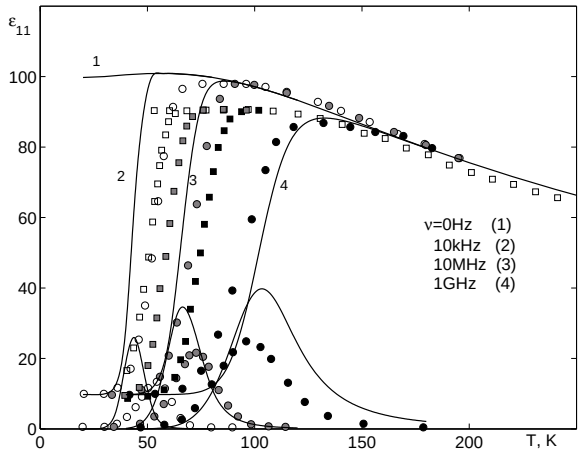


Figure 19. The temperature dependences of transverse permittivity $\varepsilon_{11}(T,\omega)$ of $Rb_{1-x}(ND_4)_xD_2PO_4$ at $x$=0.5 and different frequencies 0 Hz – 1; 1 Hz – ▫ [12]; 1 kHz – ▪ [12]; 10 kHz – 2, ○ [9]; 1 MHz – ▪ [12]; 10 MHz – 3, ● [9]; 1 GHz – 4, ● [9].

$\varepsilon'_{11}(T,\omega)$ with lowering temperature and a sharper shape and larger values of the imaginary part of the permittivity (dashed lines in fig. 17). This can be associated with an imperfect procedure of configurational averaging, as well as to neglected proton tunneling on hydrogen bonds in $Rb_{1-x}(NH_4)_xH_2AsO_4$.

### 4.7. Phase diagrams

The phase diagrams of the $Rb_{1-x}(NH_4)_xH_2PO_4$ system are constructed, using the calculated physical characteristics of the crystals. The following regions are present in these diagrams: HP (high-temperature region of paraelectric phase), LP (low-temperature region of paraelectric phase), F ( ferroelectric phase), AF (antiferroelectric phase) (figs. 21–22).

Typical peculiarities of the phase diagrams of the considered compounds will be discussed by the example of $Rb_{1-x}(ND_4)_xD_2PO_4$ ( fig.11 ). At high temperatures the system is in paraelectric phase. It region is designated like the HP, because here the reduce Edwards-Anderson parameter $Q_{EA}$ is small but different from zero and decreases with increasing temperature. For $x < 0.2$ and $x > 0.65$ a spontaneous polarization or sublattice spontaneous polarization arise at $T < T_c(x)$ and



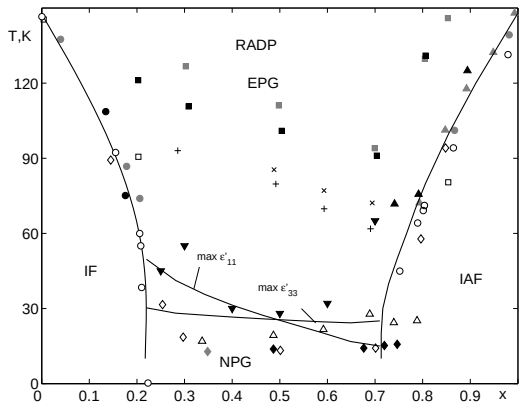


Figure 20. The phase diagram of the $Rb_{1-x}(NH_4)_xH_2PO_4$ mixture constructed using various physical characteristics ( ▼ – [2], ◇ , ◆ , ♦ – [32], ▫ , ▪ , ■ – [35], △ , ▲ , ▲ , +, × – [145], ○ , ● , ● – [146]). The solid lines are the $T_c$, $T_N$, and $T_g$ transitions obtained from the maxima of $\varepsilon'_{33}(T,0)$.

$T < T_N(x)$, respectively. As a result, the system goes to the ferroelectric or antiferroelectric state. Here the reduce Edwards-Anderson parameter $Q_{EA}$ can be significant ( fig.5) in vicinities of $T_c(x)$, $T_N(x)$ and in ferroelectric phase for $x$ close to glass phase composition region. In the central composition region we designate the low-temperature region of paraelectric phase. This region lies below the maxima of the static permittivities $\varepsilon_{11}(T)$ and $\varepsilon_{33}(T)$ ( the solid lines in fig.11, fig.12 ) and attributes large value of $Q_{EA}$. The dashed lines ($T_{g,11}(x,\nu)$ and $T_{g,33}(x,\nu)$) correspond to the low-temperature peaks of $\varepsilon''_{11}(T,\nu)$ and $\varepsilon''_{33}(T,\nu)$ at $\nu = 1$ MHz for $Rb_{1-x}(ND_4)_xD_2PO_4$ (the so-called freezing lines).These lines continue in the regions $x < 0.2$ and $x > 0.65$, where the paraelectric (or the proton glass) phase possibly coexists with ferroelectric or antiferroelectric phases, respectively. Numerical calculations show that $T_{g,11}(x,\nu) \to 0$ and $T_{g,33}(x,\nu) \to 0$ at $\nu \to 0$, so within the frame of our theory the averaged relaxation times for longitudinal and transverse permittivity have an Arrhenius-like temperature behavior that is $T_0 = 0$ (Vogel-Fulcher temperature). It should to note the approximation for averaged relaxation times on the basic of the experimental datum ( [10]) gives value $T_0 \approx$32K for x=0.5. The presented in this phase diagram experimental points of [50] were obtained by NMR studies.

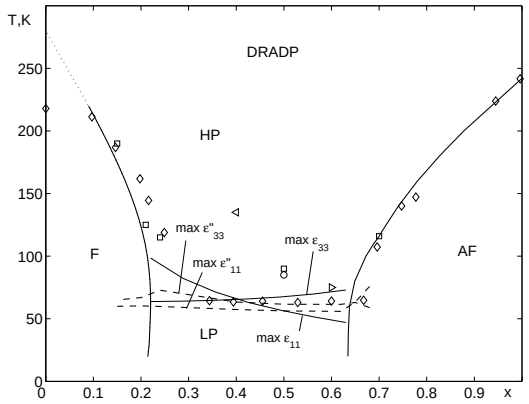


Figure 21. The phase diagram of the $Rb_{1-x}(ND_4)_xD_2PO_4$ mixture. ◁ – [7], ○ – [9], ▫ – [12], ▷– [13], ◇– [50]. The solid lines are the $T_c$, $T_N$, and $T_g$ transitions obtained from the maxima of $\varepsilon_{33}(T)$ and $\varepsilon_{11}(T)$. The dashed lines are the $T_g$ lines obtained from the maxima of $\varepsilon''_{33}(T,\nu)$ and $\varepsilon''_{11}(T,\nu)$ at frequency 1MHz.

The phase diagram of $Rb_{1-x}(NH_4)_xH_2AsO_4$ is strongly asymmetric (fig. 22), and the proton glass composition region exists at $x = (0.2; 0.45)$. The freezing lines $T_{g,11}(x,\nu)$ and $T_{g,33}(x,\nu)$ (dashed lines) correspond to the maxima of $\varepsilon''_{11}(\nu = 30$ kHz,T) and $\varepsilon''_{33}(\nu = 30$ kHz,T). The approximation on the basic of the experimental datum ( [17]) gives value $T_0 \approx$30K for x=0.36. According to the experimental data [18, 147] $T_{g,11}(x,\nu)$ is observed in the ferroelectric phase down to $x$=0.01. Also $T_{g,11}(x,\nu) \to 0$ with decreasing $x$. The calculations yield the freezing line down to $x \sim$0.15. Overall, the calculated phase diagram correctly describes the available experimental lines, even though some discrepancies are present. Thus, at the accepted values of the theory parameters the glass phase composition region is somewhat wider $x \sim [0.18; 0.46]$ than the experimental one $x \sim [0.22; 0.42]$. This difference can be related with an incorrectly determined concentration $x$ in experimental samples.

In the phase diagram of $Rb_{1-x}(NH_4)_xH_2PO_4$ (fig. 20) the temperatures of the phase transitions are lower than those of $Rb_{1-x}(ND_4)_xD_2PO_4$, whereas the glass phase region is wider. This is caused by influence of proton tunneling. The experimental points are obtained from dielectric permittivity measurements [2, 145, 146], Raman scattering [35] and X-ray diffraction [32].



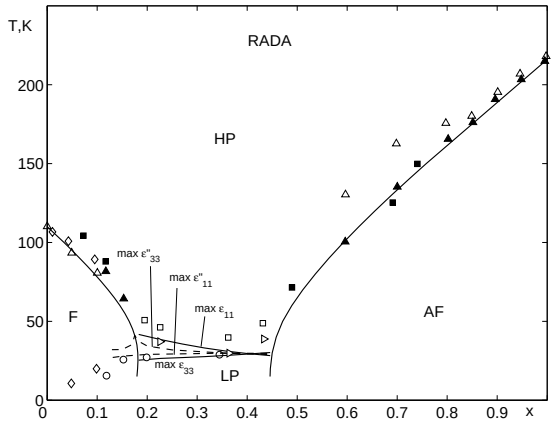


Figure 22. The phase diagram of the $Rb_{1-x}(NH_4)_xH_2AsO_4$ mixture. ▫ , ■ , ▷ - [17], ◇– [18]; ○ - [147], △ , ▲ - [148]. The solid lines are the $T_c$, $T_N$, and $T_g$ transitions obtained from the maxima of $\varepsilon_{33}(T)$ and $\varepsilon_{11}(T)$. The dashed lines are the $T_g$ lines obtained from the maxima of $\varepsilon''_{33}(T,\nu)$ and $\varepsilon''_{11}(T,\nu)$ at frequency 30kHz.

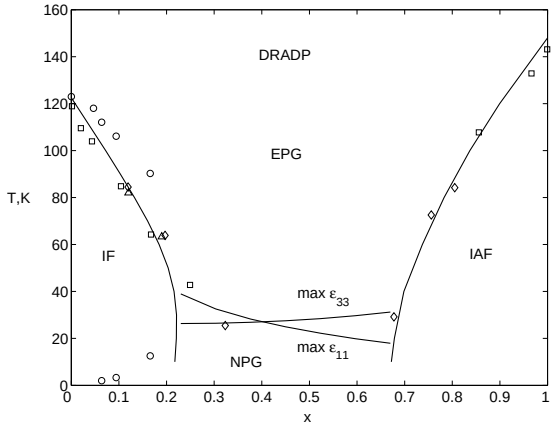


Figure 23. The phase diagram of the $K_{1-x}(NH_4)_xH_2PO_4$. ◇ - [19], ▫ – [22], ○– [54], △ - [55].The solid lines are the $T_c$, $T_N$, and $T_g$ transitions obtained from the maxima of $\varepsilon'_{33}(T,0)$ and $\varepsilon'_{11}(T,0)$.

The phase diagram of $K_{1-x}(NH_4)_xH_2PO_4$ (fig. 23) is qualitatively similar to that of $Rb_{1-x}(NH_4)_xH_2PO_4$. Its experimental points are obtained from the data for the maximum of the real part of transverse [19, 22, 54] and longitudinal [19, 22, 55] dielectric permittivities. By the circles at low temperatures in the ferroelectric phase we show the temperatures of the maximum of $\varepsilon''_{11}(T, \omega)$.

It should be noted that both for the transverse and longitudinal permittivities the best description of experimental data is obtained in the regions of the so-called "pure" phases, that is $x \to 0$, $x \to 1$, and the glass phase region at $x \sim 0.5$ for $Rb_{1-x}(NH_4)_xH_2PO_4$, $Rb_{1-x}(ND_4)_xD_2PO_4$, $K_{1-x}(NH_4)_xH_2PO_4$ and $x \sim 0.35$ for $Rb_{1-x}(NH_4)_xH_2AsO_4$.

## 5. Modified proton ordering model for the $KD_2PO_4$ type crystals

We consider a system of deuterons moving on O–D-...-O bonds in deuterated crystals of the $KD_2PO_4$ type. Axes of the reference system (x,y,z) coincide with the the tetragonal ($I\bar{4}2d$) crystallographic axes. The primitive cell of such a crystal is composed of two neighbouring $PO_4$ tetrahedra together with four hydrogen bonds attached to one of them ("$A$" type tetrahedra). Hydrogen bonds going to another ("$B$" type) tetrahedron belong to four nearest structural elements surrounding it (see fig. 24).

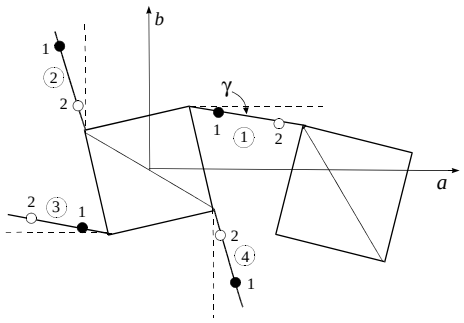


Figure 24. The primitive cell of the $KD_2PO_4$ crystal. One of possible ferroelectric proton configurations is shown.

The full model Hamitlonian of the deuteron subsystem of the $KD_2PO_4$ type ferroelectrics with taking into account the short-range and long-range interactions in presence of mechanical stresses $\sigma_6 = \sigma_{xy}$, $\sigma_4 = \sigma_{yz}$ and electric fields $+_3$, $+_1$ applied along the crystallographic axes $c$ and $a$ reads

$$\hat{H} = NU_{seed} + \hat{H}_{long} + \hat{H}_{short} - \sum_{qf}(\mu_{f1}E_1 + \mu_{f3}E_3)\frac{\sigma_{qf}}{2}, \qquad (4.1)$$

where $N$ is the number of the primitive cells; $\sigma_{qf}$ is the z-component pseudospin operator, describing the state of a deuteron in the q-th cell on the f-th bond. Two eigenvalues of the operator $\sigma_{qf} = \pm 1$ are assigned to two equilibrium positions of a deuteron on the bond. Effective dipole moments $\mu_1$, $\mu_3$, as shown in [149], are sums of the dipole moments of the tetrahedra and of hydrogen bonds, with

$$\mu_{11} = -\mu_{31} = \mu_1 \cos\gamma, \quad \mu_{21} = -\mu_{41} = \mu_2 \sin\gamma,$$
$$\mu_{13} = \mu_{23} = \mu_{33} = \mu_{43} = \mu_3.$$

The "seed" energy $U_{seed}$ is expressed in terms of the electric fields $E_1$ and $E_3$ and strains $\varepsilon_4$ and $\varepsilon_6$. It consists of the elastic, piezoelectric, and dielectric parts

$$U_{seed} = v(\frac{1}{2}c_{44}^{E0}\varepsilon_4^2 + \frac{1}{2}c_{66}^{E0}\varepsilon_6^2 - e_{14}^0\varepsilon_4 E_1 - e_{36}^0\varepsilon_6 E_3 -$$
$$-\frac{1}{2}\chi_{11}^{\varepsilon_0}E_1^2 - \frac{1}{2}\chi_{33}^{\varepsilon_0}E_3^2), \qquad (4.2)$$

where $v$ is the primitive cell volume, $c_{44}^{E0}$, $c_{66}^{E0}$, $e_{14}^0$, $e_{36}^0$, $\chi_{11}^{\varepsilon_0}$, $\chi_{33}^{\varepsilon_0}$ are the "seed" elastic constants, piezoelectric coefficients, and dielectric susceptibilities. The "seed" characteristics determine the temperature dependences of the corresponding physical characteristics far from the transition temperature $T_c$.

The Hamiltonian $\hat{H}_{long}$ includes the long-range and indirect lattice-mediated interactions between deuterons taken into account in the mean field approximation, as well as the linear over the strains $\varepsilon_4$ and $\varepsilon_6$ mean field [98, 99] induced by the piezoelectric coupling. $\hat{H}_{short}$ is the Hamiltonian of the short-range interactions between the deuterons.

The dielectric, piezoelectric, and elastic characteristics of the $KD_2PO_4$ type crystals will be explored using the thermodynamic potential. Taking into accounts the peculiarities of the crystalline structure of $KD_2PO_4$, to find the thermodynamic potential we shall use the four-particle cluster approximation [90]. In this approximation the thermodynamic potential of $KD_2PO_4$ reads

$$G = NU_{seed} + \frac{1}{2}\sum_{\substack{qq'\\ ff'}} J_{ff'}(qq')\frac{\langle\sigma_{qf}\rangle}{2}\frac{\langle\sigma_{q'f'}\rangle}{2} - \qquad (4.3)$$

$$-\frac{1}{2}T\sum_q\sum_{f=1}^{4}\ln Z_{1f}-T\sum_q\ln Z_4-Nv(\sigma_4\varepsilon_4+\sigma_6\varepsilon_6),$$

where $Z_{1f}=Spe^{-\beta\hat H_{qf}^{(1)}}$, $Z_4=Spe^{-\beta\hat H_q^{(4)}}$ are the single-particle and four-particle partition functions. The single-particle $\hat H_{qf}^{(1)}$ and four-particle $\hat H_q^{(4)}$ deuteron Hamiltonians of deformed $KD_2PO_4$ crystals are given by the expressions

$$\hat H_{qf}^{(1)}(j)=\frac{\bar x_{fj}}{\beta}\frac{\sigma_{qf}}{2}, \tag{4.4}$$

$$\begin{aligned}
&\hat H_q^{(4)}=(-\delta_{s6}\varepsilon_6-2\delta_{16}\varepsilon_6)\times \\
&\times\Big(\frac{\sigma_{q1}}{2}\frac{\sigma_{q2}}{2}\frac{\sigma_{q3}}{2}+\frac{\sigma_{q1}}{2}\frac{\sigma_{q2}}{2}\frac{\sigma_{q4}}{2}+\frac{\sigma_{q1}}{2}\frac{\sigma_{q3}}{2}\frac{\sigma_{q4}}{2}+\frac{\sigma_{q2}}{2}\frac{\sigma_{q3}}{2}\frac{\sigma_{q4}}{2}\Big)+\\
&+2(\delta_{a4}\varepsilon_4-\delta_{14}\varepsilon_4)\Big(\frac{\sigma_{q1}}{2}\frac{\sigma_{q2}}{2}\frac{\sigma_{q4}}{2}-\frac{\sigma_{q2}}{2}\frac{\sigma_{q3}}{2}\frac{\sigma_{q4}}{2}\Big)+\\
&+(V_s+\delta_{a6}\varepsilon_6)\Big(\frac{\sigma_{q1}}{2}\frac{\sigma_{q2}}{2}+\frac{\sigma_{q3}}{2}\frac{\sigma_{q4}}{2}\Big)+\\
&+(V_s-\delta_{a6}\varepsilon_6)\Big(\frac{\sigma_{q2}}{2}\frac{\sigma_{q3}}{2}+\frac{\sigma_{q4}}{2}\frac{\sigma_{q1}}{2}\Big)+\\
&+U_s\Big(\frac{\sigma_{q1}}{2}\frac{\sigma_{q3}}{2}+\frac{\sigma_{q2}}{2}\frac{\sigma_{q4}}{2}\Big)+\Phi_s\frac{\sigma_{q1}}{2}\frac{\sigma_{q2}}{2}\frac{\sigma_{q3}}{2}\frac{\sigma_{q4}}{2}-\\
&-\frac{1}{4}(\delta_{s6}\varepsilon_6-2\delta_{16}\varepsilon_6)\sum_{f=1}^{4}\frac{\sigma_{qf}}{2}-\frac{1}{2}(\delta_{a4}\varepsilon_4+\delta_{14}\varepsilon_4)\Big(\frac{\sigma_{q1}}{2}-\frac{\sigma_{q3}}{2}\Big)-\\
&-\sum_{f=1}^{4}\frac{x_{fj}}{\beta}\frac{\sigma_{qf}}{2}.
\end{aligned} \tag{4.5}$$

In (4.4), (4.5) we used the following notations

$$\begin{aligned}
x_{\frac{1}{3}j}&=\beta[-\Delta_j+2\nu_1\eta_1^{(1)}(j)+2\nu_{\frac{3}{1}}\eta_3^{(1)}(j)+2\nu_2\eta_2^{(1)}(j)+2\nu_2\eta_4^{(1)}(j)+\\
&\quad -2\psi_6\varepsilon_6\pm2\psi_4\varepsilon_4\pm\mu_1\cos\gamma E_1+\mu_3E_3],\\
x_{\frac{2}{4}j}&=\beta[-\Delta_j+2\nu_2\eta_1^{(1)}(j)+2\nu_2\eta_3^{(1)}(j)+2\nu_{\frac{3}{1}}\eta_2^{(1)}(j)+2\nu_{\frac{3}{1}}\eta_4^{(1)}(j)+\\
&\quad -2\psi_6\varepsilon_6\pm\mu_1\sin\gamma E_1+\mu_3E_3],\qquad j=4,6.
\end{aligned} \tag{4.6}$$

$$\bar x_{fj}=-\beta\Delta+x_{fj}.$$

Here $\eta_f^{(1)}(j)=\langle\sigma_{qf}\rangle$;

$$\nu_1=\frac{J_{11}}{4},\quad \nu_2=\frac{J_{12}}{4},\quad \nu_3=\frac{J_{13}}{4};$$



$J_{ff'}=\sum\limits_{R_q-R_{q'}}J_{ff'}(qq')$ is the Fourier transform of the long-range interaction constants; $\psi_4$, $\psi_6$ are the so-called deformation potentials;

$$V_s=-\frac{w_1}{2},\quad U_s=\frac{w_1}{2}-\varepsilon,\quad \Phi_s=4\varepsilon-8w+2w_1,$$

p $\varepsilon=\varepsilon_a-\varepsilon_s$, $w=\varepsilon_1-\varepsilon_s$, $w_1=\varepsilon_0-\varepsilon_s$ are the so-called Slater energies; $\Delta$ is the effective cluster field created by the neighboring bonds from outside the cluster.

If the crystal is free from external electric field and stress, the equation for the mean pseudospin value $\eta^{(1)}$ is

$$\eta^{(1)}=\frac{\mathrm{sh}(2x+\beta\delta_{s6}\varepsilon_6)+2b\,\mathrm{sh}(x-\beta\delta_{16}\varepsilon_6)}{\mathrm{ch}(2x+\beta\delta_{s6}\varepsilon_6)+4b\,\mathrm{ch}(x-\beta\delta_{16}\varepsilon_6)+2a+d},$$

where

$$x=\frac{1}{2}\ln\frac{1+\eta^{(1)}}{1-\eta^{(1)}}+\beta\nu_c\eta^{(1)}-\beta\psi_6\varepsilon_6=z_6,\quad \nu_c=\nu_1+2\nu_2+\nu_3,$$

$$a=\exp^{-\beta\varepsilon},\qquad b=\exp^{-\beta w},\qquad d=\exp^{-\beta w_1},\qquad \beta=1/k_BT.$$

## 6. Dielectric, piezoelectric, and elastic characteristics of the $MD_2XO_4$ ferroelectrics

Let us find first the dynamic characteristics of the $MD_2XO_4$ crystals, namely, the frequency dependent dielectric susceptibilities of mechanically free and clamped crystals; then the expressions for the static dielectric, piezoelectric, and elastic characteristics at $\omega\to0$ will be given.

### 6.1. Longitudinal dynamic dielectric susceptibility

The dynamic properties of the $MD_2XO_4$ crystals in presence of the stress $\sigma_6$ will be considered using the dynamic model of deuterated ferroelectric crystals of this type,nd based on the stochastic Glauber model. Using the procedure developed in [113,114], we obtain the following system of equations for the time dependent deuteron distribution functions

$$-\alpha\frac{d}{dt}\langle\prod_f\sigma_{qf}\rangle=\sum_{f'}\left\{\langle\prod_f\sigma_{qf}\left[1-\sigma_{qf'}\tanh\frac{1}{2}\beta\varepsilon_{qf'}^z(t)\right]\rangle\right\}, \tag{5.1}$$

where $\varepsilon_{qf'}^z(t)$ is the local field acting on the $f'$th deuteron in the $q$-th cell that can be determined from the Hamiltonian (4.5). Expanding

$\tanh\frac{1}{2}\beta\varepsilon^z_{qf'}(t)$ is series over the pseudospin operators entering the cluster Hamiltonains and taking into account the fact that $\sigma^2_{qf}=1$ and the symmetry of the deuteron distribution functions in the $KD_2PO_4$ type crystals in present of the electric field $E_3$

$$\eta^{(1)z}(6)=\langle\sigma_{q1}\rangle=\langle\sigma_{q2}\rangle=\langle\sigma_{q3}\rangle=\langle\sigma_{q4}\rangle, \tag{5.2}$$
$$\eta^{(3)z}(6)=\langle\sigma_{q1}\sigma_{q2}\sigma_{q3}\rangle=\langle\sigma_{q1}\sigma_{q3}\sigma_{q4}\rangle=\langle\sigma_{q1}\sigma_{q2}\sigma_{q4}\rangle=\langle\sigma_{q2}\sigma_{q3}\sigma_{q4}\rangle,$$
$$\eta^{(2)z}_1(6)=\langle\sigma_{q2}\sigma_{q3}\rangle=\langle\sigma_{q1}\sigma_{q4}\rangle,\quad \eta^{(2)z}_2(6)=\langle\sigma_{q1}\sigma_{q2}\rangle=\langle\sigma_{q3}\sigma_{q4}\rangle,$$
$$\eta^{(2)z}_3(6)=\langle\sigma_{q1}\sigma_{q3}\rangle=\langle\sigma_{q2}\sigma_{q4}\rangle,$$

we obtain a closed system of equations for the time-dependent single-particle, three-particle, and two-particle deuteron distribution functions.

We consider vibrations of a thin square plate of a $MD_2XO_4$ crystal cut in the (001) plane with sides $l$, induced by external time-dependent electric field $E_{3t}=E_3e^{i\omega t}$. The dynamics of the deformational processes in $MD_2XO_4$ will be described using the classical equation of motions of an elementary crystal volume, which read

$$\rho\frac{\partial^2u_i}{\partial t^2}=\sum_k\frac{\partial\sigma_{ik}}{\partial x_k}, \tag{5.3}$$

where $\rho$ is the crystal volume; $u_i$ are the displacements of the elementary volume along the axis $x_i$; $\sigma_{ik}$ is the mechanical stress. The sheat strain $\varepsilon_6$ is determined by the displacements $u_x=u_1$, $u_y=u_z$, that is

$$\varepsilon_6=\varepsilon_{xy}=\frac{\partial u_1}{\partial y}+\frac{\partial u_2}{\partial x}.$$

The dynamic properties of the $MD_2XO_4$ crystals will be studied at small deviations from equilibrium. Let us present these systems as sums of the static and dynamic parts. To do so, we write the distribution functions, effective fields, displacements $u_1$, $u_2$, and the strains as sums of the equilibrium functions and their deviations from equilibrium values

$$\eta^{(1)}(6)=\tilde\eta^{(1)}(6)+\eta^{(1)}_t(6),\ \eta^{(3)}(6)=\tilde\eta^{(3)}(6)+\eta^{(3)}_t(6), \tag{5.4}$$
$$\eta^{(2)}_i(6)=\tilde\eta^{(2)}_i(6)+\eta^{(2)}_t(6),\ (i=1,2,3),$$
$$\varepsilon_6=\tilde\varepsilon_6+\varepsilon_{6t},\quad u_{1,2}=\tilde u_{1,2}+u_{1,2t},$$
$$z^z_6=\tilde z_6+z_{6t}=-\beta\tilde\Delta+2\beta\nu_c\tilde\eta^{(1)}(6)-2\beta\psi_6\tilde\varepsilon_6-$$
$$-\beta\tilde\Delta_t+2\beta\nu_c\tilde\eta^{(1)}_t(6)-2\beta\psi_6\tilde\varepsilon_{6t}+\beta\mu_3E_{3t}.$$



In the result, we obtain the following system of equations for the time-dependent parts of the distribution functions

$$\frac{d}{dt}\begin{pmatrix}\eta^{(1)}_t(6)\\ \eta^{(3)}_t(6)\\ \eta^{(2)}_{1t}(6)\\ \eta^{(2)}_{2t}(6)\\ \eta^{(2)}_{3t}(6)\end{pmatrix}=\begin{pmatrix}c_{11}&c_{12}&c_{13}&c_{14}&c_{15}\\ c_{21}&c_{22}&c_{23}&c_{24}&c_{25}\\ c_{31}&c_{32}&c_{33}&c_{34}&c_{35}\\ c_{41}&c_{42}&c_{43}&c_{44}&c_{45}\\ c_{51}&c_{52}&c_{53}&c_{54}&c_{55}\end{pmatrix}\begin{pmatrix}\eta^{(1)}_t(6)\\ \eta^{(3)}_t(6)\\ \eta^{(2)}_{1t}(6)\\ \eta^{(2)}_{2t}(6)\\ \eta^{(2)}_{3t}(6)\end{pmatrix}-$$
$$-\frac{1}{2}\beta\mu_3E_{3t}\begin{pmatrix}c_1\\ c_2\\ c_3\\ c_4\\ c_5\end{pmatrix}+\beta\psi_6\varepsilon_{6t}\begin{pmatrix}c_1\\ c_2\\ c_3\\ c_4\\ c_5\end{pmatrix}-\beta\delta_{s6}\varepsilon_{6t}\begin{pmatrix}c_{1s}\\ c_{3s}\\ c_{2s}\\ c_{2s}\\ c_{2s}\end{pmatrix}+$$
$$+\beta\delta_{a6}\varepsilon_{6t}\begin{pmatrix}c_{1a}\\ -c_{1a}\\ c_{2a}\\ -c_{2a}\\ c_{3a}\end{pmatrix}-\beta\delta_{16}\varepsilon_{6t}\begin{pmatrix}\tilde c_{11}\\ \tilde c_{21}\\ \tilde c_{31}\\ \tilde c_{41}\\ \tilde c_{51}\end{pmatrix}. \tag{5.5}$$

The coefficients $c_{11},...,\tilde c_{51}$ are given in [150].

We write the equations for the displacements $u_{1t}$, $u_{2t}$ in the following form

$$\rho\frac{\partial^2u_{1t}}{\partial t^2}=c_{16}\frac{\partial\varepsilon_{6t}}{\partial y}+c_{26}\frac{\partial\eta^{(1)}_t(6)}{\partial y},\ \rho\frac{\partial^2u_{2t}}{\partial t^2}=c_{16}\frac{\partial\varepsilon_{6t}}{\partial x}+c_{26}\frac{\partial\eta^{(1)}_t(6)}{\partial x}, \tag{5.6}$$

expressions for $c_{16}$, $c_{26}$ given in [150].

Solving the systems (5.5), (5.6), we finally obtained the following expression for the longitudinal dynamic susceptibility of a mechanically free $KD_2PO_4$ type crystal [113]:

$$\chi^\sigma_{33}(\omega)=\chi^\varepsilon_{33}(\omega)+\frac{1}{R_6(\omega)}\frac{e^2_{36}(\omega)}{c^E_{66}(\omega)}, \tag{5.7}$$

where

$$\frac{1}{R_6(\omega)}=\frac{2}{k_6l}\tan\frac{k_6l}{2},\qquad k_6=\frac{\omega\sqrt{\rho}}{\sqrt{c^E_{66}(\omega)}}. \tag{5.8}$$

In (5.7) the longitudinal dynamic susceptibility of a mechanically clamped crystal is

$$\chi^\varepsilon_{33}(\omega)=\chi^{\varepsilon0}_{33}+\frac{\beta\mu_3^2}{2v}F^{(1)}(\omega), \tag{5.9}$$

$$e_{36}(\omega) = e_{36}^0 + \tag{5.10}$$
$$+\frac{\beta\mu_3}{v}\Big[-\psi_6 F^{(1)}(\omega) + \delta_{s6}F_s^{(1)}(\omega) + \delta_{16}F_1^{(1)}(\omega) - \delta_{a6}F_a^{(1)}(\omega)\Big],$$
$$c_{66}^E(\omega) = c_{66}^{E0} + \frac{4\beta\psi_6}{vD_6}f_6 + \frac{2\beta}{vD_6^2}(-\delta_{s6}M_{s6} + \delta_{16}M_{16} + \delta_{a6}M_{a6})^2 + \tag{5.11}$$
$$+\frac{4\beta\psi_6}{v}\Big[-\psi_6 F^{(1)}(\omega) + \delta_{s6}F_s^{(1)}(\omega) + \delta_{16}F_1^{(1)}(\omega) - \delta_{a6}F_a^{(1)}(\omega)\Big] -$$
$$-\frac{4\varphi_3 f_6}{vD_6}\beta\Big[-\psi_6 F^{(1)}(\omega) + \delta_{s6}F_s^{(1)}(\omega) + \delta_{16}F_1^{(1)}(\omega) - \delta_{a6}F_a^{(1)}(\omega)\Big] -$$
$$-\frac{2\beta}{vD_6}\Big[\delta_{s6}^2\cosh(2\tilde{z} + \beta\delta_{s6}\tilde{\varepsilon}_6) + 4b\delta_{16}^2\cosh(\tilde{z} - \beta\delta_{16}\tilde{\varepsilon}_6) +$$
$$+\delta_{a6}^2 2a\cosh\beta\delta_{a6}\tilde{\varepsilon}_6^2\Big],$$

where we use the following notations

$$F^{(1)}(\omega) = \frac{p^{(4)}(i\omega)^4 + p^{(3)}(i\omega)^3 + p^{(2)}(i\omega)^2 + p^{(1)}(i\omega) + p^{(0)}}{(i\omega)^5 + p_4(i\omega)^4 + p_3(i\omega)^3 + p_2(i\omega)^2 + p_1(i\omega) + p_0}, \tag{5.12}$$
$$F_s^{(1)}(\omega) = \frac{p_s^{(4)}(i\omega)^4 + p_s^{(3)}(i\omega)^3 + p_s^{(2)}(i\omega)^2 + p_s^{(1)}(i\omega) + p_s^{(0)}}{(i\omega)^5 + p_4(i\omega)^4 + p_3(i\omega)^3 + p_2(i\omega)^2 + p_1(i\omega) + p_0},$$
$$F_a^{(1)}(\omega) = \frac{p_a^{(4)}(i\omega)^4 + p_a^{(3)}(i\omega)^3 + p_a^{(2)}(i\omega)^2 + p_a^{(1)}(i\omega) + p_a^{(0)}}{(i\omega)^5 + p_4(i\omega)^4 + p_3(i\omega)^3 + p_2(i\omega)^2 + p_1(i\omega) + p_0},$$
$$F_1^{(1)}(\omega) = \frac{p_1^{(4)}(i\omega)^4 + p_1^{(3)}(i\omega)^3 + p_1^{(2)}(i\omega)^2 + p_1^{(1)}(i\omega) + p_1^{(0)}}{(i\omega)^5 + p_4(i\omega)^4 + p_3(i\omega)^3 + p_2(i\omega)^2 + p_1(i\omega) + p_0}.$$

Expressions for $p_4, \ldots, p_0$, $p^{(4)}, \ldots, p^{(0)}$, $p_s^{(4)}, \ldots, p_s^{(0)}$, $p_a^{(4)}, \ldots, p_a^{(0)}$, $p_1^{(4)}, \ldots, p_1^{(0)}$ in(5.12) are given in [150].

### 6.2. Transverse dynamic dielectric susceptibility

Performing analogous calculations for the case of the transverse electric field $E_1$, applied to the $KD_2PO_4$ type crystal, we obtain the transverse dielectric susceptibility of a mechanically free crystal [114]:

$$\chi_{11}^{\sigma}(\omega) = \chi_{11}^{\varepsilon}(\omega) + \frac{1}{R_4(\omega)}\frac{e_{14}^2(\omega)}{c_{44}^E(\omega)}, \tag{5.13}$$

where

$$\frac{1}{R_4(\omega)} = \frac{2}{k_4 l}\tanh\frac{k_4 l}{2}, \qquad k_4 = \frac{\omega\sqrt{\rho}}{\sqrt{c_{44}^E(\omega)}}.$$



In (5.13) the transverse dynamic susceptibility of a mechanically clamped crystal is

$$\chi_{11}^{\varepsilon}(\omega) = \chi_{11}^{\varepsilon 0} + \bar{v}\frac{(\mu_1\cos\gamma + \mu_2\sin\gamma)^2}{v^2}\frac{1}{4T}F_+^{(1)}(\omega) + \tag{5.14}$$
$$+\bar{v}\frac{(\mu_1\cos\gamma - \mu_2\sin\gamma)^2}{v^2}\frac{1}{4T}F_-^{(1)}(\omega).$$
$$e_{14}(\omega) = e_{14}^0 + \tag{5.15}$$
$$+\frac{\mu_1\cos\gamma + \mu_2\sin\gamma}{v}\frac{1}{4T}\Big[\tilde{\psi}_4 F_{4+}^{(1)}(\omega) + \tilde{\delta}_{a4}F_{a4+}^{(1)}(\omega) + \tilde{\delta}_{14}F_{14+}^{(1)}(\omega)\Big] +$$
$$+\frac{\mu_1\cos\gamma - \mu_2\sin\gamma}{v}\frac{1}{4T}\Big[\tilde{\psi}_4 F_{4-}^{(1)}(\omega) + \tilde{\delta}_{a4}F_{a4-}^{(1)}(\omega) + \tilde{\delta}_{14}F_{14-}^{(1)}(\omega)\Big],$$
$$c_{44}^4(\omega) = c_{44}^{E0} + \frac{2\tilde{\psi}_4}{\bar{v}DT}(\tilde{\delta}_{a4}\varkappa_1^a + \tilde{\delta}_{14}2\varkappa^b) - \frac{2}{\bar{v}DT}(\tilde{\delta}_{a4}^2\varkappa_1^a + \tilde{\delta}_{14}^2 2\varkappa^b) - \tag{5.16}$$
$$-\frac{2\tilde{\psi}_4}{\bar{v}}\frac{1}{4T}\Big\{\tilde{\psi}_4\Big[F_{4+}^{(1)}(\omega) + F_{4-}^{(1)}(\omega)\Big] +$$
$$+\tilde{\delta}_{14}\Big[F_{14+}^{(1)}(\omega) + F_{14-}^{(1)}(\omega)\Big] + \tilde{\delta}_{a4}\Big[F_{a4+}^{(1)}(\omega) + F_{a4-}^{(1)}(\omega)\Big]\Big\} +$$
$$+\frac{4\varphi_a^{\eta}}{\bar{v}DT}(\tilde{\delta}_{a4}aa_6 + \tilde{\delta}_{14}\varkappa^b)\Big\{\tilde{\psi}_4 F_{4+}^{(1)}(\omega) + \tilde{\delta}_{a4}F_{a4+}^{(1)}(\omega) + \tilde{\delta}_{14}F_{14+}^{(1)}(\omega)\Big\} +$$
$$+\frac{4\varphi_a^{\eta}}{\bar{v}DT}(\tilde{\delta}_{a4}\frac{a}{a_6} + \tilde{\delta}_{14}\varkappa^b)\Big\{\tilde{\psi}_4 F_{4-}^{(1)}(\omega) + \tilde{\delta}_{a4}F_{a4-}^{(1)}(\omega) + \tilde{\delta}_{14}F_{14-}^{(1)}(\omega)\Big\}.$$

where we use the following notations

$$F_{\pm}^{(1)}(\omega) = \frac{(i\omega)^2 m_{\pm}^{(2)} + (i\omega)m_{\pm}^{(1)} + m_{\pm}^{(0)}}{(i\omega)^3 + (i\omega)^2 m_{2\pm} + (i\omega)m_{1\pm} + m_{0\pm}}, \tag{5.17}$$
$$F_{4\pm}^{(1)}(\omega) = \frac{(i\omega)^2 m_{4\pm}^{(2)} + (i\omega)m_{4\pm}^{(1)} + m_{4\pm}^{(0)}}{(i\omega)^3 + (i\omega)^2 m_{2\pm} + (i\omega)m_{1\pm} + m_{0\pm}},$$
$$F_{14\pm}^{(1)}(\omega) = \frac{(i\omega)^2 m_{14\pm}^{(2)} + (i\omega)m_{14\pm}^{(1)} + m_{14\pm}^{(0)}}{(i\omega)^3 + (i\omega)^2 m_{2\pm} + (i\omega)m_{1\pm} + m_{0\pm}},$$
$$F_{a4\pm}^{(1)}(\omega) = \frac{(i\omega)^2 m_{a4\pm}^{(2)} + (i\omega)m_{a4\pm}^{(1)} + m_{a4\pm}^{(0)}}{(i\omega)^3 + (i\omega)^2 m_{2\pm} + (i\omega)m_{1\pm} + m_{0\pm}}.$$

The expressions for $m_{\pm}^{(2)}$, ..., $m_{a4\pm}^{(0)}$ are given in [151].

### 6.3. Static dielectric, piezoelectric, and elastic characteristics

In the static limit $\omega \to 0$ in (5.9)-(5.11), (5.14)-(5.16) we obtain the isothermic static dielectric susceptibilities of a clamped crystal

$$\chi_{33}^{\varepsilon} = \chi_{33}^{0} + \bar{v}\frac{\mu^2}{v^2}\frac{1}{T}\frac{2\varkappa_6}{D_6 - 2\varkappa_6\varphi_6^{\eta}}, \tag{5.18}$$

$$\chi_{11}^{\varepsilon} = \chi_{11}^{\varepsilon 0} + \frac{(\mu_1\cos\gamma + \mu_2\sin\gamma)^2}{v}\frac{\beta}{2}\frac{aa_6 + \varkappa^b}{D - 2(aa_6 + \varkappa^b)\varphi_a^{\eta}} + \tag{5.19}$$
$$+\frac{(\mu_1\cos\gamma - \mu_2\sin\gamma)^2}{v}\frac{\beta}{2}\frac{\frac{a}{a_6} + \varkappa^b}{D - 2(\frac{a}{a_6} + \varkappa^b)\varphi_a^{\eta}}.$$

where

$$\varkappa_6 = \mathrm{ch}(2z_6 + \beta\delta_{s6}\varepsilon_6) + b\,\mathrm{ch}(z_6 - \beta\delta_{16}\varepsilon_6) - \eta^{(1)}(6)m_6,$$
$$\varphi_6^{\eta} = \frac{1}{1 - (\eta^{(1)}(6))^2} + \beta\nu_c;$$
$$\varkappa^b = b\,\mathrm{ch}(x - \beta\delta_{16}\varepsilon_6), \qquad \varphi_a^{\eta} = \frac{1}{1 - \eta^{(1)2}} + \beta\nu_a \quad \nu_a = \nu_1 - \nu_3.$$

isothermic coefficients of piezoelectric stress

$$e_{36} = e_{36}^{0} + \frac{2\mu_3}{v}\frac{\beta\theta_6}{D_6 - 2\varphi_6^{\eta}\varkappa_6}, \tag{5.20}$$

$$e_{14} = e_{14}^{0} + \beta\frac{\mu_1\cos\gamma + \mu_2\sin\gamma}{v}\frac{\psi_4(aa_6 + \varkappa^b) - \delta_{a4}aa_6 - \delta_{14}\varkappa^b}{D - 2(aa_6 + \varkappa^b)\varphi_a^{\eta}} +$$
$$+\beta\frac{\mu_1\cos\gamma - \mu_2\sin\gamma}{v}\frac{\psi_4(\frac{a}{a_6} + \varkappa^b) - \delta_{a4}\frac{a}{a_6} - \delta_{14}\varkappa^b}{D - 2(\frac{a}{a_6} + \varkappa^b)\varphi_a^{\eta}}, \tag{5.21}$$

where

$$\theta_6 = -2\varkappa_6^c\psi_6 + f_6, \qquad f_6 = \delta_{s6}\,\mathrm{ch}(2z_6 + \beta\delta_{s6}\varepsilon_6) -$$
$$-2b\delta_{16}\,\mathrm{ch}(z_6 - \beta\delta_{16}\varepsilon_6) + \eta^{(1)z}(6)(-\delta_{s6}M_{s6} + \delta_{a6}M_{a6} + \delta_{16}M_{16});$$

isothermic elastic constants at constant field

$$c_{66}^{E} = c_{66}^{E0} + \frac{8\psi_6}{v}\cdot\frac{\beta(-\psi_6\varkappa_6^c + f_6)}{D_6 - 2\varphi_6^{\eta}\varkappa_6} - \frac{4\beta\varphi_6^{\eta}f_6^2}{vD_6(D_6 - 2\varphi_6^{\eta}\varkappa_6)} - \tag{5.22}$$
$$-\frac{2\beta}{vD_6}[\delta_{s6}^2\,\mathrm{ch}(2z_6 + \beta\delta_{s6}\varepsilon_6) + \delta_{a6}^2 2a\,\mathrm{ch}\,\beta\delta_{a6}\varepsilon_6 +$$
$$+\delta_{16}^2 4b\,\mathrm{ch}(z_6 - \beta\delta_{16}\varepsilon_6)] + \frac{2\beta}{vD_6^2}(-\delta_{s6}M_{s6} + \delta_{a6}M_{a6} + \delta_{16}M_{16})^2.$$



$$c_{44}^{E} = c_{44}^{E0} - \frac{2\psi_4}{v}\beta[\frac{\psi_4(aa_6 + \varkappa^b) - \delta_{a4}aa_6 - \delta_{14}\varkappa^b}{D - 2(aa_6 + \varkappa^b)\varphi_a^{\eta}} + \tag{5.23}$$
$$+\frac{\psi_4(\frac{a}{a_6} + \varkappa^b) - \delta_{a4}\frac{a}{a_6} - \delta_{14}\varkappa^b}{D - 2(\frac{a}{a_6} + \varkappa^b)\varphi_a^{\eta}}] +$$
$$+\frac{4\varphi_a^{\eta}}{vD}\beta(\delta_{a4}aa_6 + \delta_{14}\varkappa^b)\frac{\psi_4(aa_6 + \varkappa^b) - \delta_{a4}aa_6 - \delta_{14}\varkappa^b}{D - 2(aa_6 + \varkappa^b)\varphi_a^{\eta}} +$$
$$+\frac{4\varphi_a^{\eta}}{vD}\beta(\delta_{a4}\frac{a}{a_6} + \delta_{14}\varkappa^b)\frac{\psi_4(\frac{a}{a_6} + \varkappa^b) - \delta_{a4}aa_6 - \delta_{14}\varkappa^b}{D - 2(\frac{a}{a_6} + \varkappa^b)\varphi_a^{\eta}} +$$
$$+\frac{2\psi_4}{vD}\beta(\delta_{a4}\varkappa_1^a + \delta_{14}\varkappa^b) - \frac{2}{vD}\beta(\delta_{a4}^2\varkappa_1^a + \delta_{14}^2\varkappa^b).$$

where

$$M_{a6} = 2a\,\mathrm{sh}\,\beta\delta_{a6}\varepsilon_6, \quad M_{s6} = \mathrm{sh}(2z_6 + \beta\delta_{s6}\varepsilon_6),$$
$$M_{16} = 4b\,\mathrm{sh}(z_6 - \beta\delta_{16}\varepsilon_6), \quad \varkappa_1^a = aa_6 + \frac{a}{a_6}.$$

Using the known relations between the elastic, dielectric, and piezoelectric characteristics, we find the isothermic constants of piezoelectric stress

$$h_{36} = \frac{e_{36}}{\chi_{33}^{\varepsilon}}, \qquad h_{14} = \frac{e_{14}}{\chi_{11}^{\varepsilon}}; \tag{5.24}$$

isothermic elastic constants at constant polarization

$$c_{66}^{P} = c_{66}^{E} + e_{36}h_{36}; \qquad c_{44}^{P} = c_{44}^{E} + e_{14}h_{14}; \tag{5.25}$$

isothermic coefficients of piezoelectric strain

$$d_{36} = \frac{e_{36}}{c_{66}^{E}}; \qquad d_{14} = \frac{e_{14}}{c_{44}^{E}}; \tag{5.26}$$

isothermic constants of piezoelectric strain

$$g_{36} = \frac{h_{36}}{c_{66}^{P}}; \qquad g_{14} = \frac{h_{14}}{c_{44}^{P}}; \tag{5.27}$$

isothermic dielectric susceptibilities at $\sigma = const$:

$$\chi_{33}^{\sigma} = \chi_{33}^{\varepsilon} + e_{36}d_{36}; \qquad \chi_{11}^{\sigma} = \chi_{11}^{\varepsilon} + e_{14}d_{14}. \tag{5.28}$$

## 7. Comparison of the results of numerical calculations with experimental data. Discussion.

Let us analyze the results of numerical calculations of dielectric, piezoelectlric, and elastic characteristics of the $KH_2PO_4$ type crystals and compare them with the corresponding experimental data for these crystals. Let us note that the developed theory is valid, strictly speaking for the $KD_2PO_4$ crystals. The experimental data, on the other hand, are for the $K(H_{1-x}D_x)_2PO_4$ type crystals at different deuterations $x$.

For numerical calculations of the temperature dependences of the physical characteristics of the $K(H_{1-x}D_x)_2PO_4$ type crystals obtained in the previous section, we need to set the values of the following parameters:

- energies of proton and deuteron configurations $\varepsilon(x)$, $w(x)$, $w_1(x)$;
- long-range interaction parameters $\nu_c(x)$, $\nu_a(x)$;
- effective dipole moments $\mu_3(x)$, $\mu_1(x)$;
- deformational potentials $\psi_6(x)$, $\psi_4(x)$, $\delta_{s6}(x)$, $\delta_{a6}(x)$, $\delta_{16}(x)$, $\delta_{a4}(x)$, $\delta_{14}(x)$;
- "seed" dielectric susceptibilities $\chi^{\varepsilon 0}_{33}$, $\chi^{\varepsilon 0}_{11}$;
- "seed" coefficients of piezoelectric stress $e^0_{36}(x)$, $e^0_{14}(x)$;
- "seed" elastic constants $c^{E0}_{66}$, $c^{E0}_{44}$.
- parameter $\alpha$ that sets the time scale of the relaxational processes.

The energy $w_1(x)$ of proton configurations with four protons and without any proton is much larger than the energies of $\varepsilon$ and $w$. Therefore, we take $w_1 = \infty$ and $d = 0$.

The fitting procedure is discussed in details in [95,101,150,151]. Thus, on the first stage, the parameters $\varepsilon$, $w$ are determined [95] from the condition of the best fit of experimental data for the temperature curves of spontaneous polarization and specific heat, and to find the parameter $\nu_c$ we fit the calculated phase transition temperature to the experimental values. The values of $\mu_{3-}$ are obtained by fitting the theoretical results to the experimental values of saturation spontaneous polarization, whereas to obtain $\mu_{3+}$ we use the values of $\varepsilon_{33}(\omega)$. On the second stage, with taking into account the piezoelectric coupling, the optimum values of $\varepsilon$, $w$, $\mu_{3+}$, $\mu_{3+}$, as well as the deformational potentials $\psi_6$, $\psi_4$, $\delta_{s6}$, $\delta_{a6}$, $\delta_{16}$, $\delta_{a4}$, $\delta_{14}$ and the parameter $\nu_a$ are found from the condition of the best fit for the temperature dependences of polarization, specific heat, longitudinal and transverse static permittivities of mechanically clamped crystals, dynamic longitudinal and transverse permittivities of clamped crystals, piezoelectric coefficients, and elastic constants. Let us note that taking into account the piezoelectric coupling leads to a small increase of $w$ and $\nu_c$, as compared to their values of [95], where the piezoelectric coupling is not considered. The obtained optimum values of the model parameters for these crystals are given in Table 1.



To describe properly the temperature dependences of the dielectric permittivity $\varepsilon^{T\sigma}_{11}$ [144] we should take $\mu_1(x)$ to increase slightly with temperature as $\mu_1(x) = \mu^0_1(x) + k\mu(T - T_c)$. To describe the temperature curves of polarization and static dielectric permittivity in the paraelectric phase the values of $\mu_3$ must be different, with $\mu^+_3 > \mu^-_3$. In [152] the deviation of the ratio $\frac{\mu^+_3}{\mu^-_3}$ from unity is ascribed to existence of underdamped soft mode.

The parameter $\alpha_H$ was determined by fitting the theoretically calculated $\varepsilon_{33}(\omega)$ curves to the experimental points. It was assumed that $\alpha$ is temperature dependent

$$\alpha = [P + R|\Delta T|] \cdot 10^{-14},\ \Delta T = T - T_c.$$

The primitive cell volume of the $K(H_{1-x}D_x)_2PO_4$ crystals consisting of two $PO_4$ groups was taken to be equal to $v = 0,1936 \cdot 10^{-21}$ cm$^3$ at $x = 0$, $v = 0,1954 \cdot 10^{-21}$ cm$^3$ at $x = 0,88$, $v = 0,2090 \cdot 10^{-21}$ cm$^3$ for $RbH_2PO_4$, $v = 0,2052 \cdot 10^{-21}$ cm$^3$ for $KH_2AsO_4$, and $v = 0,2065 \cdot 10^{-21}$ cm$^3$ for $KH_2AsO_4$.

Let us analyze the results of numerical calculations of the physical characteristics of the $K(H_{1-x}D_x)_2PO_4$ type crystals and compare them with the corresponding experimental data for these crystals.

### 7.1. Static dielectric, piezoelectric, and elastic characteristics

The calculated temperature dependences of isothermic inverse static dielectric permittivities of free $\varepsilon^{\sigma}_{33}(0,T)$ and clamped $\varepsilon^{\varepsilon}_{33}(0,T)$ $K(H_{1-x}D_x)_2PO_4$ crystals at different $x$, as well as of $RbH_2PO_4$, $KH_2AsO_4$, and $KD_2AsO_4$ crystals along with the experimental data are given in fig. 25. When approaching the transition temperature $T_c$ in the paraelectric phase, the magnitude of $\varepsilon^{\sigma}_{33}$ increases according to the hyperbolic law, reaching very high values at $T = T_c$. With increasing $x$ the value of $\varepsilon^{\sigma\,\max}_{33}$ decreases. Below the transition temperature $\varepsilon^{\sigma}_{33}$ drops very fast. At $x = 0,88$ $(\varepsilon^{\sigma}_{33})^{-1}$ obeys the Curie-Weiss law in a wide temperature range. At $x = 0,00$ this range is narrower; a notable

Table 5. Sets of the optimum values of the model parameters for the $K(H_{1-x}D_x)_2PO_4$ type crystals.

| $x$ | $T_c$ (K) | $\frac{\varepsilon}{k_B}$ (K) | $\frac{w}{k_B}$ (K) | $\frac{\nu_c}{k_B}$ (K) | $\frac{\nu_a}{k_B}$ (K) |
|---|---|---|---|---|---|
| 0.00 | 122.5 | 56.00 | 422.0 | 17.91 | 7.00 |
| 0.88 | 211.0 | 88.60 | 815.0 | 34.90 | 17.00 |
| RDP | 147.6 | 60.00 | 440.0 | 29.13 | 28.00 |
| KDA | 97.0 | 35.50 | 385.0 | 17.43 | 20.00 |

| $x$ | $\mu_{3-}, 10^{-18}$ $(esu\cdot cm)$ | $\mu_{3+}, 10^{-18}$ $(esu\cdot cm)$ | $\mu_1^{(0)}, 10^{-18}$ $(esu\cdot cm)$ | $k_\mu, 10^{-21}$ $(\frac{esu\cdot cm}{K})$ | $\chi_{33}^0$ | $\chi_{11}^0$ |
|---|---|---|---|---|---|---|
| 0.00 | 1.46 | 1.71 | 4.27 | 5.7 | 0.73 | 0.80 |
| 0.88 | 1.79 | 2.05 | 5.52 | 4.2 | 0.39 | 0.65 |
| RDP | 1.50 | 2.00 | 3.68 | 5.7 | 0.40 | 1.25 |
| KDA | 1.61 | 1.65 | 4.85 | 6.4 | 0.70 | 0.70 |

| $x$ | $\frac{\psi_6}{k_B}$ $(K)$ | $\frac{\delta_{s6}}{k_B}$ $(K)$ | $\frac{\delta_{a6}}{k_B}$ $(K)$ | $\frac{\delta_{16}}{k_B}$ $(K)$ | $\frac{\psi_4}{k_B}$ $(K)$ | $\frac{\delta_{a4}}{k_B}$ $(K)$ | $\frac{\delta_{14}}{k_B}$ $(K)$ |
|---|---|---|---|---|---|---|---|
| 0.00 | -150 | 82 | -500 | -400 | 124.0 | 92.0 | 80.0 |
| 0.88 | -140 | 50 | -1000 | -400 | 188 | 95 | 300 |
| RDP | -130 | 50 | -500 | -300 | 152.0 | 80.0 | 5.0 |
| KDA | -170 | 130 | -500 | -500 | 370.0 | 70.0 | 30.0 |

| $x$ | $c_{66}^0 \cdot 10^{-10}$ $(dyn/cm^2)$ | $c_{44}^0 \cdot 10^{-10}$ $(dyn/cm^2)$ | $e_{36}^0$ $(esu/cm^2)$ | $e_{14}^0$ $(esu/cm^2)$ |
|---|---|---|---|---|
| 0.00 | 7.10 | 13.00 | 1000 | 500 |
| 0.88 | 6.40 | 12.85 | 2000 | 500 |
| RDP | 5.90 | 10.60 | 3000 | 2000 |
| KDA | 7.50 | 10.80 | 3000 | 2000 |

| $x$ | $P_-$ $(s)$ | $R_-$ $(\frac{s}{K})$ | $P_+$ $(s)$ | $R_+$ $(\frac{s}{K})$ | $P$ $(s)$ | $R$ $(\frac{s}{K})$ |
|---|---|---|---|---|---|---|
| 0.00 | 0.35 | 0.0100 | 0.43 | 0.0160 | 0.46 | 0.0130 |
| RDP | 0.55 | 0.0080 | 0.93 | 0.0140 | 0.56 | 0.0107 |
| KDA | 0.47 | 0.0160 | 0.61 | 0.0190 | 3.20 | 0.0140 |

nonlinearity of the temperature dependence of $(\varepsilon_{33}^\sigma)^{-1}$ is observed. The dielectric permittivity of $\varepsilon_{33}$ in $KH_2PO_4$ calculated without taking into account the piezoelectric coupling coincides with $\varepsilon_{33}^\sigma$ at $\Delta T < 50$ K and is smaller than $\varepsilon_{33}^\sigma(T)$ at larger values of $\Delta T$.



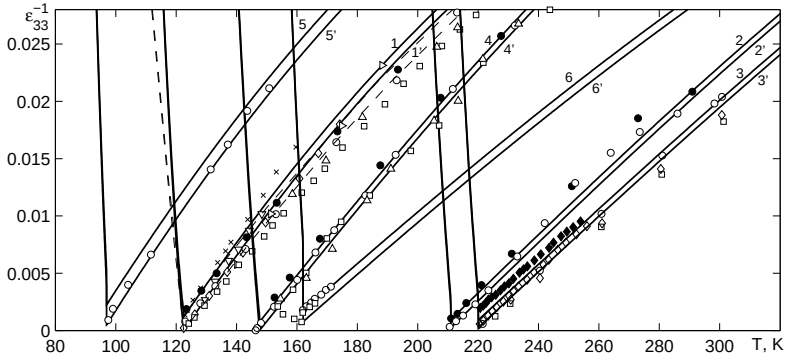


Figure 25. The temperature dependences of inverse static dielectric permittivities of clamped $(\varepsilon_{33}^\varepsilon)^{-1}$ (1) and free $(\varepsilon_{33}^\sigma)^{-1}$ (2) $K(H_{1-x}D_x)_2PO_4$ crystals: $x$=0.0 – 1, 1', ○ , ● [139], ▫ [153], ◇ [154], ▷ [131], ◁ [155], ▽ [156], △ [144], × [157]; $x$=0.88 – 2, 2', ○ [140], ● $((\varepsilon_{33}^\sigma\text{-}1)/4\pi$ [158]-$d_{36}^2$ [158]$/s_{66}^E)4\pi$+1; $x$=1.0 – 3, 3', ◆ , ◇ [159], ○ [154], ▫ [160]; $RbH_2PO_4$ – 4, 4' ○ [140], ● $((\varepsilon_{33}^\sigma\text{-}1)/4\pi$ [158]- $d_{36}^2$ [158]$/s_{66}^E)4\pi$+1, ▫ [132], △ [131]; $KH_2AsO_4$ – 5, 5' ○ [155]; $KD_2AsO_4$ – 6, 6' ○ [161], ▫ [162]. Lines are the theoretical results; dashed lines are the results of [93] for $KH_2PO_4$.

The values of the longitudinal static permittivity increase with replacing K → Rb at all temperatures and decrease with P → As.

In figure 26 we depict the temperature curves of $\varepsilon_{11}^\sigma(0)$ in $KH_2PO_4$, $K(H_{0,12}D_{0,88})_2PO_4$, $RbH_2PO_4$, and $KH_2AsO_4$.

In the $KH_2PO_4$, $K(H_{0,12}D_{0,88})_2PO_4$, $RbH_2PO_4$ crystals the values of transverse permittivities of mechanically free and clamped crystals practically coincide. For the case of $KH_2AsO_4$ the curve 4 corresponds to $\varepsilon_{11}^\sigma(0)$, whereas the curve 4' to $\varepsilon_{11}^\varepsilon(0)$. The theory does not reproduce the dome-shaped curve of the permittivity $\varepsilon_{11}^{\sigma,\varepsilon}$ at small $\Delta T$. The values of $\varepsilon_{11}^\sigma$ hardly depend on the deuteron concentration $x$. At the transition point $\varepsilon_{11}^\sigma$ has a jump, which increases with $x$. The calculated difference $\varepsilon_{11}^\sigma(+)$ - $\varepsilon_{11}^\sigma(-)$ is 3,25 at $x = 0$ and 30,9 at *x=0,88*, which accords with the experimental 4,0 and 34,6 [144].

At isomorphic replacement K → Rb the permittivity $\varepsilon_{11}^\sigma(0)$ slightly decreases in the paraelectric phase and increases in the ferroelectric phase. At replacing P → As the value $\varepsilon_{11}^\sigma(0)$ strongly increases in the paraelectric phase.

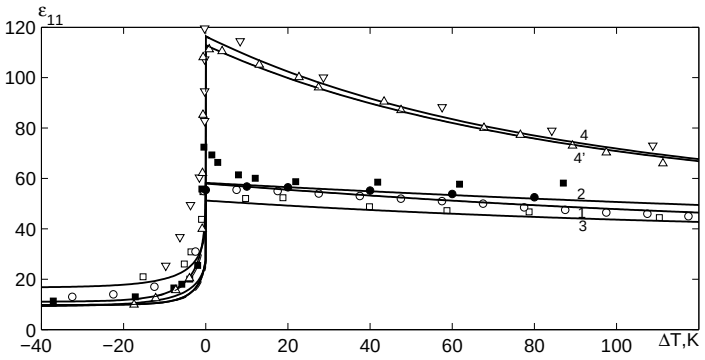


Figure 26. The temperature dependence of the transverse permittivity of the ferroelectric crystals: $KH_2PO_4$ – 1, ○ [144]; $K(H_{0.12}D_{0.88})_2PO_4$ – 2, ● [144], ■ [140]; $RbH_2PO_4$ – 3, ▫ [140]; $KH_2AsO_4$ – 4, △ [118]. Symbols are experimental points; solid lines are the theoretical values.

In figures 27 and 28 we plot the temperature dependences of the coefficients of piezoelectric strain $d_{36}$ and stress $e_{36}$ of the $KH_2PO_4$, $K(H_{0,12}D_{0,88})_2PO_4$, $RbH_2PO_4$, and $KH_2AsO_4$ crystals. Using the experimental points for $d_{36}$, $\varepsilon_{33}^{\sigma}$, and $c_{66}^{E}$ ($s_{66}^{E}$), we find $e_{36}$, also shown in fig. 28 as the experimental points.

The temperature dependences of the coefficients of piezoelectric strain $d_{14}$ and stress $e_{14}$ are shown in figs. 29 and 30 along with the experimental data. It should be mentioned that the piezoelectric coefficients $d_{14}$, $e_{14}$ do not have any anomalies in their temperature behavior. At $T \to T_c$ the values of $d_{36}$ and $e_{36}$ increase. With increasing $\Delta T$ from 0 to 170 K in $KH_2PO_4$ the values $d_{36}$ decreases by 88 times, whereas $e_{36}$ by 44,5 times. With increasing the deuteration level $x$ the longitudinal piezoelectric coefficients decrease, whereas the transverse coefficients decrease.

The calculated temperature dependences of the piezoelectric constants $h_{36}$ and $g_{36}$ of the $M(H_{1-x}D_x)_2XO_4$ crystals are given in [101], whereas the dependences of $h_{14}$ and $g_{14}$ in [151].

The calculated temperature dependences of the isothermic elastic constants $c_{jj}^{E}$ along with the experimental data are given in fig. 31 for $K(H_{1-x}D_x)_2PO_4$ crystals, whereas the temperature curves of $c_{66}^{E}$ and $c_{66}^{P}$ of $KH_2PO_4$, $K(H_{0,12}D_{0,88})_2PO_4$, $RbH_2PO_4$, $KH_2AsO_4$, and $KD_2AsO_4$ are shown in fig. 32. At the transition temperature the elastic constant



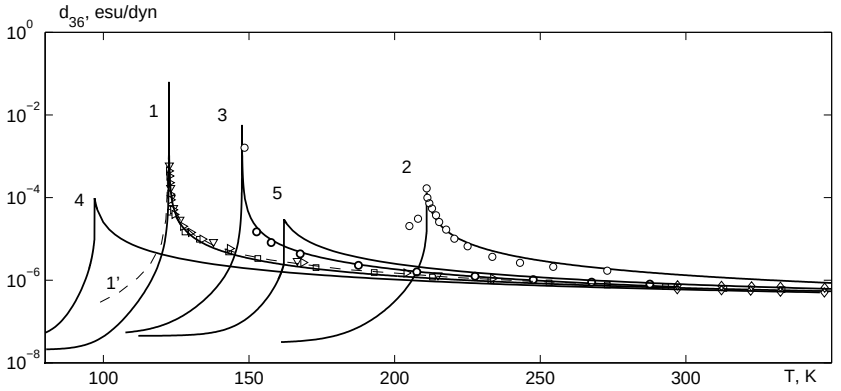


Figure 27. The temperature dependence of the coefficient of piezoelectric strain $d_{36}$ of $KH_2PO_4$ – 1, ▫ [139], ▽ [163], ▷ [164]; $K(H_{0.12}D_{0.88})_2PO_4$ – 2, ○ [140]; $RbH_2PO_4$ – 3, ○ [140]; $KH_2AsO_4$ – 4, ◇ [165]; $KD_2AsO_4$ – 5, ◆ [165]. Lines are the theoretical results; dashed lines are the theoretical curves of [93] for $KH_2PO_4$.

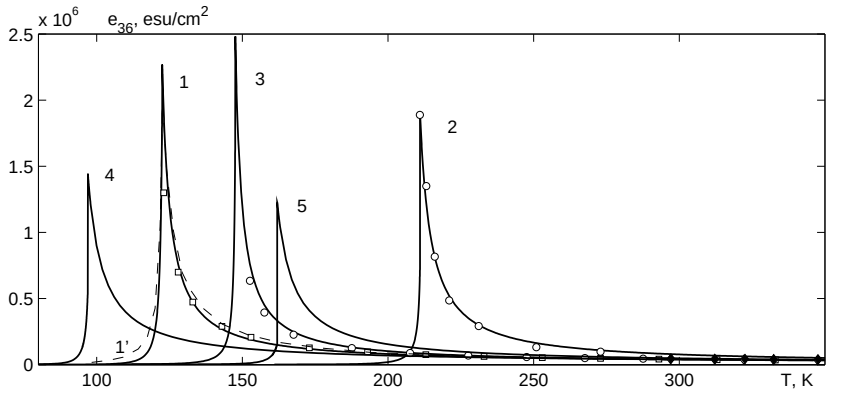


Figure 28. The temperature dependence of the coefficient of piezoelectric stress $e_{36}$ of $KH_2PO_4$ – 1, ▫ [139]; $K(H_{0.12}D_{0.88})_2PO_4$ – 2, ○ $-d_{36}$ [140]$/s_{66}^{E}$ [166]; $RbH_2PO_4$ – 3, ○ $-d_{36}$ [140]$/s_{66}^{E}$ [166]; $KH_2AsO_4$ – 4, ◇ $-d_{36}/s_{66}^{E}$ [165]; $KD_2AsO_4$ – 5, ◆ $-d_{36}/s_{66}^{E}$ [165]. Lines are the theoretical results; dashed lines are the theoretical curves of [93] for $KH_2PO_4$.

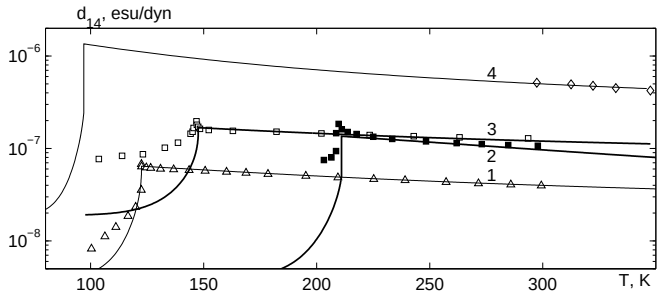


Figure 29. The temperature dependence of the coefficient of piezoelectric strain $d_{14}$ of $KH_2PO_4$ – 1, △ [167], $K(H_{0,12}D_{0,88})_2PO_4$ – 2, ■ [140], $RbH_2PO_4$ – 3, ▫ [140], $KH_2AsO_4$ – 4, ◇ [165].

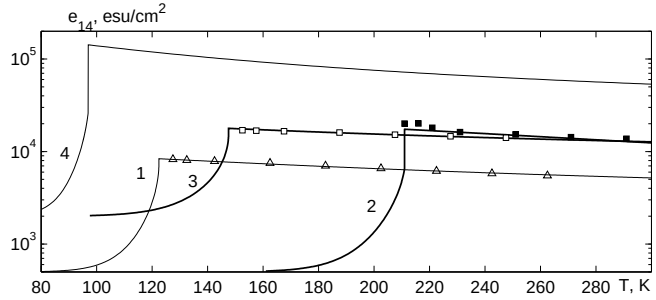


Figure 30. The temperature dependence of the coefficient of piezoelectric stress $e_{14}$ of $KH_2PO_4$ – 1, △ – $d_{14}$ [167]/$s^E_{44}$ [139], $K(H_{0,12}D_{0,88})_2PO_4$ – 2, ■ – $d_{14}$ [140]/$s^E_{44}$ [132], $RbH_2PO_4$ – 3, ▫ – $d_{14}$ [140]/$s^E_{44}$ [132], $KH_2AsO_4$ – 4, ◇ – $d_{14}/s^E_{44}$ [165].

$c^E_{66}$ goes to zero in $KH_2PO_4$ and $RbH_2PO_4$ and have some finite values in other crystals. The temperature dependence of $c^E_{44}$ does not have anomalies at the transition point. With increasing $x$ the values of the elastic constants slightly decrease.

Hence, the proposed theory, as see in figs. 25-32 well describes the experimental data for the static dielectric, piezoelectric, and elastic characteristics of the $KH_2PO_4$ type crystals.



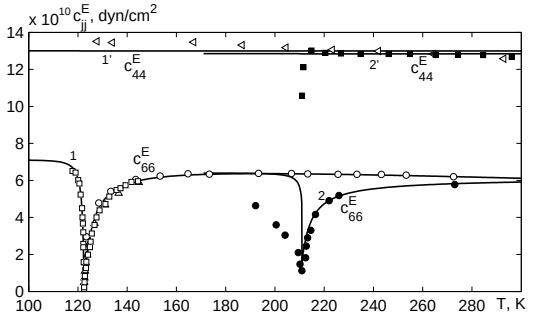


Figure 31. The temperature dependences of the elastic constants $c^E_{jj}$ of $KH_2PO_4$ (1) and $K(H_{0,12}D_{0,88})_2PO_4$ (2): ○ [139], ▫ [168], △ [169], ● $1/s^E_{66}$ [166], ◁ [139], ■ [166].

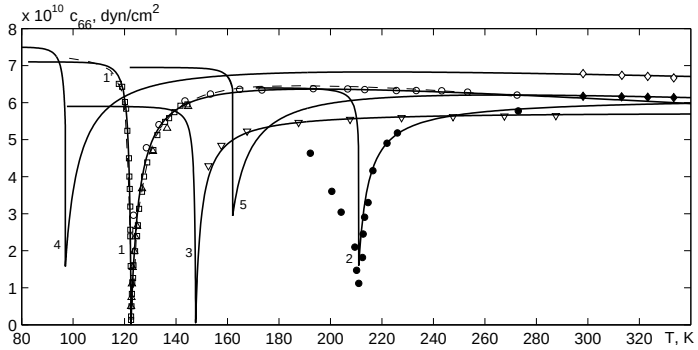


Figure 32. The temperature dependence of the elastic constants $c^E_{66}$ of different crystals: $KH_2PO_4$ – 1, ○ [139], ▫ [168], △ [169]; $K(H_{0.12}D_{0.88})_2PO_4$ – 2, ○ $-1/s^E_{66}$ [166]; $RbH_2PO_4$ – 3, ○ $-1/s^E_{66}$ [166]; $KH_2AsO_4$ – 4, ◇ $-1/s^E_{66}$ [165]; $KD_2AsO_4$ – 5, ◇ $-1/s^E_{66}$ [165]. Lines are the theoretical results; the dashed line is the theoretical curve of [93] for $KH_2PO_4$.

### 7.2. Dynamic longitudinal and transverse dielectric permittivities

Let us calculate the longitudinal dynamic characteristics of the mechanically free crystals of the $KH_2PO_4$ type cut as square plates $l \times l$

($l = 1$ mm) in the (0,0,1) plane.

In figures 33-36 we showed the frequency dependences of the real

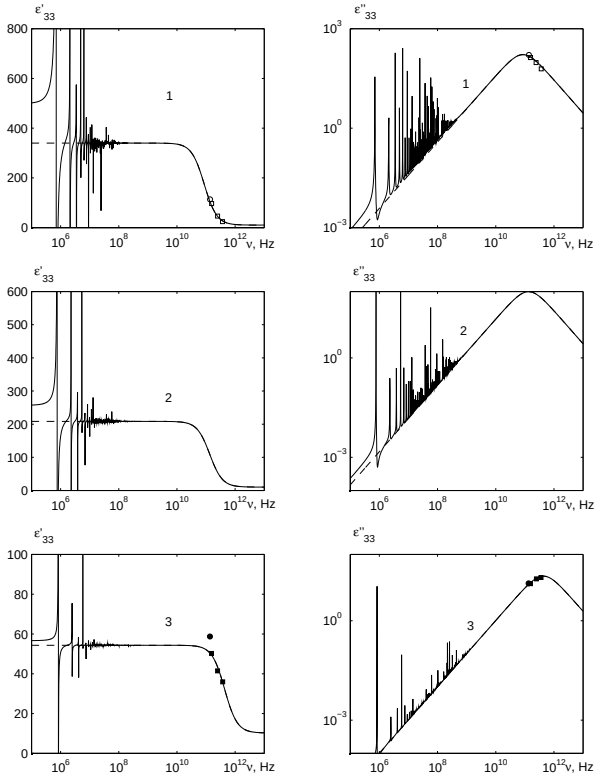


Figure 33. The frequency dependences of the real and imaginary parts of the dielectric susceptibilities of free and clamped $KH_2PO_4$ crystals at different $\Delta T$,K: 1 – 5, 2 – 10, 3 – 50.

and imaginary parts of the dielectric susceptibilities of free and clamped $MH_2XO_4$ crystals in the paraelectric phase at different temperatures. In the frequency range $3 \cdot 10^5$–$3 \cdot 10^8$ Hz the susceptibility of $MH_2XO_4$ has a resonant dispersion, with numerous peaks at frequencies where $Re(R_6(\omega)) = 0$ or $Re(k_6 l/2) = \pi/2(2n+1)$. Taking into account the



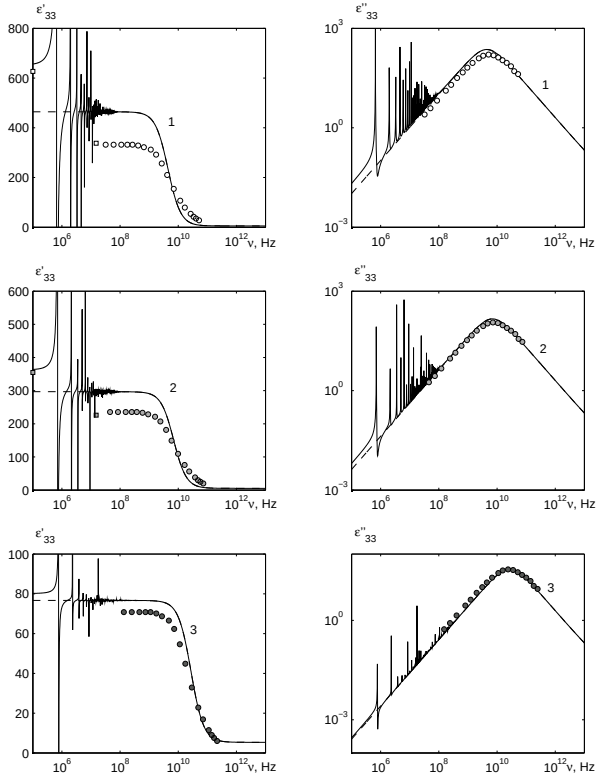


Figure 34. The frequency dependences of the real and imaginary parts of the dielectric susceptibilities of free and clamped $KD_2PO_4$ crystals at different $\Delta T$,K: 1 – 5, 2 – 10, 3 – 50.

dispersion law (5.8), we find an equation for the resonant frequencies

$$\omega_n = \frac{\pi(2n+1)}{l}\sqrt{\frac{c_{66}^E}{\rho}},$$

where it has been taken into account that in the frequency range $5 \cdot 10^5$–$5 \cdot 10^8$ Hz $c_{66}^E(\omega)$ is practically frequency independent. The resonant frequencies are inversely proportional to the sample dimensions. The dashed lines in figs. 33-36 correspond to the low-frequency limit of the clamped susceptibility. With increasing frequency and temperature $\Delta T$ the am-

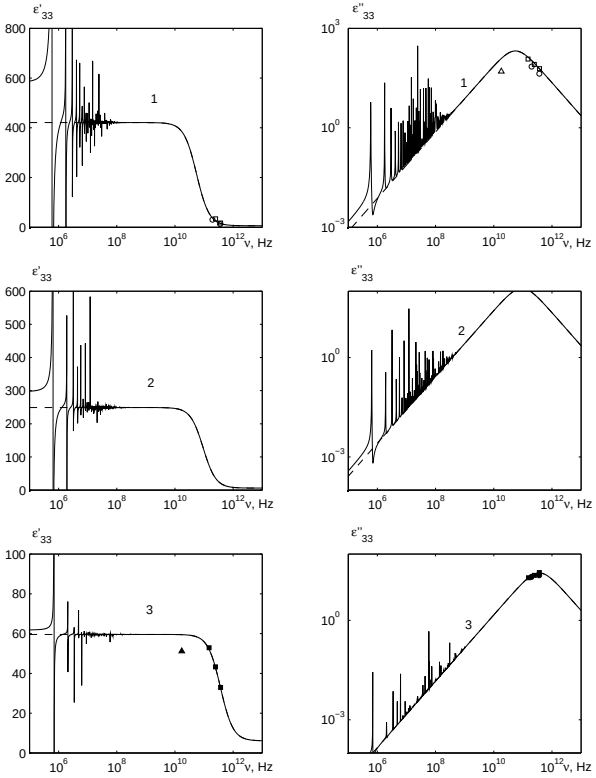


Figure 35. The frequency dependences of the real and imaginary parts of the dielectric susceptibilities of free and clamped $RbH_2PO_4$ crystals at different $\Delta T$,K: 1 – 5, 2 – 10, 3 – 50.

plitudes of the resonant peaks decrease. With increasing temperature $\Delta T$ the last resonant peak shifts to higher frequencies. A similar multi-peak resonant dispersion is observed in the ferroelectric phase. Above the resonant frequencies the crystal is clamped by the high-frequency field; the permittivity of a clamped crystal has a relaxational dispersion above $10^9$ Hz. At $\omega \to 0$ we get the static dielectric permittivity of a free crystal.

Let us analyze the calculated temperature and frequency dependences of the dynamic characteristics of mechanically free



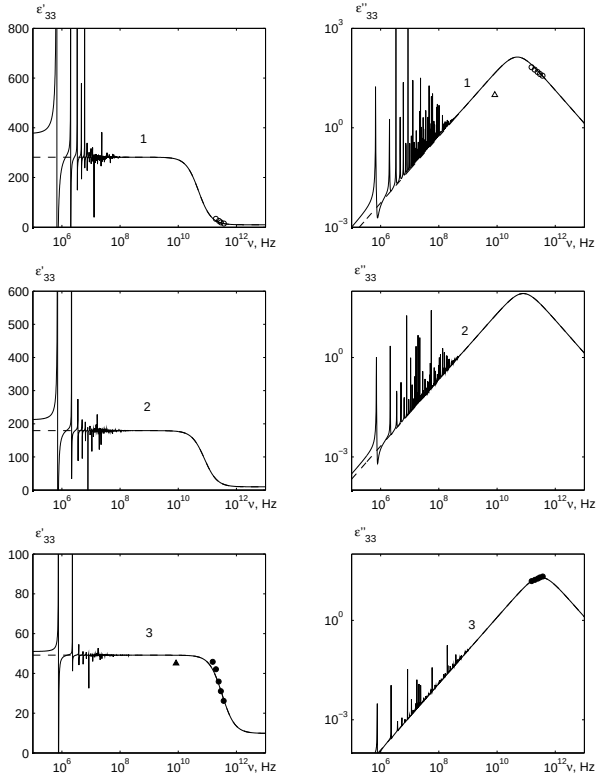


Figure 36. The frequency dependences of the real and imaginary parts of the dielectric susceptibilities of free and clamped $KH_2AsO_4$ crystals at different $\Delta T$,K: 1 – 5, 2 – 10, 3 – 50.

$M(H_{1-x}D_x)_2XO_4$ crystals cut as square plates with sides $l = 1$ mm in the (1, 0, 0) plane.

The frequency dependences of real and imaginary parts of the dielectric permittivity $\varepsilon_{11}^{\sigma}$ of $KH_2PO_4$, $RbH_2PO_4$, and $KH_2AsO_4$ at $\Delta T = 5$ K are shown in fig. 37. In the frequency range $10^6 - 10^8$ Hz the susceptibility has a resonant dispersion.At $\omega \to 0$ we get the static dielectric permittivity of a free crystal. The dashed lines in fig. 37 correspond to the low-frequency limit of the clamped susceptibility. Above the resonant frequencies the crystal is clamped by the high-frequency field; the

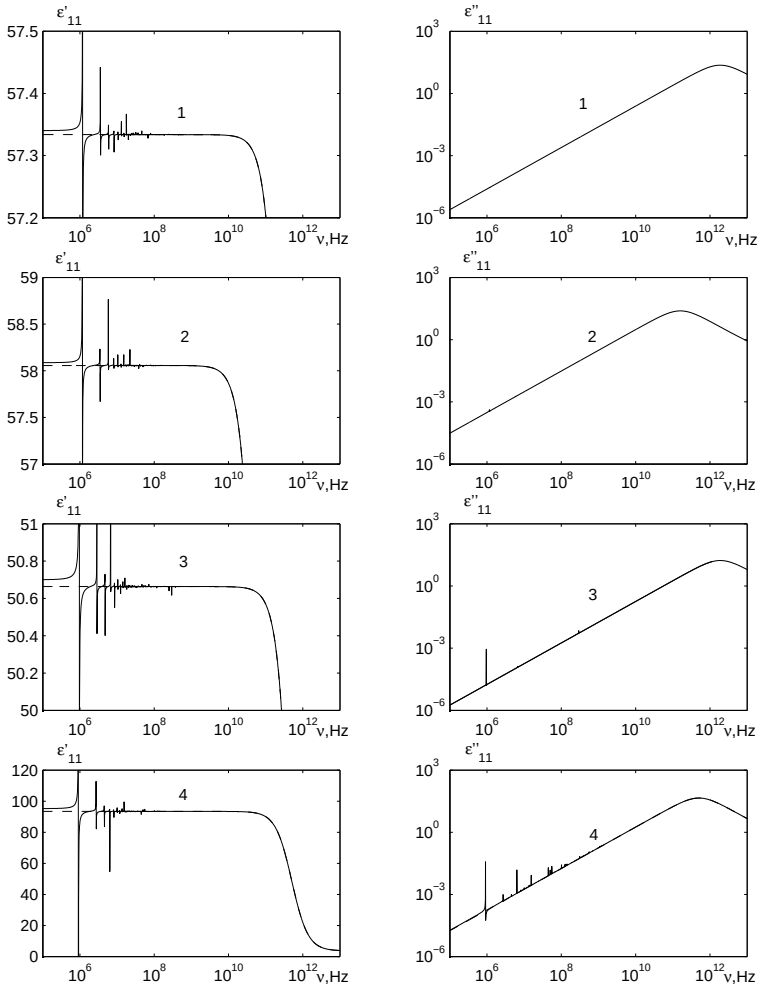


Figure 37. The frequency dependences of the real and imaginary parts of the dielectric permittivity of free $KH_2PO_4$ (1), $K(H_{0.07}D_{0.93})_2PO_4$ (2), $RbH_2PO_4$ (3), $KH_2AsO_4$ (4) crystals at $\Delta T$=5K.

permittivity of a clamped crystal has a relaxational dispersion above $10^9$ Hz.

The dashed and solid lines in fig. 38 correspond to the tempera-



ture dependences of $\varepsilon'_{33}(\omega,T)$ and $\varepsilon''_{33}(\omega,T)$ calculated without and with taking into account the piezoelectric coupling, respectively. It should be

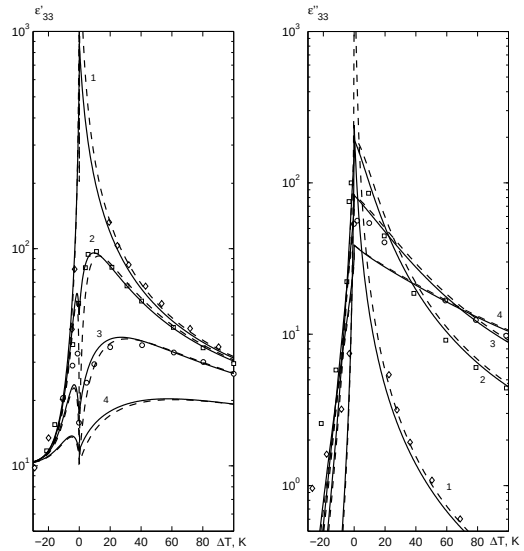


Figure 38. The temperature dependence of $\varepsilon'_{33}$ and $\varepsilon''_{33}$ of $KH_2PO_4$ at different frequencies $\nu$ (GHz): 9.2 – 1, ◇ [170]; 154.2 – 2, ▫ [171]; 372 – 3, ○ [171]; 800 – 4. Symbols are experimental points; the lines are the theoretical values.

mentioned that when the piezoelectric coupling is taken into account, the minimal values of $\varepsilon'_{33}(\omega)$ at $\Delta T = 0$ and at different frequencies are smaller than when the piezoelectric coupling is neglected; it accords with the experiment.

## 8. Modified proton ordering model for the $ND_4D_2PO_4$ type crystals

We consider a system of deuterons moving on O–D-. . .-O bonds in deuterated crystals of the $ND_4D_2PO_4$ type. primitive cell of such a crystal is composed of two neighboring $PO_4$ tetrahedra together with four hydrogen bonds attached to one of them ("$A$" type tetrahedra). Hydrogen bonds going to another ("$B$" type) tetrahedron belong to four nearest structural elements surrounding it (see fig. 39). The deuteron

configuration of the ground state in $ND_4D_2PO_4$ is shown. The spontaneous polarization in these crystals is zero due to antipolar ordering of dipole moments of hydrogen bonds. If an external electric field is applied along the crystallographic axes $a, b$, or $c$, then the different from zero net polarizations are induced.

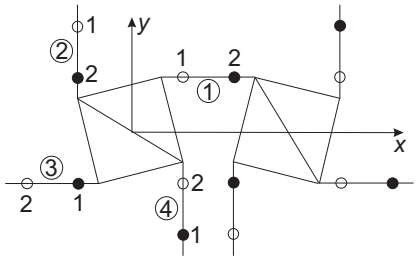


Figure 39. The primitive cell of the $ND_4D_2PO_4$: ①, ②, ③, ④ are the bonds numbers; 1,2 are the deuteron equilibrium sites. One of possible antiferroelectric deuteron configurations is shown..

The model Hamiltonian of the deuteron subsystem of $ND_4D_2PO_4$ with taking into account the short-range and long-range interactions, in presence of mechanical stresses $\sigma_6 = \sigma_{xy}$ and $\sigma_4 = \sigma_{yz}$, as well as external electric fields $E_3$ and $E_1$, directed along the crystallographic axes $c$ and $a$, consists of the "seed" and pseudospin parts. The "seed" energy corresponds to the lattice of heavy ions, and it is not explicitly dependent on the deuteron subsystem configuration. The pseudospin part takes into account the long-range ($\hat{H}_{long}$) and short-range ($\hat{H}_{short}$) interactions between the deuterons near the $PO_4$ tetrahedra and the interaction with the electric fields $E_1$ and $E_3$. Hence,

$$\hat{H} = NU_{seed} + \hat{H}_{long} + \hat{H}_{short} - \sum_{qf}(\mu_{f1}E_1 + \mu_{f3}E_3)\frac{\sigma_{qf}}{2}, \qquad (8.1)$$

where $N$ is the number of the primitive cells; $\sigma_{qf}$ is the z-component pseudospin operator, describing the state of a deuteron in the q-th cell on the f-th bond. Two eigenvalues of the operator $\sigma_{qf} = \pm 1$ are assigned to two equilibrium positions of a deuteron on the bond. Effective dipole moments of the primitive cell along the crystallographic axes per one deuteron bond have the following symmetry

$$\mu_3 = \mu_{13} = \mu_{23} = \mu_{33} = \mu_{43}, \quad \mu_1 = -\mu_{11} = \mu_{31}, \quad \mu_{21} = \mu_{41} = 0.$$



The "seed" energy $U_{seed}$ is expressed in terms of the electric fields $E_1$ and $E_3$, as well as strains $\varepsilon_i$, $\varepsilon_4$, and $\varepsilon_6$. It consists of the elastic, piezoelectric, and dielectric contributions

$$U_{seed} = v(\frac{1}{2}c_{44}^{E0}\varepsilon_4^2 + \frac{1}{2}c_{66}^{E0}\varepsilon_6^2 - e_{14}^0\varepsilon_4 E_1 - e_{36}^0\varepsilon_6 E_3 - \\ -\frac{1}{2}\chi_{11}^{\varepsilon_0}E_1^2 - \frac{1}{2}\chi_{33}^{\varepsilon_0}E_3^2), \qquad (8.2)$$

where $v$ is the primitive cell volume; $c_{ij}^{E0}$, $c_{44}^{E0}$, $c_{66}^{E0}$, $e_{14}^0$, $e_{36}^0$, $\chi_{11}^{\varepsilon_0}$, $\chi_{33}^{\varepsilon_0}$ are the "seed" elastic constants, piezoelectric coefficients, and dielectric susceptibilities. The "seed" characteristics determine the temperature dependences of the corresponding physical characteristics far from the transition temperature $T_N$.

The dielectric, piezoelectric, and elastic characteristics of the $ND_4D_2PO_4$ type crystals will be explored using the thermodynamic potential. Taking into accounts the peculiarities of the crystalline structure of $ND_4D_2PO_4$, to find the thermodynamic potential we shall use the four-particle cluster approximation [90]. In this approximation the thermodynamic potential of $ND_4D_2PO_4$ reads

$$G = NU_{seed} + \frac{1}{2}\sum_{\substack{qq'\\ ff'}} J_{ff'}(qq')\frac{\langle\sigma_{qf}\rangle}{2}\frac{\langle\sigma_{q'f'}\rangle}{2} - \qquad (8.3)$$

$$-\frac{1}{2}T\sum_q\sum_{f=1}^{4}\ln Z_{1f} - T\sum_q \ln Z_4 - N\bar{v}(\sigma_4\varepsilon_4 + \sigma_6\varepsilon_6),$$

where $Z_{1f} = Spe^{-\beta\hat{H}_{qf}^{(1)}}$, $Z_4 = Spe^{-\beta\hat{H}_q^{(4)}}$ are the single-particle and four-particle partition functions. The single-particle $\hat{H}_{qf}^{(1)}$ and four-particle $\hat{H}_q^{(4)}$ Hamiltonians of strains $ND_4D_2PO_4$ crystals are given by the expressions

$$\hat{H}_{q_3^1}^{(1)} = \mp\frac{1}{\beta}\bar{x}_q\frac{\sigma_{q_3^1}}{2} \mp \frac{1}{\beta}\bar{x}_{13}\frac{\sigma_{q_3^1}}{2} + \frac{1}{\beta}\bar{z}\frac{\sigma_{q_3^1}}{2}, \qquad (8.4)$$
$$\hat{H}_{q_4^2}^{(1)} = \pm\frac{1}{\beta}\bar{x}_q\frac{\sigma_{q_4^2}}{2} \pm \frac{1}{\beta}\bar{x}_{24}\frac{\sigma_{q_4^2}}{2} + \frac{1}{\beta}\bar{z}\frac{\sigma_{q_4^2}}{2},$$

$$\hat{H}_q^{(4)} = \left(\frac{\delta_{a4}}{2} + \frac{\delta_{14}}{2}\right)\varepsilon_4\left(-\frac{\sigma_{q1}}{2} + \frac{\sigma_{q3}}{2}\right) + \qquad (8.5)$$
$$+\left(-\frac{\delta_{s6}}{4} + \frac{\delta_{16}}{2}\right)\varepsilon_6\left(\frac{\sigma_{q1}}{2} + \frac{\sigma_{q2}}{2} + \frac{\sigma_{q3}}{2} + \frac{\sigma_{q4}}{2}\right) +$$

$$+2\,(\delta_{a4}-\delta_{14})\,\varepsilon_4\left(\frac{\sigma_{q1}}{2}\frac{\sigma_{q2}}{2}\frac{\sigma_{q4}}{2}-\frac{\sigma_{q1}}{2}\frac{\sigma_{q3}}{2}\frac{\sigma_{q4}}{2}\right)+$$
$$+\,(-\delta_{s6}-2\delta_{16})\,\varepsilon_6\times$$
$$\times\left(\frac{\sigma_{q1}}{2}\frac{\sigma_{q2}}{2}\frac{\sigma_{q3}}{2}+\frac{\sigma_{q1}}{2}\frac{\sigma_{q2}}{2}\frac{\sigma_{q4}}{2}+\frac{\sigma_{q1}}{2}\frac{\sigma_{q3}}{2}\frac{\sigma_{q4}}{2}+\frac{\sigma_{q2}}{2}\frac{\sigma_{q3}}{2}\frac{\sigma_{q4}}{2}\right)+$$
$$+(V_a+\delta_{a6}\varepsilon_6)\left(\frac{\sigma_{q1}}{2}\frac{\sigma_{q2}}{2}+\frac{\sigma_{q3}}{2}\frac{\sigma_{q4}}{2}\right)+$$
$$+(V_a-\delta_{a6}\varepsilon_6)\left(\frac{\sigma_{q2}}{2}\frac{\sigma_{q3}}{2}+\frac{\sigma_{q4}}{2}\frac{\sigma_{q1}}{2}\right)+$$
$$+U_a\left(\frac{\sigma_{q1}}{2}\frac{\sigma_{q3}}{2}+\frac{\sigma_{q2}}{2}\frac{\sigma_{q4}}{2}\right)+\Phi_a\frac{\sigma_{q1}}{2}\frac{\sigma_{q2}}{2}\frac{\sigma_{q3}}{2}\frac{\sigma_{q4}}{2}-$$
$$-\frac{1}{\beta}x_q\Big(-\frac{\sigma_{q1}}{2}+\frac{\sigma_{q2}}{2}+\frac{\sigma_{q3}}{2}-\frac{\sigma_{q4}}{2}\Big)-$$
$$-\frac{1}{\beta}x_{13}\Big(-\frac{\sigma_{q1}}{2}+\frac{\sigma_{q3}}{2}\Big)-\frac{1}{\beta}x_{24}\Big(\frac{\sigma_{q2}}{2}-\frac{\sigma_{q4}}{2}\Big)-$$
$$-\frac{1}{\beta}z\left(\frac{\sigma_{q1}}{2}+\frac{\sigma_{q2}}{2}+\frac{\sigma_{q3}}{2}+\frac{\sigma_{q4}}{2}\right).$$

Here we use the following notations

$$V_a=\frac{1}{2}\varepsilon'-\frac{1}{2}w_1',\qquad U_a=\frac{1}{2}\varepsilon'+\frac{1}{2}w_1',\qquad \Phi_a=2\varepsilon'-8w'+2w_1',$$
$$\varepsilon'=\varepsilon_s-\varepsilon_a,\quad w'=\varepsilon_1-\varepsilon_a,\quad w_1'=\varepsilon_0-\varepsilon_a,$$

where $\varepsilon_s$, $\varepsilon_a$, $\varepsilon_1$, $\varepsilon_0$ are the configurational energies of deuterons near a $PO_4$ tetrahedron, whereas $\varepsilon'$, $w'$, $w_1'$ are the antiferroelectric energies of the extended Slater-Takagi model [90];

$$x_q=\beta(-\Delta_a e^{i\mathbf{k}^z\mathbf{a}_q}+2\nu_a(\mathbf{k}^z)\eta^{(1)}e^{i\mathbf{k}^z\mathbf{a}_q}),$$
$$x_{13}=\beta(-\Delta_{13}+2\nu_a(0)\eta_{13}^{(1)x}+2\psi_4\varepsilon_4+\mu_1E_1),$$
$$x_{24}=\beta(-\Delta_{24}+2\nu_a(0)\eta_{24}^{(1)x}),$$
$$z=\beta(-\Delta_c+2\nu_c(0)\eta^{(1)z}-2\psi_6\varepsilon_6+\mu_3E_3),$$
$$\bar{x}_q=-\beta\Delta_a e^{i\mathbf{k}^z\mathbf{a}_q}+x_q,$$
$$\bar{x}_{24}^{13}=-\beta\Delta_{24}^{13}+\bar{x}_{24}^{13},\qquad \bar{z}=-\beta\Delta_c+z,$$

where

$$4\nu_a^0(\mathbf{k}^z)=J_{11}(\mathbf{k}^z)-J_{13}(\mathbf{k}^z),\quad J_{ff'}(\mathbf{k}^z)=\sum_{\mathbf{a}_q-\mathbf{a}_{q'}}J_{ff'}(qq')e^{-i\mathbf{k}^z(\mathbf{a}_q-\mathbf{a}_{q'})},$$
$$4\nu_a^0(0)=J_{11}(0)-J_{13}(0),\quad 4\nu_c^0(0)=J_{11}(0)+2J_{12}(0)+J_{13}(0),$$



where $\mathbf{k}^z=1/2(\mathbf{b}_1+\mathbf{b}_2+\mathbf{b}_3)$, $\mathbf{b}_1$, $\mathbf{b}_2$, $\mathbf{b}_3$ are vectors of the reciprocal lattice; $e^{i\mathbf{k}^z\mathbf{a}_q}=\pm1$, $\psi_4$, $\psi_6$ are the deformational potentials; $\Delta_a$, $\Delta_{13}$, $\Delta_{24}$, $\Delta_c$ are the effective fields created by the neighboring bonds from outside the cluster.

If the crystal is free from external fields and stresses, then

$$\eta^{(1)}=-\langle\sigma_1\rangle=\langle\sigma_2\rangle=\langle\sigma_3\rangle=-\langle\sigma_4\rangle=\frac{1}{D}(\operatorname{sh}2x+2b\operatorname{sh}x),\qquad(8.6)$$

фx

$$D=a+\operatorname{ch}2x+d+4b\operatorname{ch}x+1,\qquad x=\frac{1}{2}\ln\frac{1+\eta^{(1)}}{1-\eta^{(1)}}+\beta\nu_a(\mathbf{k}^z)\eta^{(1)}.$$
$$a=e^{-\beta\varepsilon'},\qquad b=e^{-\beta w'},\qquad d=e^{-\beta w_1'}.$$

In contrast to the ferroelectric $KD_2PO_4$ type crystals, where the energy of the up/down configurations $\varepsilon_s$ is the lowest configurational energy of deuterons around a $PO_4$ group, in the $ND_4D_2PO_4$ type crystals the lowest is the energy of the lateral configurations $\varepsilon_a$. In addition, in these crystals the character of deuteron ordering and symmetry of their distribution functions are also different.

## 9. Dielectric, piezoelectric, and elastic characteristics of the $ND_4D_2PO_4$ type antiferroelectrics

### 9.1. Longitudinal dynamic dielectric susceptibility

The procedure that can be used to find the dynamic characteristics of the $ND_4D_2PO_4$ type crystals is analogous to the presented above procedure for the $KD_2PO_4$ type crystals [113, 114]. Therefore, here we give only the find results.

The expression for the longitudinal dynamic susceptibility of a mechanically free $ND_4D_2PO_4$ type crystal reads [115]:

$$\chi_{33}^{\sigma}(\omega)=\chi_{33}^{\varepsilon}(\omega)+\frac{1}{R(\omega)}\frac{e_{36}^2(\omega)}{c_{66}^E(\omega)}.\qquad(9.1)$$

where

$$\frac{1}{R(\omega)}=\frac{2}{k_6l}\tan\frac{k_6l}{2},\qquad k_6=\frac{\omega\sqrt{\rho}}{\sqrt{c_{66}^E(\omega)}},$$

In (9.1) longitudinal dynamic susceptibility of a mechanically clamped crystal is

$$\chi_{33}^{\varepsilon}(\omega)=\chi_{33}^{\varepsilon 0}+\frac{\beta\mu_3^2}{v}F^{(1)}(\omega),\qquad(9.2)$$

$$e_{36}(\omega) = e_{36}^{0} + \\ + \frac{\beta\mu_3}{v}\Big[-2\psi_6 F^{(1)}(\omega) + \delta_{s6}F_s^{(1)}(\omega) - \delta_{a6}F_a^{(1)}(\omega) + \delta_{16}F_1^{(1)}(\omega)\Big], \quad (9.3)$$

$$c_{66}^{E}(\omega) = c_{66}^{E0} + \quad (9.4)$$
$$+ \frac{4\beta\psi_6}{vD}\Big[-2\psi_6 F^{(1)}(\omega) + \delta_{s6}F_s^{(1)}(\omega) + \delta_{16}F_1^{(1)}(\omega) - \delta_{a6}F_a^{(1)}(\omega)\Big] -$$
$$- \frac{4\varphi_c^{\eta} f_6}{vD}\beta\Big[-2\psi_6 F^{(1)}(\omega) + \delta_{s6}F_s^{(1)}(\omega) + \delta_{16}F_1^{(1)}(\omega) - \delta_{a6}F_a^{(1)}(\omega)\Big] +$$
$$+ \frac{4\beta\psi_6}{vD}f_6 - \frac{2\beta}{vD}\Big[\delta_{s6}^2 a + \delta_{16}^2 4b + \delta_{a6}^2(1+\cosh 2x)\Big],$$

where we use the following notations

$$F^{(1)}(\omega) = \frac{(i\omega)^2 r^{(2)} + (i\omega)r^{(1)} + r^{(0)}}{(i\omega)^3 + (i\omega)^2 r_2 + (i\omega)r_1 + r_0}, \quad (9.5)$$
$$F_s^{(1)}(\omega) = \frac{(i\omega)^2 r_s^{(2)} + (i\omega)r_s^{(1)} + r_s^{(0)}}{(i\omega)^3 + (i\omega)^2 r_2 + (i\omega)r_1 + r_0},$$
$$F_a^{(1)}(\omega) = \frac{(i\omega)^2 r_a^{(2)} + (i\omega)r_a^{(1)} + r_a^{(0)}}{(i\omega)^3 + (i\omega)^2 r_2 + (i\omega)r_1 + r_0},$$
$$F_1^{(1)}(\omega) = \frac{(i\omega)^2 r_1^{(2)} + (i\omega)r_1^{(1)} + r_1^{(0)}}{(i\omega)^3 + (i\omega)^2 r_2 + (i\omega)r_1 + r_0},$$

whereas the expressions for $r_2$, ..., $r_1^{(0)}$ are given in [172].

### 9.2. Transverse dynamic dielectric susceptibility

The transverse dynamic susceptibility of mechanically free $ND_4D_2PO_4$ crystal reads [173]:

$$\chi_{11}^{\sigma}(\omega) = \chi_{11}^{\varepsilon}(\omega) + \frac{1}{R_4(\omega)}\frac{e_{14}^2(\omega)}{c_{44}^{E}(\omega)}, \quad (9.6)$$

ф-х

$$\frac{1}{R_4(\omega)} = \frac{2}{k_4 l}\tanh\frac{k_4 l}{2}, \qquad k_4 = \frac{\omega\sqrt{\rho}}{\sqrt{c_{44}^{E}(\omega)}},$$

In (9.6) the transverse dynamic susceptibility of a mechanically clamped crystal is

$$\chi_{11}^{\varepsilon}(\omega) = \chi_{11}^{\varepsilon 0} + \bar{v}\frac{\mu_1}{v^2}\frac{1}{4T}\Big[F_+^{(1)}(\omega) + F_-^{(1)}(\omega)\Big]. \quad (9.7)$$



$$e_{14}(\omega) = e_{14}^{0} + \frac{\mu_1}{v}\frac{1}{2T}\Big\{\tilde{\psi}_4\Big[F_+^{(1)}(\omega) + F_-^{(1)}(\omega)\Big] + \quad (9.8)$$
$$+ \tilde{\delta}_{14}\Big[F_{14+}^{(1)}(\omega) + F_{14-}^{(1)}(\omega)\Big] + \tilde{\delta}_{a4}\Big[F_{a4+}^{(1)}(\omega) + F_{a4-}^{(1)}(\omega)\Big]\Big\},$$

$$c_{44}^{E}(\omega) = c_{44}^{E0} + \frac{2\tilde{\psi}_4}{\bar{v}DT}\Big[\tilde{\delta}_{a4}(\varkappa+1) + \tilde{\delta}_{14}(\varkappa_2^b + \varkappa^b)\Big] + \quad (9.9)$$
$$+ \left\{-\frac{2\tilde{\psi}_4}{\bar{v}T} + \frac{2\varphi_a^{\eta}(0)}{\bar{v}DT}\Big[\tilde{\delta}_{14}(\varkappa_2^b + \varkappa^b) + \tilde{\delta}_{a4}(\varkappa+1)\Big]\right\} \times$$
$$\times\frac{1}{2T}\Big\{\tilde{\psi}_4\Big[F_+^{(1)}(\omega) + F_-^{(1)}(\omega)\Big] +$$
$$+ \tilde{\delta}_{14}\Big[F_{14+}^{(1)}(\omega) + F_{14-}^{(1)}(\omega)\Big] + \tilde{\delta}_{a4}\Big[F_{a4+}^{(1)}(\omega) + F_{a4-}^{(1)}(\omega)\Big]\Big\} +$$
$$+ \frac{2\varphi_a^{\eta}(0)}{\bar{v}D}\Big[\tilde{\delta}_{a4}(\varkappa-1) + \tilde{\delta}_{14}(\varkappa_2^b - \varkappa^b)\Big] \times$$
$$\times\frac{1}{2T}\Big\{\tilde{\psi}_4\Big[F_+^{(1)}(\omega) - F_-^{(1)}(\omega)\Big] +$$
$$+ \tilde{\delta}_{14}\Big[F_{14+}^{(1)}(\omega) - F_{14-}^{(1)}(\omega)\Big] + \tilde{\delta}_{a4}\Big[F_{a4+}^{(1)}(\omega) - F_{a4-}^{(1)}(\omega)\Big]\Big\} +$$
$$+ \frac{2}{\bar{v}D^2T}\Big(\tilde{\delta}_{a4}\sinh 2x + \tilde{\delta}_{14}2b\sinh x\Big)^2 -$$
$$- \frac{2}{\bar{v}DT}\Big[\tilde{\delta}_{a4}^2(\cosh 2x + 1) + \tilde{\delta}_{14}^2 2b\cosh x\Big].$$

Here we use the following notations

$$F_+^{(1)}(\omega) = \frac{(i\omega)^4 n^{(4)} + (i\omega)^3 n^{(3)} + (i\omega)^2 n^{(2)} + (i\omega)n^{(1)} + n^{(0)}}{(i\omega)^5 + (i\omega)^4 n_4 + (i\omega)^3 n_3 + (i\omega)^2 n_2 + (i\omega)n_1 + n_0},$$
$$F_-^{(1)}(\omega) = \frac{(i\omega)^2 m^{(2)} + (i\omega)m^{(1)} + m^{(0)}}{(i\omega)^3 + (i\omega)^2 m_2 + (i\omega)m_1 + m_0}, \quad (9.10)$$
$$F_{14+}^{(1)}(\omega) = \frac{(i\omega)^4 n_{14}^{(4)} + (i\omega)^3 n_{14}^{(3)} + (i\omega)^2 n_{14}^{(2)} + (i\omega)n_{14}^{(1)} + n_{14}^{(1)}}{(i\omega)^5 + (i\omega)^4 n_4 + (i\omega)^3 n_3 + (i\omega)^2 n_2 + (i\omega)n_1 + n_0},$$
$$F_{14-}^{(1)}(\omega) = \frac{(i\omega)^2 m_{14}^{(2)} + (i\omega)m_{14}^{(1)} + m_{14}^{(0)}}{(i\omega)^3 + (i\omega)^2 m_2 + (i\omega)m_1 + m_0},$$
$$F_{a4+}^{(1)}(\omega) = \frac{(i\omega)^4 n_{a4}^{(4)} + (i\omega)^3 n_{a4}^{(3)} + (i\omega)^2 n_{a4}^{(2)} + (i\omega)n_{a4}^{(1)} + n_{a4}^{(1)}}{(i\omega)^5 + (i\omega)^4 n_4 + (i\omega)^3 n_3 + (i\omega)^2 n_2 + (i\omega)n_1 + n_0},$$
$$F_{a4-}^{(1)}(\omega) = \frac{(i\omega)^2 m_{a4}^{(2)} + (i\omega)m_{a4}^{(1)} + m_{a4}^{(0)}}{(i\omega)^3 + (i\omega)^2 m_2 + (i\omega)m_1 + m_0},$$

whereas the expressions for $n^{(4)}$, ..., $m_0$ are given in [173].

### 9.3. Static dielectric, piezoelectric, and elastic characteristics

In the static limit $\omega \to 0$ in (9.2)-(9.4), (9.7)-(9.9), we obtain the isothermic static dielectric susceptibility of a mechanically clamped crystals, piezoelectric coefficient, and elastic constant at constant field in the following form

$$\chi_{33}^{\varepsilon} = \chi_{33}^{\varepsilon 0} + \frac{\mu_3^2}{v}\beta\frac{2\varkappa_6}{D-2\varkappa_6\varphi_c^{\eta}}, \tag{9.11}$$

$$\chi_{11}^{\varepsilon} = \chi_{11}^{\varepsilon 0} + \bar{v}\frac{\mu_1^2}{v^2}\frac{1}{2T}\left[\frac{\varkappa_1^b}{D-2\varkappa_1^b\varphi_a^{\eta}(0)} + \frac{\varkappa_2}{D-2\varkappa_2\varphi_a^{\eta}(0)}\right], \tag{9.12}$$

$$e_{36} = e_{36}^0 + 2\frac{\mu_3}{v}\beta\frac{-2\varkappa_6+f_6}{D-2\varkappa_6\varphi_c^{\eta}}, \tag{9.13}$$

$$e_{14} = e_{14}^0 + \tag{9.14}$$
$$+\frac{\mu_1}{v}\frac{1}{T}\left[\frac{\tilde{\psi}_4\varkappa_1^b - \tilde{\delta}_{a4} - \tilde{\delta}_{14}\varkappa^b}{D-2\varkappa_1^b\varphi_a^{\eta}(0)} + \frac{\tilde{\psi}_4\varkappa_2 - \tilde{\delta}_{a4}\varkappa - \tilde{\delta}_{14}\varkappa_2^b}{D-2\varkappa_2\varphi_a^{\eta}(0)}\right],$$

$$c_{66}^E = c_{66}^{E0} + \frac{8\psi_6}{v}\frac{\beta(-\psi_6\varkappa_6+f_6)}{D-2\varkappa_6\varphi_c^{\eta}} - \frac{4\beta\varphi_c^{\eta}f_6^2}{vD(D-2\varkappa_6\varphi_c^{\eta})} -$$
$$-\frac{2\beta}{vD}(\delta_{16}^2 4b\,\mathrm{ch}\,x + \delta_{s6}^2 a + \delta_{a6}^2 2\,\mathrm{ch}^2\,x). \tag{9.15}$$

$$c_{44}^E = c_{44}^{E0} - \frac{2\tilde{\psi}_4}{\bar{v}T}\frac{\tilde{\psi}_4\varkappa_1^b - (\tilde{\delta}_{a4}+\tilde{\delta}_{14}\varkappa^b)}{D-2\varkappa_1^b\varphi_a^{\eta}(0)} - \tag{9.16}$$
$$-\frac{4\varphi_a^{\eta}(0)}{\bar{v}T}\frac{(\tilde{\delta}_{a4}+\tilde{\delta}_{14}\varkappa^b)(\tilde{\delta}_{a4}\varkappa+\tilde{\delta}_{14}\varkappa_2^b)}{D[D-2\varkappa_1^b\varphi_a^{\eta}(0)]} -$$
$$-\frac{2\tilde{\psi}_4}{\bar{v}T}\frac{\tilde{\psi}_4\varkappa_2 - (\tilde{\delta}_{a4}\varkappa+\tilde{\delta}_{14}\varkappa_2^b)}{D-2\varkappa_2\varphi_a^{\eta}(0)} -$$
$$-\frac{4\varphi_a^{\eta}(0)}{\bar{v}T}\frac{(\tilde{\delta}_{a4}+\tilde{\delta}_{14}\varkappa^b)(\tilde{\delta}_{a4}\varkappa+\tilde{\delta}_{14}\varkappa_2^b)}{D[D-2\varkappa_2\varphi_a^{\eta}(0)]} -$$
$$-\frac{2}{\bar{v}DT}\left[\tilde{\delta}_{a4}^2(\mathrm{ch}\,2x+1) + \tilde{\delta}_{14}^2 2bb_1\,\mathrm{ch}\,x\right] +$$
$$+\frac{2}{\bar{v}D^2T}(\tilde{\delta}_{a4}\,\mathrm{sh}\,2x + \tilde{\delta}_{14}2bb_1\,\mathrm{sh}\,x)^2,$$

$$\varkappa_6 = a + b\,\mathrm{ch}\,x,\ \varkappa_1^b = 1 + b\,\mathrm{ch}\,x,$$
$$\varkappa^b = b\,\mathrm{ch}\,x,\ f_6 = \delta_{s6}a - \delta_{16}2b\,\mathrm{ch}\,x;$$
$$\varkappa_2 = \varkappa + \varkappa_2^b = \mathrm{ch}\,2x - \eta^{(1)}\,\mathrm{sh}\,2x + b\,\mathrm{ch}\,x - \eta^{(1)}2b\,\mathrm{sh}\,x,$$
$$\varphi_a^{\eta}(0) = \frac{1}{1-\eta^{(1)2}} + \beta\nu_a(0),\quad \varphi_c^{\eta} = \frac{1}{1-\eta^{(1)2}} + \beta\nu_c(0).$$



Using the known relations between the elastic, dielectric, and piezoelectric characteristics of the $ND_4D_2PO_4$ crystal, we find, just like we did for $KD_2PO_4$, the other thermodynamic quantities, such as $\chi_{33}^{\sigma}$, $\chi_{11}^{\sigma}$, $h_{36}$, $h_{14}$, $d_{36}$, $d_{14}$, $g_{36}$, $g_{14}$, $c_{66}^P$, $c_{44}^P$.

## 10. Comparison of the numerical results with experimental data

Let us analyze the results of numerical calculations of dielectric, piezoelectric, and elastic characteristics of the $NH_4H_2PO_4$ (ADP) and $ND_4D_2PO_4$ (DADP) crystals and compare them with the corresponding experimental data. It should be noted that the developed in the previous sections theory, strictly speaking, is valid for the DADP crystals only. But taking into account the effect of tunneling suppression by the short range correlations, we shall assume that the proposed in the two previous sections theory is valid for ADP as well.

In order to calculate the temperature dependences of the physical characteristics of ADP and DADP crystals in the paraelectric phase, obtained within the developed theory, we need to set the values of the following parameters:

- energies of proton and deuteron configurations $\varepsilon_H'^0$, $w_H'^0$, $\varepsilon_D'^0$, $w_D'^0$;
- long-range interaction parameters $\nu_{cH}^0(0)$, $\nu_{cD}^0(0)$, $\nu_{aH}^0(0)$, $\nu_{aD}^0(0)$;
- deformational potentials $\psi_6$, $\delta_{s6}$, $\delta_{16}$, $\delta_{a6}$, $\delta_{1i}$; $\psi_4$, $\delta_{a4}$, $\delta_{14}$;
- effective dipole moments $\mu_{3H}$, $\mu_{3D}$, $\mu_{1H}$, $\mu_{1D}$;
- "seed" static dielectric susceptibility $\chi_{33}^{\varepsilon 0}$, $\chi_{11}^{\varepsilon 0}$, piezoelectric coefficients $e_{36}^0$, $e_{14}^0$, elastic constants $c_{66}^{E0}$, $c_{44}^{E0}$.

In order to determine the listed above parameters we used [172, 173] the experimental data for the temperature dependences of the calculated physical characteristics of the ADP and DADP crystals. The fitting procedure is analogous to that for the $KH_2PO_4$ crystals. The optimum set of the parameters used in numerical calculations of the physical characteristics of the considered crystals is given in Table 2.

In calculations the primitive cell volume $v$ was taken to be equal to $0{,}2110{\cdot}10^{-21}$ cm$^3$ for ADP [174], and $v = 0{,}213{\cdot}10^{-21}$ cm$^3$ for DADP [175].

Since most of experimental data for the calculated physical characteristics of the DADP type antiferroelectrics are available only for the paraelectric phase, the numerical calculations will be performed for $T > T_N$ only.

Table 6. The sets of the optimum model parameters for ADP and DADP

| | $T_N$ (K) | $\frac{\varepsilon'^0}{k_B}$ (K) | $\frac{w'^0}{k_B}$ (K) | $\frac{\nu_a^0(0)}{k_B}$ (K) | $\frac{\nu_c^0}{k_B}$, (K) | $\mu_1, 10^{-18}$ (esu·cm) | $\mu_3, 10^{-18}$, (esu· cm) | $\chi_{11}^{0\varepsilon}$ | $\chi_{33}^{0\varepsilon}$ |
|---|---|---|---|---|---|---|---|---|---|
| ADP | 148 | 20 | 490,0 | -40,00 | -10,00 | 6,45 | 2,10 | 0,70 | 0,23 |
| DADP | 240 | 78,8 | 715,4 | -54,70 | -17.35 | 7.29 | 2,75 | 0,58 | 0,34 |

| | $\frac{\psi_4}{k_B}$ (K) | $\frac{\delta_{s4}}{k_B}$ (K) | $\frac{\delta_{14}}{k_B}$ (K) | $e_{14}^0, 10^4$ (esu·cm$^2$) | $c_{44}^{E0} \cdot 10^{-10}$ (dyn/cm$^2$) |
|---|---|---|---|---|---|
| ADP | 120 | 94 | 82 | 250 | 8.9 |
| DADP | 225 | 100 | 100 | 3000 | 9.0 |

| | $\frac{\psi_6}{k_B}$, (K) | $\frac{\delta_{s6}}{k_B}$, (K) | $\frac{\delta_{a6}}{k_B}$, (K) | $\frac{\delta_{16}}{k_B}$, (K) | $e_{36}^0$ $(esu/cm^2)$ | $c_{66}^0 \cdot 10^{-10}$ $(dyn/cm^2)$ |
|---|---|---|---|---|---|---|
| ADP | -160 | 1400 | 100 | -300 | 10000 | 7.9 |
| DADP | -200 | 2000 | 200 | -100 | 28000 | 7.6 |

| | $P_{long}$ (s) | $R_{long}$ (s/k) | $P_{transv}$ (s) | $R_{transv}$ (s/k) |
|---|---|---|---|---|
| ADP | 0,38 | 0,0090 | 0,95 | 0,0110 |
| DADP | 6,72 | 0,0090 | 5,90 | 0,0032 |

### 10.1. Static dielectric, piezoelectric and elastic characteristics

Let us discuss now the results of calculations of the physical characteristics of ADP and DADP crystals within the proposed theory and compare the obtained results with the corresponding experimental data. In figure 40 along with the available experimental data we plot the calculated temperature dependences of the transverse and longitudinal static dielectric permittivities of ADP (a) and DADP (b) antiferroelectrics. It can be seen, that the calculated $\varepsilon_{11}^{\sigma}$ and $\varepsilon_{11}^{\varepsilon}$ practically coincide (the difference is less than 0.02%), that agrees with the experimental data. At the same time $\varepsilon_{33}^{\sigma}$ is by $\sim 18\%$ larger than $\varepsilon_{33}^{\varepsilon}$; this difference does not depend on temperature.

In figure 41 we plot the temperature dependences of the piezoelectric coefficients of the ADP and DADP crystals along with the experimental data. The coefficients $d_{36}$ and $e_{36}$ are finite at $T = T_N$ and decrease with further increase of temperature. It should be noted that with increasing temperature $\Delta T$ from 0 up to 170 K the coefficient $d_{36}$ of ADP becomes 2.1 times smaller, whereas $e_{36}$ halves. The values of the piezoelectric coefficients $d_{14}$, $e_{14}$ of $N(H_{1-x}D_x)_4(H_{1-x}D_x)_2PO_4$ are of the same order



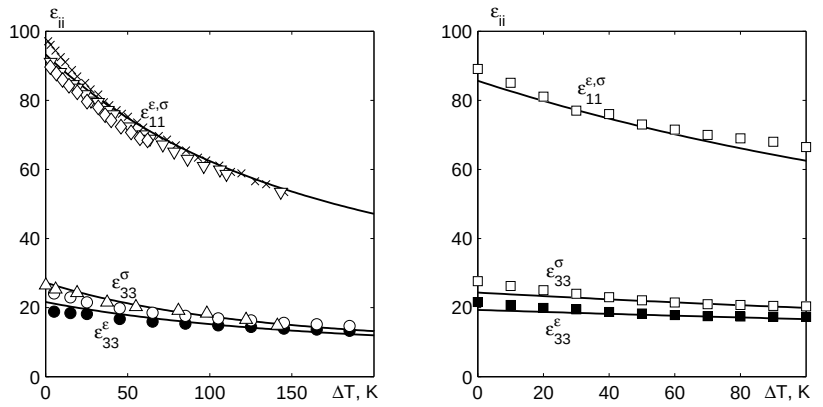


Figure 40. The temperature dependence of the the transverse and longitudinal static dielectric permittivities of ADP (a) and DADP (b): × – [141]; ◇ – [22]; ▽ – [142]; △ – [133]; ○ , ● – [139]; □ , ■ , – [135].

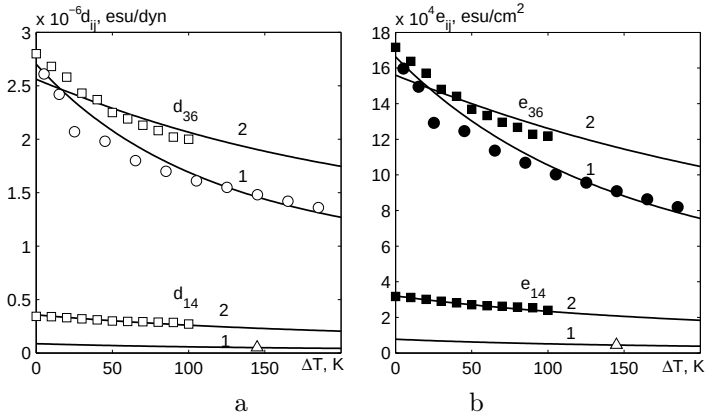


Figure 41. The temperature dependence of the piezoelectric coefficients of ADP (1) and DADP (2) crystals: □ , ■ – [135]; ○ , ● – [139]; △ – [176].

as these characteristics of $K(H_{1-x}D_x)_2PO_4$.

The calculated temperature dependences of the elastic constants $c_{44}^{E,P}$

and $c_{66}^{E,P}$ of ADP (a) and DADP (b) along with the available experimental data are shown in fig. 42.

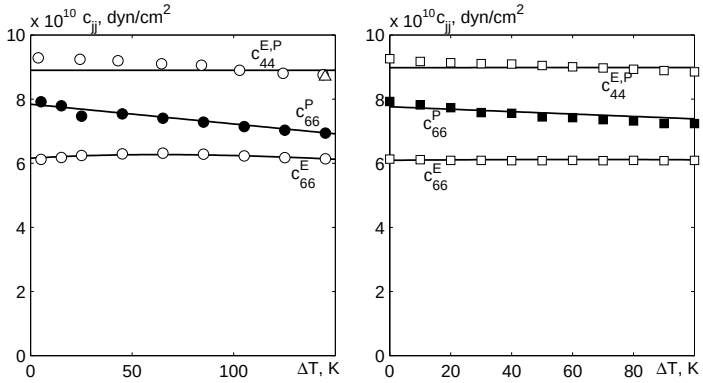


Figure 42. The temperature dependence of the elastic constants of ADP (c) and DADP (d) crystals: ▫ , ▪ – [135]; ○ , ● – [139]; △ – [176].

As one can see in figs. 40-42, the proposed theory provides a good agreement with experiment for the thermodynamic characteristics of ADP and DADP crystals.

### 10.2. Dynamic longitudinal and transverse permittivities

Let us analyze now the temperature and frequency dependences of the calculated dynamic characteristics of mechanically free ADP and DADP crystals, cut as thin square plates with sides $l = 1$ mm in the plane (0,0,1). Due to the lack of available experimental data, we are not able to make a quantitative comparison of the theoretical temperature and frequency dependences of the characteristics of a mechanically free crystal in the piezoelectric resonance region with experiment. Depending on the relation between the frequency $\nu$ from the piezoelectric resonance region and temperature $\Delta T$, the temperature curves of the real and imaginary parts of the dielectric permittivity of mechanically free ADP and DADP crystal, one can observe one, two, or more resonance peaks.

In figure 43 for ADP at $\Delta T = 28$ K and in figure 44 for DADP at $\Delta T = 64$ K we depict the calculated frequency curves of the real and imaginary parts of the dielectric permittivity $\varepsilon_{33}(\omega, T)$ along with the experimental data of [177]. At $10^6 - 10^8$ Hz the permittivity has the



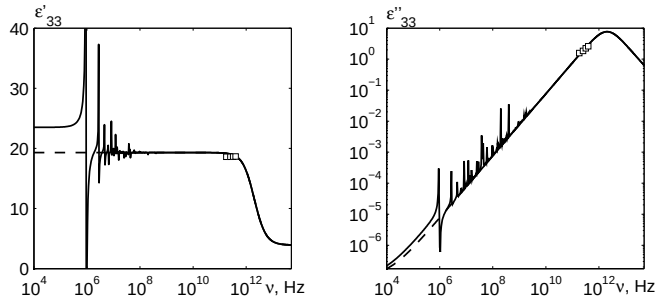


Figure 43. The frequency dependences of the real and imaginary parts of the dynamic dielectric permittivity of a free and clamped (dashed line) ADP crystal at $\Delta T = 28$ K; □ – [177].

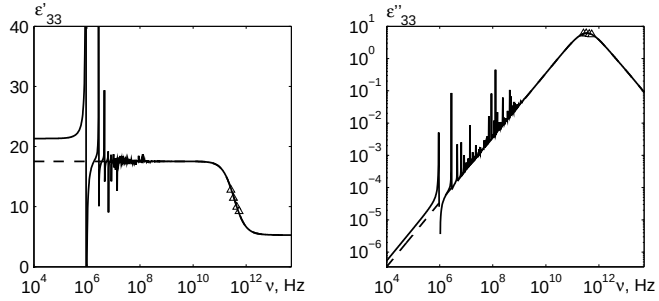


Figure 44. The frequency dependences of the real and imaginary parts of the dynamic dielectric permittivity of a free and clamped (dashed line) DADP crystal at $\Delta T = 64$ K; △ – [177, 178].

resonance dispersion. At $\omega \to 0$ we obtain the static dielectric permittivity of a free crystal. The dashed line corresponds to the low-frequency limit of the clamped permittivity. Above the resonances the permittivity corresponds to a crystal clamped by the high-frequency field and has a relaxational dispersion.

Let us analyze now the temperature and frequency dependences of the calculated dynamic characteristics of mechanically free ADP and DADP crystals, cut as square plates with sides $l = 1$ mm in the plane (1,0,0).

In figures 45 and 46 we show the frequency dependences of the real

and imaginary parts of the dynamic dielectric permittivity $\varepsilon_{11}$ of ADP at $\Delta T = 35$ K and DADP at $\Delta T = 62$ K. In the frequency range

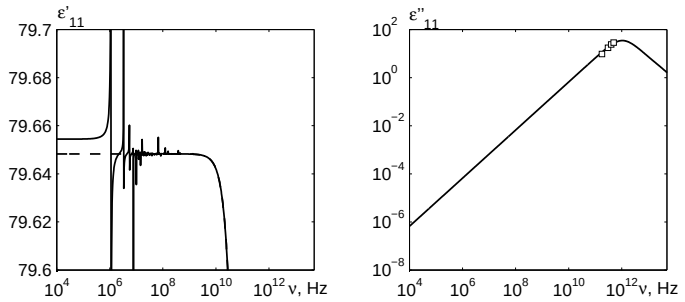


Figure 45. The frequency dependences of the real and imaginary parts of the dynamic dielectric permittivity $\varepsilon_{11}$ of a free and clamped (dashed line) ADP crystal at $\Delta T = 35$ K, ▫ [177].

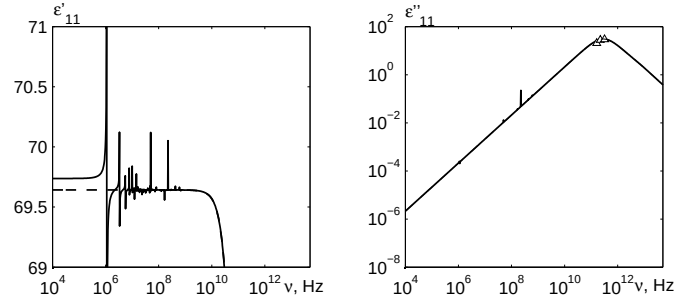


Figure 46. The frequency dependences of the real and imaginary parts of the dynamic dielectric permittivity $\varepsilon_{11}$ of a free and clamped (dashed line) DADP crystal at $\Delta T = 62$ K, ▵ [177, 178].

$10^6 - 10^8$ Hz the resonance dispersion is observed. At $\omega \to 0$ we obtain the static dielectric permittivity of a free crystal. The dashed line corresponds to the low-frequency limit of the clamped permittivity. The resonance peaks of $\varepsilon_{11}^{\sigma}$ are also very small. Above the resonances, the crystal clamping by the high-frequency field is observed; the dielectric permittivity of the clamped crystal has a relaxational dispersion above $10^9$ Hz.



## 11. Electromechanical coupling coefficient

In figure 47 we show the temperature dependence of the electromechanical coupling coefficient $k_3^2 = (\varepsilon_{33}^{\sigma} - \varepsilon_{33}^{\varepsilon})/\varepsilon_{33}^{\sigma}$ for different crystals of the KDP family. $k_3^2$ has a maximum at the transition point and drops at moving away from $T_c$, especially in the ferroelectric phase. In ADP and DADP $k_3^2$ has a maximum at $T = T_N$ at decreases slowly with increasing temperature. At $\Delta T \approx$10K the magnitude of $k_3^2$ in ADP is much larger than in RDP. The frequency dependence of the real part of the

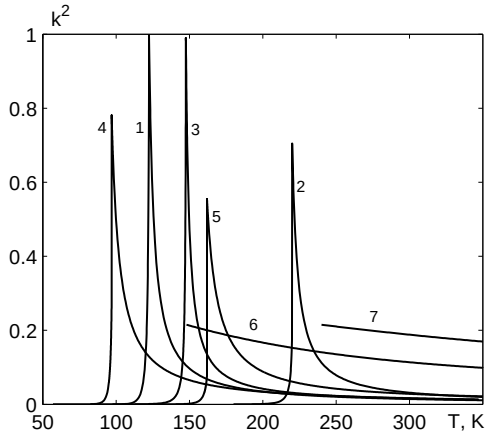


Figure 47. The temperature dependence of the electromechanical coupling coefficient $k^2 = (\varepsilon^{\sigma} - \varepsilon^{\varepsilon})/\varepsilon^{\sigma}$ of KDP (1), DKDP (2), RDP (3), KDA (4), DKDA (5), ADP (6), DADP (7) crystals.

electromechanical coupling coefficient $k_3^2(\nu) = (\varepsilon_{33}^{\sigma}(\nu) - \varepsilon_{33}^{\varepsilon}(\nu))/\varepsilon_{33}^{\sigma}(\nu)$ of KDP at $\Delta T$=5K is shown in fig. 48 At frequencies below the piezoelectric resonance frequency, where the crystal is mechanically free, $k_3^2(\nu) \approx 0.4$, whereas at frequencies where the crystal is clamped, $k_3^2(\nu) \approx 0$.

To estimate the piezoelectric coefficients and elastic constants of the KDP family crystals, we calculate the presented in fig. 49 temperature dependence of the difference $\varepsilon_{33}^{\sigma} - \varepsilon_{33}^{\varepsilon} = 4\pi e_{36} d_{36} = 4\pi e_{36}^2/c_{66}^E = 4\pi d_{36}^2 c_{66}^E$.

The results of this section indicate that the presence of piezoelectric coupling in the $KH_2PO_4$ family crystals gives rise to the difference between the dielectric permittivities of mechanically free and clamped crystals, non-zero piezoelectric coefficients, and piezoelectric resonance.

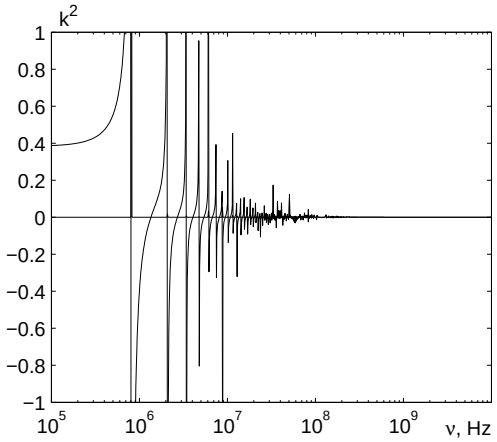


Figure 48. The frequency dependence of the real part of the electromechanical coupling coefficient $k^2 = (\varepsilon^\sigma(\omega) - \varepsilon^\varepsilon(\omega))/\varepsilon^\sigma(\omega)$ of KDP at $\Delta T$=5K.

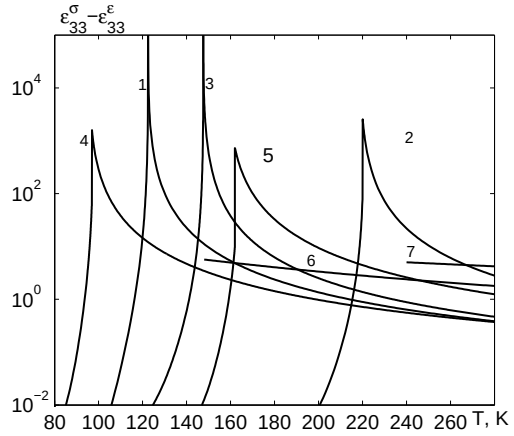


Figure 49. Temperature dependence of the difference $\varepsilon^\sigma - \varepsilon^\varepsilon$ of KDP (1), DKDP (2), RDP (3), KDA (4), DKDA (5), ADP (6), DADP (7) crystals.



Unfortunately, there was no similar theoretical or experimental studies carried out for the disordered compounds of the $Rb_{1-x}(NH_4)_xH_2PO_4$ type. Principally important is to explore the permittivities $\varepsilon'_{33}(\nu T)$ and $\varepsilon''_{33}(\nu T)$ in wide temperature and frequency ranges, in order to estimate the electromechanical coupling coefficient and the difference between the permittivities of free and clamped crystals, which would indicate that the piezoelectric coefficients in these systems are different from zero.

The measurements of dielectric, piezoelectric, and elastic characteristics of the compounds of this type were carried out (by L.M. Korotkov and his group). Below we give some of the obtained results for the longitudinal dielectric permittivity (fig. 50) and coefficients of piezoelectric strain (fig. 51) $d_{36}$ of the $K_{1-x}(NH_4)_xH_2PO_4$ compounds. The obtained

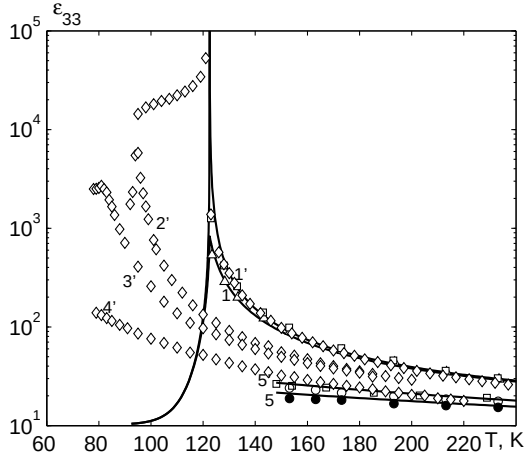


Figure 50. The temperature dependence of the dielectric permittivity of clamped ($\varepsilon^\varepsilon_{33}$) (curves 1,5) and free $\varepsilon^\sigma_{33}$ (1',2',3',4',5') $K_{1-x}(NH_4)_xH_2PO_4$ crystals at different $x$: 0.0 – 1, 1', ▫ , [139], ◇ , [Коротков] 1', △ [139]; 0.09 – 2', ◇ , [Коротков]; 0.12 – 3', ◇ , [Коротков]; 0.24 – 4', ◇ , [Коротков]; 1.0 – 5, • [139], 5', ○ [139], ▫ [133].

results along with the available structural data confirm our assumption about non-centrosymmetric structure of the K1-x(NH4)xH2PO4 type systems. They form a basis for development of a consistent statistical theory of the K1-x(NH4)xH2PO4 type systems that takes into account the piezoelectric coupling.

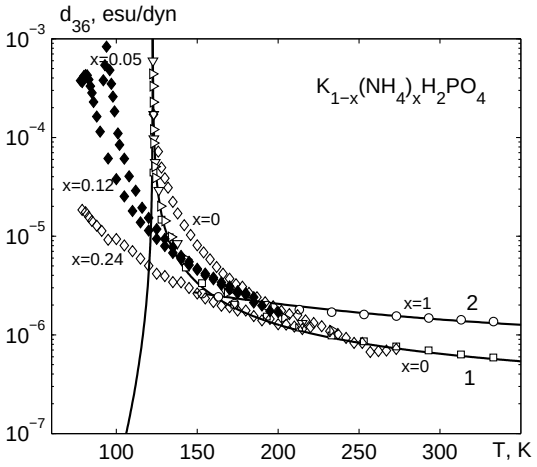


Figure 51. The temperature dependence of the coefficient of piezoelectric strain $d_{36}$ of KDP – 1, ▫ [139], ▽ [163], ▷ [164]; ADP – 2, ○, [139]. ◊, ⧫ – [Коротков].

## 12. Conclusions

In the framework of the four-particle cluster approximation for the short-range interactions and the mean field approximation for the long-range interactions, we explored the free energy, a system of equations for variation parameters, expression for spontaneous polarization, Edwards-Anderson parameter, molar specific heat, longitudinal and transverse dielectric permittivities of the $Rb_{1-x}(NH_4)_xH_2PO_4$ type compounds for all compositions $x$. The theoretical results are compared with experimental data.

In the ferroelectric phase composition region the spontaneous polarization decreases with increasing $x$ and vanishes at the transition to the glass phase region. The molar specific heat of the $Rb_{1-x}(NH_4)_xH_2PO_4$ type compounds in the regions of the ferroelectric and antiferroelectric phases has jumps, which vanish at the transition to the glass phase. The Edwards-Anderson parameter is different from zero at all compositions $0 < x < 1$ and temperatures, which is explained by the internal random deformational fields

For the $Rb_{1-x}(ND_4)_xD_2PO_4$ mixture the proposed theory satisfactorily describes the temperature curves of the real and imaginary parts of



the longitudinal and transverse permittivities in the regions of "pure" phases ($x \sim 1$, 0.5, 0). At the same time, for $Rb_{1-x}(NH_4)_xH_2PO_4$, $Rb_{1-x}(NH_4)_xH_2AsO_4$, $K_{1-x}(NH_4)_xH_2PO_4$ at low temperatures in the glass phase composition region the theory incorrectly describes the shape of the imaginary part of the permittivity curves $\varepsilon''_{aa}(T,\nu)$ (the theoretical peak is too narrow and too high). This is partially caused by the neglected within the Glauber approach tunneling of protons, which plays an essential role in the dynamic processes in these systems at low temperatures. It is established that in this model the dynamics in the proton glass composition region is of the Debye relaxation type only at high temperatures. In our model the temperature curves of the averaged relaxation times for longitudinal and transverse permittivities for proton-glass composition region at $T \to 0$ are close to the Arrhenius law. The phase diagrams constructed using the calculated dielectric characteristics are close to the experimental ones.

Absence of reliable experimental data for the physical characteristics of the $Rb_{1-x}(NH_4)_xH_2PO_4$ type proton glasses in a wide composition range creates large difficulties for verifying the validity of the proposed theory. Possible further improvement of the theory of proton glasses also requires reliable experimental data for the temperature dependences of all calculated characteristics of these crystals in a wide composition range.

Using the proposed modified proton ordering model with taking into account linear over the $\varepsilon_6$ and $\varepsilon_4$ strains contributions into the energy of the proton system but without tunneling, within the framework of the four-particle cluster approximation we calculate the dielectric, piezoelectric, elastic, and dynamic characteristics of the $KH_2PO_4$ type ferroelectrics and $NH_4H_2PO_4$ type antiferroelectrics. A thorough numerical analysis of the dependences of the calculated physical characteristics of the crystals on the values of the model parameters is carried out. The optimal sets of the values of these parameters are found for the considered crystals; it allowed us to properly describe the available experimental data. The physical characteristics of partially deuterated crystals is performed within the mean crystal approximation.

With taking into account the piezoelectric coupling we obtained the expressions for the susceptibilities of mechanically free and clamped crystals, piezoelectric coefficients, and elastic constants. The calculations of the temperature dependences of these characteristics confirm the experimentally obtained significant difference between the values of $\varepsilon^{\sigma}_{33}$ and $\varepsilon^{\xi}_{33}$ in the $K(H_{1-x}D_x)_2PO_4$ type crystal and the very small difference between these quantities for ADP and DADP. On the other hand,

the values of $\varepsilon_{11}^{\sigma}$ and $\varepsilon_{11}^{\varepsilon}$ in the ferroelectric compounds of the $KH_2PO_4$ family almost coincide.

It has been shown that the minimal value of $\varepsilon'_{33}(\omega)$ at different frequencies is larger when the piezoelectric coupling is taken into account than when it is neglected, which is consistent with experiment. The dispersion frequency of $\varepsilon_{33}(\omega)$ in the ferroelectric compoundsof the $KH_2PO_4$ family increases with incrasing $\varepsilon_6$. The phenomena of crystal clamping and piezoelectric resonance in the considered crystals have been described for the first time.

It has been established [101–103, 179] that taking into account the piezoelectric coupling weakly affects the spontaneous polarization and molar specific heat of partially deuterated ferroelectrics of the $K(H_{1-x}D_x)_2PO_4$ type. It should be noted that tunneling hardly influences the dielectric, piezoelectric, and elastic characteristics of the considered crystals, but essentially changes the difference between the Curie and Curie-Weiss temperatures of a free crystal.

## 13. Acknowledgement

The authors acknowledge support from the State Foundation for Fundamental Studies of Ukraine, Project "The phase transitions and physical properties of the $KH_2PO_4$-$NH_4H_2PO_4$ systems with competing ferroelectric and antiferroelectric interactions" No. F40.2/099.

## References

1. Courtens E. Competing structural ordering and transitions to glass in mixed crystals of $Rb_{1-x}(NH_4)_xH_2PO_4$. //J. Phys. (Paris) Lett.– 1982.– Vol. 43.– L199.
2. Nagata T., Iwata M., Orihara H., Ishibashi Y., Miura Y., Mamiya T., Terauchi H. Measurement of Nonlinear Dielectric Constant in $Rb_{1-x}(NH_4)_xH_2PO_4$ Mixed Crystals. // J. Phys. Soc. Jpn. – 1997. – Vol. 66, N 5. – P. 1503-1507.
3. Takashige M., Terauchi H., Miura Y., Hoshino S., Nakamura T. Dielectric Dispersion of $Rb_{1-x}(NH_4)_xH_2PO_4$. // Jap. J. Appl. Phys.– 1985.– 24 Suppl. 24-2– P. 947-949.
4. Iida S., Terauchi H. Dipole-Glass Phase in Random Mixture of Ferroelectric and Antiferroelectric $Rb_{1-x}(NH_4)_xH_2PO_4$. // J. Phys. Soc. Jpn. – 1983. – Vol. 52. – P. 4044-4047.
5. Courtens E..Scaling dielectric data on $Rb_{1-x}(NH_4)_xH_2PO_4$ structural glasses and their deuterated isomorph// Phys.Rev. B.– 1986.– Vol. 33,N4.– P. 2975-2978.
6. Samara G.A., Terauchi H. Pressure-Induced Suppression of the Proton-Glass Phase and Isotope Effects in $Rb_{1-x}(NH_4)_xH_2PO_4$ at High Pressure. // Phys. Rev. Lett. – 1987. – Vol. 59, N 3. – P. 347-350.
7. Ko J.H., Kim B.G., Kim J.J., Fujimori H., Miyajima S. Anisotropic glass freezing in rubidium/ammonium dihydrogen phosphate mixed crystal and its deuterated analogue // J. Phys.: Condens. Matter. – 1995. – Vol. 14. – P. 4403-4410.
8. Miura Y., Takashige M., Terauchi H., Takano Y., Ishimoto H., Ogawa S. Dielectric Constant of $Rb_{0.25}(NH_4)_{0.75}H_2PO_4$ below 1K // Jap. J. Appl. Phys. – 1985. – Vol. 24, Suppl. 24-2, P.950-951.
9. He P. Dielectric Dispersion in $Rb_{1-x}[N(H_{1-y}D_y)_4]_x(H_{1-y}D_y)_2PO_4$ Mixed Crystal System. // J. Phys. Soc. Jpn. – 1991. – Vol. 60, N 1. – P. 313-323.
10. Banys J., Kajokas A., Lapinskas S., Brillingas A., Grigas J., Petzelt J., Kamba S. Microwave and millimetre-wave dielectric response of $Rb_{1-x}(ND_4)_xD_2PO_4$ dipolar glass. // J.Phys.B. – 2002. – Vol. 14. – P. 3725 -3733.
11. Courtens E., Vogt H. Observation of Freezing in a Structural Glass over an Exceptionally Broad Range of Frequencies.// Z.Phys.B.– 1986.– Vol. 62.– P. 143-151.
12. Kutnjak Z., Pirc R., Levstik A., Levstik I., Filipic C., Blinc R. Observation of the freezing line in a deuteron glass. //Phys.Rev. – 1994. – Vol. 50, N 17. – P. 12421-12428.
13. Levstik A., Filipic C., Kutnjak Z., Levstik I., Pirc R., Tadic B., Blinc R. Field-Cooled and Zero-Field-Cooled Dielectric Susceptibility in Deuteron Glasses // Phys. Rev. Lett. – 1991. – Vol. 66, N 18. – P. 2368-2371.
14. Kim B.G., Kim J.J. Relaxation-time distribution function of deuterated dipole glass in the low frequency region. // Phys.Rev.B. – 1997. – Vol. 55, N 9. – P. 5558-5561.
15. Trybula Z., Schmidt V.H., Drumheller J.E., He D., Li.Z. Dielectric measurements of proton-glass state in $Rb_{0.65}(NH_4)_{0.35}H_2AsO_4$ // Phys. Rev. B. – 1989. – Vol. 40, No.7. – P.5289-5291.
16. Trybula Z., Schmidt V.H. Drumheller E.J. Coexistence of proton-glass and ferroelectric order in $Rb_{1-x}(NH_4)_xH_2AsO_4$. // Phys. Rev. – 1991. – Vol. 43, No. 1. – P. 1287-1289.
17. Kim S., Kwun S. Proton-glassy behavior in $Rb_{1-x}(NH_4)_xH_2AsO_4$ mixed crystal. // Phys. Rev. B. – 1990. – Vol. 42, No.1. – P. 638-

642.
18. Pinto J., Schmidt V.H. Spontaneous polarization in the deuterated and undeuterated proton glass $Rb_{1-x}(NH_4)_xH_2AsO_4$ // Ferroelectrics. – 1993. – Vol. 141. P.207-213.
19. Gridnev S.A., Korotkov L.N., Shuvalov L.A., Rogova S.P.,Fedosyuk R.M. Dielectric properties and $x - T$ phase diagram of mixed $K_{1-x}(NH_4)_xH_2PO_4$ crystals // Ferroelectrics Lett. – 1991. – Vol. 13. – P. 67-72.
20. Gridnev S.A. Dipolar glasses // Soros Educational Journal – 1998. - No. 8. – P. 95-101. (in Russian)
21. Tu C.S., Schmidt V.H., Saleh A.A. Dielectric relaxation and piezoelectric coupling in the mixed proton-glass crystall $K_{0.61}(NH_4)_{0.39}H_2PO_4$ // Phys. Rev. B. - 1993. – Vol. 48, No 17. – P. 12483-12487.
22. Ono Y., Hikita T., Ikeda T. Phase transitions in mixed crystal system $K_{1-x}(NH_4)_xH_2PO_4$ // J. Phys. Soc. Jpn. – 1987. – Vol. 56, No. 2. – P. 577-588.
23. Kwon O.J., Kim J.J. Proton glass behavior and phase diagram of the $K_{1-x}(NH_4)_xH_2PO_4$ system. //Phys.Rev B. – 1993. – Vol. 48, No. 9. – P. 6639-6642.
24. Cevc P., Zalar B., and Blinc R. EPR study of random field smearing of the proton glass transition in $Tl^{2+}$ doped $Rb_{1-x}(NH_4)_xH_2PO_4$. // Solid state Comm. – 1989. – Vol. 70, N 4. – P. 461-464.
25. Kind R., Blinc R., Dolinsek J., Korner N., Zalar B., Cevc P., Dalal N., DeLooze J. $Tl^{2+}$ EPR study of the dynamics of the proton-glass transition in $Rb_{1-x}(NH_4)_xH_2PO_4$. //Phys.Rev.B. – 1991. – Vol. 43, No. 4. – P. 2511-2518.
26. Grinberg E.S., Izotov V.V., Efimov V.N. $Tl^{2+}$ EPR with electric field application study of ferro- and antiferroelectrics parts of mixed $Rb_{1-x}(NH_4)_xH_2PO_4$ system phase diagram // Ferroelectrics Letters. – 1993. – Vol. 15, P. 61-68.
27. Smolyaninov I., Glinchuk M.D. The peculiarities of glass state formation and the role of random elastic field in mixed crystal of the $KH_2PO_4$ family. // J.Phys.: Condens.Matter. – 1994. – Vol. 6. – P. 2869-2880.
28. Slak J., Kind R., Blinc R., Courtens E., Zumer S. NMR relaxation study of the H-bonded glass $Rb_{1-x}(NH_4)_xH_2PO_4$ // Phys. Rev. B. – 1984. – Vol. 30, No.1. – P. 85-92.
29. Chen S., Ailion D.C., Laicher G. $^{31}P$ NMR spin-lattice relaxation: Structural glass dynamics in $Rb_{1-x}(ND_4)_xD_2PO_4$ // Phys. Rev. B. – 1993. – Vol. Vol. 47, No.6, P. 3047-3052.



30. Terauchi H. Dipole-glass phase in $Rb_{1-x}(NH_4)_xH_2PO_4$ // Ferroelectrics. – 1985. – Vol. 64. – P. 87-96.
31. Cowley R.A., Ryan T., Courtens E. The structure of the glass phase in $Rb_{1-x}(NH_4)_xH_2PO_4$ // J. Phys. C: Solid State Phys. – 1985. – Vol. 18. – P. 2793-2798.
32. Hayase S., Sakashita H., Terauchi H. Temperature and concentration dependence of x-ray diffuse scattering in a random mixture $Rb_{1-x}(NH_4)_xH_2PO_4$. // Ferroelectrics. – 1987. – Vol. 72. – P. 245-256.
33. Yuzyuk Yu.I., Gregora I., Vorlicek V., Pokorny J., Petzelt J. Raman spectra of DRADP-50 dipolar glass // J. Phys.: Condens. Matter. – 1995. – Vol. 7. – 683-695.
34. Yuzyuk Yu.I., Gregora I., Vorlicek V., Petzelt J. Raman spectra of DRADP-25 dipolar glass: evidence for the mixed ferroelectric-glass phase // J. Phys.: Condens. Matter. – 1996. – Vol. 8. – P. 619-629.
35. Hattori T., Araki H., Nakashima S., Mitsuishi A., Terauchi H. Temperature Dependence of the $\nu_2$ Band of $PO_4$ tetrahedrons in $Rb_{1-x}(NH_4)_xH_2PO_4$ Mixed Crystals. // J. Phys. Soc. Jpn. – 1988.– Vol. 57, No. 3.– P. 1127-1135.
36. Popkov Yu.A., Vankevych A.V., Shuvalov L.A., Fedosyuk R.M. Phase states in mixed crystals $K_{1-x}(NH_4)_xH_2PO_4$. Behaviour of fully symmetric $\nu_1$ – oscillation mode of tetrahedra $PO_4$ // Low Temperature Physics. – 1993. – Vol. 19, No. 2, C. 195-200. (in Russian)
37. Kim J.J., Shin H.K. Raman study of $Rb_{1-x}(NH_4)_xH_2P_{1-y}As_yO_4$ mixed crystal: order parameters in competing and frustrated interactions // Ferroelectrics. – 1992. – Vol. 135. – P. 319-332.
38. Blinc R., Dolinsek J., Schmidt V.H., Ailion D.C. $ND_4$ Deuteron NMR and the Smearing of the Glass Transition in $Rb_{1-x}(ND_4)_xD_2PO_4$ // Europhys. Lett. – 1988. – Vol. 6, No. 1. – P. 55-60.
39. Chen S., Ailion D.C. NMR determination of the Edwards-Anderson order parameter in the deuterated pseudo-spin-glass $Rb_{1-x}(ND_4)_xD_2PO_4$: Anisotropy and concentration dependence of the $ND_4^+$ deuteron second moment // Phys.Rev.B. – 1990. – Vol. 42, N 10. – P. 5945-5952.
40. Gridnev S.A., Korotkov L.N., Fedosyuk R.M. Edwards-Anderson order parameter in proton glass of KDP-ADP system // Ferroelectrics. – 1995. – Vol. 167. P. 15-19.
41. Seliger J., Zagar V., Blinc R. $^{17}O$ NQR study of glass order in $Rb_{0.5}(NH_4)_{0.5}H_2PO_4$ // Phys. Rev. B. – 1995. – Vol. 52, No.17. –

12519-12521.
42. Grimm H., Parlinski K., Schweika W., Courtens E., Arend H. Neutron scattering study of freezing in $Rb_{1-x}(ND_4)_xD_2PO_4$ // Phys. Rev. B. – 1986. – Vol. 33, No.7, P. 4969-4976.
43. Choi Y.S., Kim J.J. Coexistence of two universal relaxations in the glassy freezing of a deuteron dipole glass. // Eur.Lett. – 2004. – Vol. 65, No. 1. – P. 55-60.
44. Chamberlin R.V. and Haines D.N. Percolation model for relaxation in random systems [dilute systems] // Phys.Rev.Lett. – 1990. – Vol. 65, N 17. – P. 2197-2200.
45. Chamberlin R.V. Non-Arrhenius response of glass-forming liquids. // Phys.Rev.B. – 1993. – Vol. 48, No. 21. – P. 15638-15645.
46. Blinc R., Dolinsek J., Zalar B. Low temperature properties of proton and deuteron glasses // Z. Phys. B. – 1997. – Vol. 104. P. 629–634.
47. Sinitskii A., Schmidt V.H. Monte-Carlo stochastic-dynamic study of dielectric response and nonergodicity in proton glass. // Phys.Rev.B. – 1996. – Vol. 54, No.2. – P.842-848.
48. Moriya K., Matsuo T., Suga H., Terauchi H. Heat Capacities and Phase Transitions of the $(NH_4)_xRb_{1-x}H_2PO_4$ System. // Jap. J. Appl. Phys. – 1985. – 24 Suppl. 24-2. – P. 955-957.
49. Papantopoulos G., Papavassiliou G., Milia F., Schmidt V.H., Drumheller J.E., Pinto N.J., Blinc R. Zalar B. $^{75}As$ Nuclear Quadrupole Resonance in Weakly Substitutionally Disordered $Rb_{1-x}(NH_4)_xH_2AsO_4$ // Phys. Rev. Lett. – 1994. – Vol. 73, No.2. – P. 276-279.
50. Korner N., Pfammatter Ch., Kind R. Soft mode, "Relaxor", and glassy-type dynamics in the solid solution $Rb_{1-x}(ND_4)_xD_2PO_4$. // Phys. Rev. Lett. – 1993. – Vol. 70, N 9. – P. 1283-1286.
51. Noh K.H., Kwun S., Yoon J.G. Study of the anisotropic dielectric behavior of $Rb_{1-x}(NH_4)_xH_2PO_4$ ($x$=0.15 and 0.17) mixed crystals. // Phys. Rev. B. – 2000. – Vol. 62, P. 223.
52. Trybula Z. and Kaszynski J. Phase coexistence of hydrogen-bonded mixed ferroelectric and antiferroelectric crystal. // Ferroelectrics. – 2004. – Vol. 298. – P. 347-351.
53. Eom J., Yoon J., Kwun S. Proton glass with remaining ferroelectric order in $Rb_{1-x}(NH_4)_xH_2AsO_4$ mixed crystals // Phys. Rev. B. – 1991. – Vol. 44, No.6, P. 2826-2829.
54. Trybula Z. and Kaszynski J., Maluszynska H. Phase coexistence of hydrogen-bonds $K_{1-x}(NH_4)_xH_2PO_4$ crystal.// Ferroelectrics. – 2005. – Vol. 316. – P. 125-129.



55. Korotkov L.N., Shuvalov L.A., Dielectric Relaxation in Mixed Ferro-Glassy State in Solid Solutions of $K_{1-x}(NH_4)_xH_2PO_4$ Type // Ferroelectrics. – 2003. – Vol. 285. – P. 67-74.
56. Kaszynski J., Trybula Z., Maluszynska H. Dielectric Properties of $K_{1-x}(NH_4)_xH_2PO_4$ (x = 0:095) Crystal // Acta Physica Polonica A. – 2005. – Vol. 108, No. 1. – P. 103-106.
57. Lanceros-Mendez S., Schmidt V.H., and Shapiro S.A. Phase Coexistence in the Deuteron Glass $Rb_{0.9}(ND_4)_{0.1}D_2AsO_4$ Proven by Neutron Diffraction // Ferroelectrics. – 1999. – Vol. 223. – P. 203-210.
58. Howell F.L., Pinto N.J., Schmidt V.H. Complex permittivity of the deuterated and undeuterated proton glass $Rb_{1-x}(NH_4)_xH_2AsO_4$ // Phys.Rev.B. – 1992. – Vol. 16, No.21. – P. 13762-13766.
59. Trybula Z. and Kaszynski J., Los Sz., Mielcarek S., and Trybula M. Two relaxation processes in the inhomogeneous deuterated ferroelectric $Rb_{0.96}(ND_4)_{0.04}D_2AsO_4$. //Phys.Stat.Sol.(b). – 2004. – Vol. 241, N 2. – P. 447-452.
60. Gregorovic A., Zalar B., Blinc R., Ailion D.C. $^{14}$N NMR study of the role of N-D...O bonds in the deuteron glass transition // Phys.Rev.B. – 1999. – Vol. 60, N 1. – P. 76-79.
61. Schmidt V.H., Lanceros-Menndez S., Meschia S.C., Pinto N.J. Anomalous and normal protonic conductivity in $Cs_{1-x}(NH_4)_xH_2PO_4$, $Cs_{1-x}(ND_4)_xD_2PO_4$ and $K_{1-x}(NH_4)_xH_2PO_4$ // Solid State Ionics. – 1999. – Vol. 125. – P. 147-157.
62. Tu C.S., Schmidt V.H. Phases in Antiferroelectrics-side $Rb_{1-x}(ND_4)_xD_2AsO_4$ crystals studied by complex permittivity // Ferroelectrics. – 1999. – Vol. 227. – P.141-151.
63. Schmidt V.H. Phase Coexistence in Proton Glass // J.Korean Phys.Soc. – 1998. – Vol. 32. P.S803-S806.
64. Dobrosavljevic V., Stratt R.M. Mean-field theory of the proton glass // Phys. Rev. B. – 1987. – Vol. 36, No.16. – P. 8484-8496.
65. Tadic B., Pirc R., Blinc R. Isotope effect and pressure dependence of the freezing temperature in proton glasses // Phys. Rev. B. – 1988. – Vol. 37, No.1. – P. 679-682.
66. Sherrington D., Kirkpatrick S. Solvable Model of Spin Glass. // Phys.Rev. Lett. – 1975.–Vol. 35. – P. 1792-1796.
67. Pirc R., Tadic B., and Blinc R. Random-Field Smearing of the Proton-Glass Transition. // Phys.Rev.B. – 1987. – Vol. 36, N 16. – P. 8607-8615.
68. Kim D.H., Kim J.J. Replica Symmetric Solution of Random Field

Tunneling Model for Proton Glasses. // Ferroelectrics. – 2002. – Vol. 268. – P. 263-268.
69. Blinc R., Dolinsek J., Pirc R., Tadic B., Zalar B., Kind R., Liechti O. Local-polarization Distribution in Deuteron Glasses. // Phys. Rev. Lett. – 1989. – Vol. 63, N 20. – P. 2248-2251.
70. Pirc R., Tadic B., Blinc R., Kind R. Dynamic approach to local-polarization distribution and NMR line shape in deuteron glasses. // Phys. Rev. B. – 1991. – Vol. 43, No.4. – P. 2501-2510.
71. Crokidakis N., Nobre F.D. Ising spin glass under continuous-distribution random magnetic fields: Tricritical points and instability lines // Phys. Rev. E. – 2008. – Vol. 77. – P. 041124 (9).
72. Banerjee V., Dattagupta S. Dielectric relaxation in a deuteron glass. // Phys.Rev B. – 2003. – Vol. 68. – P. 054202.
73. Prelovcek P., Blinc R. Spin glass phase in mixed ferroelectric-antiferroelectric hydrogen bonded systems. // J. Phys. C.: Solid State Phys. – 1982. – Vol. 15. – P. L985-L990.
74. Matsushita E., Matsubara T. Theory of Phase Transition in Mixed Crystals $Rb_{1-x}(NH_4)_xH_2PO_4$. //Prog.Theor.Phys. - 1984. - Vol. 71, N 2. - P. 235-241.
75. Matsushita E., Matsubara T. Matsubara: Cluster Theory of Glass in $Rb_{1-x}(NH_4)_xH_2PO_4$. // J.Phys.Soc.Jap. – 1985. – Vol. 54, N 3. – P. 1161-1167.
76. Korynevskii N.A., Solovyan V.B. On the Phase Transitions in Ferroelectric-Antiferroelectric Mixed Systems. // Ferroelectrics. – 2005. – Vol. 317. – P. 19-24.
77. Korynevskii N.A., Solovyan V.B. Investigation of ferroelectric-antiferroelectric mixed compound of RADA type. //Phase Transition. – 2007. – Vol. 80, N 1-2. – P. 55-61.
78. Korynevskii N.A., Solovyan V.B. On the problem of low-temperature ordering in ferro-antiferroelectric mixed compounds // Condens. Matter Phys. – 2009. – Vol. 12, No 2. – P. 267-273.
79. Levitskii R.R., Sorokov S.I., Vdovych A.S. Spin model with different types of competing interactions. // Ferroelectrics. – 2005. – Vol. 316. – P. 111-119.
80. Sorokov S.I., Levitskii R.R., Vdovych A.S. Spin-glass model with essential short-range competing interactions. // Condens. Matter Phys. – 2005, – Vol. 8, No. 3(43). – P. 603-622.
81. Sorokov S.I., Vdovych A.S., Levitskii R.R. Relaxation and thermodynamic properties of the proton-glass model with essential short-range competing interactions // J. Phys. Study. - 2009. - Vol.13, N 1. - 1701 (9p.). (in Ukrainian)



82. Sorokov S.I., Vdovych A.S., Levitskii R.R. Thermodynamic and relaxation dynamics of simple model of proton glass. - Lviv, 2009. - 34 p. (Prepr. / NAN of Ukraine. Institute for Condensed Matter Physics; ICMP-09-06U). (in Ukrainian)
83. Levitskii R.R., Sorokov S.I., Stankowski J., Trybula Z., Vdovych A.S. Termodynamics and complex dielectric permittivity of mixed crystals of the $Rb_{1-x}(NH_4)_xH_2PO_4$ type. // Condens. Matter Phys. – 2008. – Vol. 11, No. 3(55). – P. 523-542.
84. Sorokov S.I., Levitsky R.R., Vdovych A.S. Thermodynamics, dielectric permittivity and phase diagrams of the $Rb_{1-x}(NH_4)_xH_2PO_4$ type proton glasses // Condens. Matter Phys. - 2010. - Vol. 13, No 1. - P. 13706: 1-26.
85. Sorokov S.I., Levitskii R.R., Vdovych A.S., Trybula Z. Termodynamics and dielectric properties of $Rb_{1-x}(NH_4)_xH_2PO_4$ type proton glasses. – Lviv, 2009. – 62 c. (Prepr. / NAN of Ukraine. Institute for Condensed Matter Physics; ICMP-09-08U). (in Ukrainian)
86. Sorokov S.I., Levitskii R.R., Vdovych A.S. Microscopic Theory of $Rb_{1-x}(NH_4)_xH_2PO_4$ Type Compounds // Ferroelectrics. – 2009. – Vol. 379, Issue 1. – P. 101 - 106.
87. Sorokov S.I., Levitsky R.R., Vdovych A.S., Korotkov L.N. Thermodynamic and Dielectric Properties of $K_{1-x}(NH_4)_xH_2PO_4$ Mixed Crystal // Ferroelectrics. - 2010. - Vol. 397, Issue 1. - P. 43 - 53.
88. Sorokov S.I. Thermodynamic and Dielectric Properties of $Rb_{1-x}(NH_4)_xH_2PO_4$ mixed crystals // Izv. RAN. Ser. Fiz. - 2010 - Vol.74, N9. - P.1268-1272. (in Russian)
89. Vaks V.G., Introduction into microscopic theory of ferroelectrics. - M.: Nauka, 1973. - 327 p. (in Russian)
90. Levitskii R.R., Korynevskii N.A., Stasyuk I.V. Theory of proton ordering in ferro- and antiferroelectrics of orthophosphate type // Ukr. J. Phys. - 1974. - Vol.19, №8. - P.1289-1297. (in Ukrainian)
91. Blinc R., Zeks B. Ferroelectrics and antiferroelectrics. Lattice dynamics. - M.: Mir, 1975. - 398 p. (in Russian)
92. Levitskii R.R., Lisnii B.M., Baran O.R. Thermodynamics and dielectric properties of $KH_2PO_4$, $RbH_2PO_4$, $KH_2As0_4$, $RbH_2As0_4$ ferroelectrics // Condens. Matter Phys. - 2001. - Vol. 4, №3. - P. 523-552.
93. Levitskii R.R., Lisnii B.M. Thermodynamics and dielektric properties of the $KH_2PO_4$ type ferroelectrics with hydrogen bonds in cluster approximation // J. Phys. Study. - 2002. - T. 6, №1. - C 91-108. (in Ukrainian)
94. Levitskii R.R., Lisnii B.M., Baran O.R. Thermodynamics and di-

elektric properties of the $NH_4H_2PO_4$ type antiferroelectrics // Condens. Matter Phys. - 2002. - Vol. 5, №3. - P. 553-577.
95. Levitskii R.R., Zachek I.R., Vdovych A.S., Sorokov S.I. Thermodynamics and dynamical properties of the $KH_2PO_4$ type ferroelectric compounds. A unified model // Condens. Matter Phys. – 2009. – Vol. 12, No 1, pp. 75-119.
96. Yomosa Sh., Nagamiya T. The phase transition and the piezoelectric effect of $KH_2PO_4$. // Progr. Theor. Phys., 1949, v. 4, № 3, p. 263–274.
97. Slater J.C. Theory of the transition in $KH_2PO_4$. // J. Chem. Phys., 1941, v. 9, № 1, p. 16–33.
98. Stasyuk I.V., Biletskii I.N. Influence of uniform and uniaxial pressure on ferroelectric phase transition in the $KH_2PO_4$ type crystals // Izv. AN SSSR, ser. fiz., 1983, Vol.47, P.705. (in Russian)
99. Stasyuk I.V., Biletskii I.N., Styagar O.N. Induced by external pressure phase transition in the $KD_2PO_4$ type crystals // Ukr. J. Phys. – 1986, Vol. 31, № 4, P. 567–571. (in Russian)
100. Stasyuk I.V., Levitskii R.R., Zachek I.R., Moina A.P. The $KD_2PO_4$ ferroelectrics in external fields conjugate to the order parameter: Shear stress $\sigma_6$. // Phys. Rev. B, 2000, v. 62, №. 10, p. 6198–6207.
101. Levitsky R.R., Zachek I.R., Vdovych A.S., Moina A.P. Longitudinal dielectric, piezoelectric, elastic, and thermal characteristics of the $KH_2PO_4$ type ferroelectrics // J. Phys. Study. - 2010. - Vol. 14, No 1. - P. 1701(17p.)
102. Levitskii R.R., Lisnii B.M., Theory of piezoelectric, elastic and dielectric properties of the $KH_2PO_4$ family crystals at strain $u_6$. Phase transition and piezoeffect in $KH_2PO_4$ crystal // J. Phys. Study., 2003, Vol. 7, №4, c. 431-445. (in Ukrainian)
103. Levitskii R.R., Lisnii B.M. Theory of related to shear strain $u_6$ physical properties of ferroelectrics and antiferroelectrics of the $KH_2PO_4$ family // phys. stat. sol. (b). - 2004. -Vol.241, №6.-P.1350-1368.
104. Lisnii B.M., Levitskii R.R. Theory of physical properties of ferro- and antiferroelectrics of the $KH_2PO_4$ family related to strains $u_4$ and $u_5$ // Ukr. J. Phys., 2004, v. 49, №7, p.701-709.
105. Stasyuk I.V., Levitskii R.R., Moina A.P., Lisnii B.M. Longitudinal field influence on phase transition and physical properties of the $KH_2PO_4$ family ferroelectrics. // Ferroelectrics, 2001, v. 254, p. 213–227.
106. Lisnii B.M., Levitskii R.R., Baran O.R. // Phase Transitions. 2007. **80**. N 1-2. 25-30.



107. Stasyuk I.V., Levitskii R.R., Moina A.P., Velychko O.V. // Ukr. J. Phys.: Reviews. 2008. N 1. P. 3-6. (in Ukrainian)
108. Stasyuk I.V., Kaminska N.M. Theory of spontaneous polarization and strain of сегнетоелектриків типу $KH_2PO_4$. // УФЖ, 1974, т. 19, в. 2, с. 237–252. (in Ukrainian)
109. Levitsky R.R., Zachek I.R., Vdovych A.S. Static dielectric, piezoelectric and elastic properties of antiferroelectrics $NH_4H_2PO_4$ and $ND_4D_2PO_4$ // Physics and chemistry of solid state. - 2009. - Vol. 13, N 2. - P. 635-646. (in Ukrainian)
110. Stasyuk I.V., Levitskii R.R., Korinevskii N.A. Collective vibrations of protons in compounds of $KH_2PO_4$-type. The cluster approximation // Phys. Stat. Sol. (b). - 1979. - Vol. 91,№2. - P. 541-550.
111. Levitskii R.R., Stasyuk I.V., Korinevsky H.A. Dynamics of ferroactive crystals of orthophosphate type // Ferroelectrics. - 1978. - Vol. 21. - P. 481-483.
112. Korinevskii N.A., Levitskii R.R. Dynamic theory of orthophosphates in cluster approximation // Theoretical and Mathematical Physics. - 1980. - Vol. 42, №3. - P. 416-429. (in Russian)
113. Levitsky R.R., Zachek I.R., Moina A.P., Vdovych A.S. Longitudinal relaxation of mechanically free $KH_2PO_4$ type crystals. Piezoelectric resonance and sound attenuation // Condens. Matter Phys. - 2008. - Vol. 11, No 3(55). - P. 555-570.
114. Levitsky R.R., Zachek I.R., Vdovych A.S. Transverse relaxation in the ferroelectrics with hydrogen bonds of $KH_2PO_4$ family // Physics and chemistry of solid state. - 2009. - Vol. 10, N 2. - C. 377-388. (in Ukrainian)
115. Levitsky R.R., Zachek I.R., Moina A.P., Vdovych A.S. Longitudinal relaxation of $ND_4D_2PO_4$ type antiferroelectrics. Piezoelectric resonance and sound attenuation // Condens. Matter Phys. - 2009. - Vol. 12, No 2. - P. 275-294.
116. Stasyuk I.V., Levitskii R.R. The role proton-phonon Interaction in the phase transition of ferroelectrics with hydrogen bonds // Phys. Stat. Sol.b. – 1970. – Vol. 39, No1. – P. K35-K38.
117. Levitsky R.R., Zachek I.R., Vdovych A.S. Thermodynamics and dynamical properties of the $KH_2PO_4$ type ferroelectric compounds. Unified model. - Lviv, 2008. - 150 p. (Prepr. / NAN of Ukraine. Institute for Condensed Matter Physics; ICMP-08-04U). (in Ukrainian)
118. Gilletta P., Chabin M. Longitudinal and transverse dielectric properties of KDP type crystals // Phys. Stat. Sol. b. – 1980. – Vol. 100. – P. K77-K82.

119. Fairall C.W., Reese W. Thermodynamic properties of $RbH_2AsO_4$ // Phys. Rev. B. – 1974. – Vol. 10, No. 3. - P. 882-885.
120. Zolototrubov Yu.S., Strukov B.A., Taraskin S.A., Kamysheva L.N. Phase transition in crystal $RbH_2As0_4$ // Izv. AN SSSR. Ser. Fiz. – 1975. – Vol. 39, N 4. – C. 782-786. (in Russian)
121. Lains M., Glass A. ferroelectrics and Related Materials. - M.: Mir, 1981. - 736 p. (in Russian)
122. Wiseman G.G. Electrocaloric effect on potassium dihydrogen phosphate // Iee Transactions on Electron Devices. – 1969. – Vol. ED-16, No. 6. - P. 588-593.
123. Strukov B.A., Korzhuev M.A., Baddur A., Koptsik V.A. Spontaneous polarization of crystal $KH_2PO_4$ near Curie point // Fiz. Tverd. Tela. – 1971. – Vol.13, No. 7. – P. 1872-1877. (in Russian)
124. Amin M., Strukov B.A. Heat capacity of monocrystal $RbH_2PO_4$ // Fiz. Tverd. Tela. – 1968. – Vol.10, No. 10. – P. 3158 - 3160. (in Russian)
125. Strukov B.A., Baddur A., Zinenko V.N., Mishchenko A.V., Koptsik V.A. Isotopic effect in crystals $RbH_2PO_4$// Fiz. Tverd. Tela. - 1973. - T.15, №6. - C. 1388-1394. (in Russian)
126. Amin M., Strukov B.A. Influence of deuteration on Heat capacity of crystals $NH_4H_2PO_4$ (ADP) // Fiz. Tverd. Tela. – 1970. – T.12, No. 7. – C. 2035-2038. (in Russian)
127. Stephenson C.C., Adams H.E. The heat capacity of ammonium dihydrogen arsenate from 15 to 300 K. The anomaly at the Curie temperature // J. Am. Chem. Soc. – 1944. – Vol. 66, No.8. – P. 1409-1412.
128. Strukov B.A., Baddur A., Koptsik V.A., Velichko I.A. Electric and thermal properties of mixed ferroelectric crystals $KH_{2(1-x)}D_{2x}PO_4$ // Fiz. Tverd. Tela. – 1972. – T.14, No 4. – C. 1034-1039. (in Russian)
129. Strukov B.A., Amin M., Kopsik V.A. The specific heat of some KDP - type crystals // J. Phys. Soc. Japan. – 1970. – Vol. 28, Suppl. – P. 207-209.
130. Reese W., May L.F. Critical phenomena in order-disorder ferroelectrics. I. Calorimetric studies of $KH_2PO_4$ // Phys. Rev. – 1967. – Vol. 162, No2. - P. 510-518.
131. Vasilevskaya A.S., Sonin A.S. Relation of dielectric and electrooptic properties of ferroelectric crystals of KDP group in paraelectric phase. // Fiz. Tverd. Tela. – 1971. – Vol.13, №6. – C. 1550-1556. (in Russian)
132. Pereverzeva L.P. peculiarities of dispersion $\varepsilon$ in ferroelectrics with order-disorder phase transition // Izv. AN SSSR, Ser. Fiz. - 1971. - Vol.35, №12. - P. 2613-2614. (in Russian)
133. Matthias B., Merz W., Scherrer P. Das seignetteelektrische Gitter vom $KH_2PO_4$ -Typus und das Verhalten der $NH_4$ - Rotationsumwandlung bei $(NH_4, T1)H_2PO4$ -Mischkristallen // Helv. Phys. Acta. - 1947. - Vol. 20. - P. 273-306.
134. Mason W.P. The elastic, piezoelectric, and dielectric constants of potassium dihydro-gen phosphate and ammonium dihydrogen phosphate // Phys. Rev. - 1946. - Vol. 69, №5-6. - P. 173-194.
135. Mason W.P., Mattias B.T. The piezoelectric, dielectric and elastic properties at $ND_4D_2PO_4$ (deuterated ADP) // Phys. Rev. - 1952. - Vol. 88, №3. - P. 477-479.
136. Blinc R., Burgar M., Levstik A. On the order of the phase transition in KDA type ferroelectric crystals // Sol. Stat Commun. - 1973. - Vol. 12, No 6. - P. 573-576.
137. Berdowski J., Opilski A. Crystal Growth of the para- and antiferroelectric phases of deuterium ammonium dihydrogen arsenate (DADA) // J. Crystal Growth. - 1978. -Vol. 43. - P. 381-384.
138. Baumgartner H. Untersehied der Dielektrizitats-konstanten zwischen einem freien und einem geklemmten $KH_2PO_4$-kristall // Helv. phys. acta. – 1951. – Vol.24. – P. 326-329.
139. Mason W. Piezoelectric crystals and its application in ultraacoustics. - M.: IL, 1952. - 447 c. (in Russian)
140. Shuvalov L.A., Zheludev I.S., Mnatsakanyan A.V., Lupudov Ts.Zh., Fiala I. Ferroelectric anomalies of dielectric and piezoelectric properties of crystals $RbH_2PO_4$ and $KD_2PO_4$ // Izv. AN SSSR, Ser. Fiz. - 1967. - Vol.31, №11. - P.1919-1922. (in Russian)
141. Volkova E.N., Izrailenko A.N. Some physical properties of solid mixtures ADP - DADP // Kristallografiya. - 1983. - Lov.28, №6. - P. 1217-1219. (in Russian)
142. Lee K.S., Kim K.T., Kim J.J. KDP impurity effects on antiferroelectric phase transition of ADP crystal // Jpn. J. of Appl. Phys. - 1985. - Vol. 24, Suppl. 24-2. - P. 969-971.
143. Gesi K., Ozawa K. Effect of hydrostatic pressure on the antiferroelectric phase transitions in ammonium dihydrogen arsenate $NH_4H_2AsO_4$ and deuterated analogue // J. Phys. Soc. Jpn. - 1984. - Vol. 53, No. 12. - P. 4405-4412.
144. Volkova E.N. Physical properties of ferroelectric solid mixtures $K(D_xH_{1-x})_2PO_4$ // Candidate dissertation. Moscow, 1991, 152p. (in Russian)
145. Takashige M., Terauchi H., Miura Y., Hoshino S. A Re-Entrant

Glasslike Phase in $Rb_{1-x}(NH_4)_xH_2PO_4$. // J. Phys. Soc. Jpn. – 1985.– Vol. 54, N 9.– P. 3250-3253.
146. Courtens E. Experimental Studies on Mixed Ferro-Antiferroelectric Glasses. // Jap. J. Appl. Phys. – 1985.– Vol. 24.– P. 70-74.
147. Trybula Z., Stankowski J. Coexistence of paraelectric/proton-glass and ferroelectric (antiferroelectric) orders in $Rb_{1-x}(NH_4)_xH_2AsO_4$ crystals // Condens. Matter Phys. – 1998. – Vol. 1, No. 3. P. 311-330.
148. Trybula Z., Stankowski J., Szczepanska L., Blinc R., Weiss Al., Dalal N.S. Proton glass state in $Rb_{1-x}(NH_4)_xH_2AsO_4$ // Ferroelectrics. – 1988. – Vol. 79. P.335-338.
149. Levitskii R.R., Moina A.P., Lisnii B.M. Influence of longitudinal electric field on phase transition and physical properties of $KH_2PO_4$ family ferroelectrics. - Lviv, 2000, 36 c. (Prepr. / NAN of Ukraine. Institute for Condensed Matter Physics; ICMP-00-12U) (in Ukrainian).
150. Levitskii R.R., Zachek I.R., Vdovych A.S. Longitudinal dielectric, piezoelectric, elastic, dynamic and thermal properties of $KH_2PO_4$ type ferroelectrics. - Lviv, - 2006. - 116 p. (Prepr. / NAN of Ukraine. Institute for Condensed Matter Physics; ICMP-06-08U ). (in Ukrainian)
151. Levitskii R.R., Zachek I.R., Vdovych A.S. Transverse dielectric, piezoelectric, elastic and dynamic properties of $KH_2PO_4$ type ferroelectrics. - Lviv, 2007. - 80 c. (Prepr. / NAN of Ukraine. Institute for Condensed Matter Physics; ICMP-07-24U). (in Ukrainian)
152. Tokunaga M. Two different mechanismus of the Curie-Weiss dielectric susceptibility in dispersive-type ferroelectrics // J. Phys. Soc. Jpn. - 1987. - Vol. 56. -P. 1653-1656.
153. Deguchi K., Nakamura E. Deviation from the Curie-Weias law in $KH_2PO_4$ // J.Phys.Soc.Japan. -1980. - Vol. 49, №5. -P. 1887-1891.
154. Samara G.A. The effects of deuteration on the static ferroelectric properties of $KH_2PO_4$ (KDP) // Ferroelectrics. - 1973. - Vol. 5. - P. 25-37.
155. Chabin M., Gilletta F. Polarization and dielectric constant of KDP-type crystals // Ferroelectrics. - 1977. - Vol. 15. - P. 149-154.
156. Mayer R.J., Bjorkstam J.L. Dielectric properties of $KD_2PO_4$ // J. Phys. Chem. Solids. - 1962. - Vol. 23. - P. 619-620.
157. Kobayashi J., Uesu Y., Mizutani I., Enomoto Y. X-ray study on thermal expansion of ferroelectric $KH_2PO_4$. // Phys. stat. sol. (a), 1970, vol. 3, p. 63-69.
158. Strukov B.A., Baddur A., Velichko I.A. About first order phase transition in crystals $KD_2PO_4$ // Fiz. Tverd. Tela. - 1971. - Vol.13, №8. - P. 2484-2485. (in Russian)
159. Hill R.M., Ichiki S.K. Paraelectric response of $KD_2PO_4$ // Phys. Rev. - 1963. - Vol. 130, №1. - P. 150-151.
160. Breziria B., Fouskova A., Smutny P. Regular behaviour of solid solutions of $KH_{2(1-n)}D_{2n}PO_4$ single crystals // Phys.Stat. Sol. a. - 1972. - Vol. 11, №2. -P. K149-K152.
161. Fairall C.W., Reese W. Thermodynamic properties of $KH_2AsO_4$ and $KD_2As0_4$ // Phys. Rev. B. -1972. - Vol. 6, №1. - P. 193-199.
162. Blinc R., Burgar M., Levstik A. On the order of the phase transition in KDA type ferroelectric crystals // Sol. Stat Commun. - 1973. - Vol. 12, №6. - P. 573-576.
163. Bantle W., Caflish C. Der Piezoeffekt des seignette-elektrischen Kristalls $KH_2PO_4$ // Helv. Phys. Acta. - 1943. - Vol. 16. - P. 235-250.
164. Von Arx A., Bantle W. // Helv. Phys. Acta, 1943, vol. 16, p. 211.
165. Adhav.R.S. // J.Appl.Phys., 1968, v.39, p.4095.
166. Shuvalov L.A., Mnatsakanyan A.V. The elastic properties of $KD_2PO_4$ crystals over a wide temperature range. // Sov. Phys. Crystall., 1966, vol. 11, №2, p. 210-212.
167. Iona F., Shirane D. Ferroelectric crystals. - M.: Mir, 1965. - 555p.
168. Brody E.M., Cummins H.Z. // Phys. Rev. Lett., 1968, vol. 21, p. 1263.
169. Garland C.W., Novotny D.B. Ultrasonic velocity and attenuation in $KH_2PO_4$ // Phys. Rev. -1969. - Vol. 177, №2. -P. 971-975.
170. Kaminov I.P. Microwave dielectric properties of $NH_4H_2PO_4$, $KH_2As0_4$ and partially deuterated $KH_2PO_4$ // Phys. Rev. -1965, Vol. 138, №5A. - p. 1539-1543.
171. Volkov A.A., Kozlov G.V., Lebedev S.P., Velichko I.A. Dielectric spectra of mixed crystals KDP-DKDP in submillimetric wave region // Fiz. Tverd. Tela, - 1979. - Vol.21, №11. - P. 3304-3309 (in Russian).
172. Levitskii R.R., Zachek I.R., Vdovych A.S. Longitudinal static dielectric, piezoelectric, elastic, electrostrictive and dynamic dielectric properties of $ND_4D_2PO_4$ type antiferroelectrics. - Lviv, 2008. - 61p. (Prepr. / NAN of Ukraine. Institute for Condensed Matter Physics; ICMP-08-19U) (in Ukrainian).
173. Levitskii R.R., Zachek I.R., Vdovych A.S. Transverse static dielectric, piezoelectric, elastic, electrostrictive and dynamic dielectric properties of $ND_4D_2PO_4$ type antiferroelectrics. - Lviv, 2008. - 46p. (Prepr. / NAN of Ukraine. Institute for Condensed Matter Physics;

ICMP-08-20U) (in Ukrainian).
174. Kentsig V. Ferroelectrics and antiferroelectrics. - M.: IL, 1960. - 234 p. (in Russian).
175. Fukami T. X-ray Study of crystal structure of $ND_4D_2PO_4$ in the antiferroelectric phase // J. Phys. Soc. Jpn. - 1988. - Vol. 57, №4. - P. 1287-1290.
176. Zheludev I.S. Physics of crystal dielectrics. - M.: Nauka, 1968. - 463p.
177. Kozlov G.V., Lebedev S.P., Prokhorov A.M., Volkov A.A. Investigation of ferroelectric excitations in hydrogen-bond crystals using the method of submillimeter spectroscopy // J.Phys.Soc.Japan. - 1980. - Vol. 49, Suppl. - P. 188-190.
178. Levitskii R.R., Zachek I.R., Mits Ye.V., Volkov. A.A., Kozlov G.V., Lebedev S.P. Longitudinal and transverse relaxation in $ND_4D_2PO_4$. - Kyiv, 1982. - 30 p. - (Preprint of the Bogolyubov Institute for Theoretical Physics; ITP-82-2R). (in Russian).
179. Stasyuk I.V., Levitskii R.R., Moina A.P., Slivka A.G., Velychko O.V. Field and deformational effects in complex ferroelectric compounds. – Uzhgorod: Grazhda, 2009. – 392p. (in Ukrainian)

# CONDENSED MATTER PHYSICS

The journal **Condensed Matter Physics** is founded in 1993 and published by Institute for Condensed Matter Physics of the National Academy of Sciences of Ukraine.

**AIMS AND SCOPE:** The journal **Condensed Matter Physics** contains research and review articles in the field of statistical mechanics and condensed matter theory. The main attention is paid to physics of solid, liquid and amorphous systems, phase equilibria and phase transitions, thermal, structural, electric, magnetic and optical properties of condensed matter. Condensed Matter Physics is published quarterly.

**ABSTRACTED/INDEXED IN:**
- Chemical Abstract Service, Current Contents/Physical, Chemical&Earth Sciences
- ISI Science Citation Index-Expanded, ISI Alrting Services
- INSPEC
- Elsevier Bibliographic Databases (EMBASE, EMNursing, Compendex, GEOBASE, Scopus)
- "Referativnyi Zhurnal"
- "Dzherelo"



**CONTACT INFORMATION:**
Institute for Condensed Matter Physics
of the National Academy of Sciences of Ukraine
1 Svientsitskii Str., 79011 Lviv, Ukraine
Tel: +38(032)2760908; Fax: +38(032)2761978
E-mail: cmp@icmp.lviv.ua http://www.icmp.lviv.ua